Title
Modeling and Analysis of Tritium Transport in Multi-Region Lead-Lithium Liquid Metal Blankets

Author
Zhang, Hongjie

Publication Date
2014

Peer reviewed|Thesis/dissertation

UNIVERSITY OF CALIFORNIA

Los Angeles

Modeling and Analysis of Tritium Transport in Multi-Region Lead-Lithium Liquid Metal Blankets

A dissertation submitted in partial satisfaction

of the requirements for the degree

Doctor of Philosophy in Mechanical Engineering

by

Hongjie Zhang

2014

ABSTRACT OF THE DISSERTATION

Modeling and Analysis of Tritium Transport in Multi-Region Lead-Lithium Liquid Metal Blankets

by

Hongjie Zhang

Doctor of Philosophy in Mechanical Engineering

University of California, Los Angeles, 2014

Professor Mohamed A Abdou, Chair

It is critical to be able to predict tritium transport in lead-lithium liquid metal (LM) blankets with great accuracy to provide information for fusion reactor safety and economy analyses. However, tritium transport processes are complex and affected by multiple physics such as magnetohydrodynamic (MHD) flow, yet there is no single computer code capable of simulating these phenomena inclusively. Thus the objectives of this research are: 1) to develop mathematical models and computational codes to quantify both tritium distributions throughout the blanket and the permeation loss rate from LM to helium coolant, and 2) to evaluate the key factors that govern tritium permeation and distribution.

To accomplish these objectives, a computational framework for analyzing tritium transport phenomena affected by multi-physics and geometric features has been developed. Models have been proposed to integrate multiple tritium transfer processes, including transport inside the LM MHD flow, transfer across the material interface, and permeation through the structural materials and into the helium coolant. Numerical schemes have been developed and implemented in the code to link the different

transport mechanisms. The developed model and code have been validated against the data from the US-JA TITAN experiments on hydrogen transport through an α-Fe/PbLi system and in-reactor tritium release data from lead-lithium, and the modeling results agree well with the experimental data.

Parametric studies are performed to quantify the MHD effects, buoyancy effects, PES effects, and the uncertainties of transport properties. The MHD effects reduce the tritium permeation rate due to the higher velocity near the wall. However, the rate of decrease is reduced at higher Hartmann numbers. The buoyancy effect on tritium transport in the LM MHD flows is revealed. Its tritium inventory drops by 80%, and the permeation rate drops by 20% for an upward flow compared to a downward flow. If a PES is introduced on the wall parallel to the magnetic field, tritium loss rate increases by 15% because the velocity is reduced near the front wall. The range of permeation rate change on the basis of uncertainties of transport properties is also provided, and the effect of the uncertainty of tritium solubility is significant. Furthermore, as the FCI electric conductivity increases from 5 to 500 $\Omega^{-1}m^{-1}$, the tritium permeation rate decreases by 46% due to the increasing velocity in the gap. Lastly, the difference in tritium permeation rates between dual coolant lead lithium (DCLL) and helium-cooled lead lithium (HCLL) blanket concepts is quantified. The tritium permeation loss percentage from the HCLL concept is about one order of magnitude higher than from the DCLL concept (~ 17%. vs. 1.2%). This is mainly due to a much lower velocity and thus a much higher tritium partial pressure for the HCLL concept.

The computational models and results stated in this work provide guidance on the lead-lithium liquid metal blanket designs to comply tritium control requirements with regard to the reduction in tritium permeation and inventory and on planning the experiments for database evaluation.

The dissertation of Hongjie Zhang is approved.

_____

Mohamed A Abdou, Committee Chair

_____

Jaime Marian

_____

Adrienne Lavine

_____

Alice Ying

_____

Xiaolin Zhong

University of California, Los Angeles

2014

Table of Contents

Figures

Tables

NOMENCLATURE

Symbols or Abbreviations

B	Magnetic field vector
c	Concentration
CORE	PbLi flow region inside flow channel insert
D	Diffusivity
DCLL	Dual coolant lead lithium
FCI	Flow channel insert
GAP	PbLi flow region between structure wall and flow channel insert
Gr	Grashoff number
Ha	Hartmann number
HC	Helium coolant
HCLL	Helium-cooled lead-lithium
He	Helium
ITER	International Thermonuclear Experimental Reactor
j	Current density or species flux
*K*r	Recombination coefficient
*K*s	Solubility
Li	Lithium
LM	Liquid metal
MHD	Magnetohydrodynamics
p	Pressure / Partial pressure
PbLi	Lead-lithium
PES	Pressure equalization slot
Re	Reynolds number

S	Tritium generation rate
SiC	Silicon carbide
TBM	Test Blanket Module
u, U	**V**elocity vector
t	Time
T	Temperature

Greek Symbols

ρ	Density
σ	Electrical conductivity
φ	Electric potential
Ω	Domain
∂Ω	Domain boundary

Acknowledgments

I would like to express my deepest gratitude to my dissertation advisor, Professor Mohamed A Abdou for his support and encouragement during this work. Without his guidance, I might not have accomplished my thesis research. I would also like to express my special appreciation to Dr. Alice Ying for her valuable advice, patience and helpful suggestions throughout this process, and for her helpful edits of this document.

My thanks extend to other committee members: Professors Jaime Marian, Professor Adrienne Lavine, and Professor Xiaolin Zhong for their helpful career advice and suggestions in general.

I am also grateful to UCLA Fusion personnel for their help and positive discussions and valuable comments.

A special mention goes to my family for my spiritual support, and constant encouragement throughout my life.

.

Vita

1998	B.S., University of Science and Technology of China, Mechanical Engineering
2010	M.S., University of California, Los Angeles, Mechanical Engineering

Publications

H. Zhang, (2014). Quantification of Dominating Factors in Tritium Permeation in PbLi Blankets. Fusion Science & Technology (to be published).

H. Zhang, (2013). Impact of pressure equalization slot in flow channel insert on tritium transport in a DCLL-type poloidal duct. Fusion Science and Technology 64 (3), 651-656.

H. Zhang, (2011). Modeling Tritium Transport in PbLi Breeder Blankets Under Steady State. Fusion Science and Technology 60 (2), 814-818.

H. Zhang, (2010). Integrated simulation of tritium permeation in solid breeder blankets. Fusion Engineering and Design 85 (10), 1711-1715.

ABSTRACT OF THE DISSERTATION

Modeling and Analysis of Tritium Transport in Multi-Region Lead-Lithium Liquid Metal Blankets

by

Hongjie Zhang

Doctor of Philosophy in Mechanical Engineering

University of California, Los Angeles, 2014

Professor Mohamed A Abdou, Chair

It is critical to be able to predict tritium transport in lead-lithium liquid metal (LM) blankets with great accuracy to provide information for fusion reactor safety and economy analyses. However, tritium transport processes are complex and affected by multiple physics such as magnetohydrodynamic (MHD) flow, yet there is no single computer code capable of simulating these phenomena inclusively. Thus the objectives of this research are: 1) to develop mathematical models and computational codes to quantify both tritium distributions throughout the blanket and the permeation loss rate from LM to helium coolant, and 2) to evaluate the key factors that govern tritium permeation and distribution.

To accomplish these objectives, a computational framework for analyzing tritium transport phenomena affected by multi-physics and geometric features has been developed. Models have been proposed to integrate multiple tritium transfer processes, including transport inside the LM MHD flow, transfer across the material interface, and permeation through the structural materials and into the helium coolant. Numerical schemes have been developed and implemented in the code to link the different

transport mechanisms. The developed model and code have been validated against the data from the US-JA TITAN experiments on hydrogen transport through an α-Fe/PbLi system and in-reactor tritium release data from lead-lithium, and the modeling results agree well with the experimental data.

Parametric studies are performed to quantify the MHD effects, buoyancy effects, PES effects, and the uncertainties of transport properties. The MHD effects reduce the tritium permeation rate due to the higher velocity near the wall. However, the rate of decrease is reduced at higher Hartmann numbers. The buoyancy effect on tritium transport in the LM MHD flows is revealed. Its tritium inventory drops by 80%, and the permeation rate drops by 20% for an upward flow compared to a downward flow. If a PES is introduced on the wall parallel to the magnetic field, tritium loss rate increases by 15% because the velocity is reduced near the front wall. The range of permeation rate change on the basis of uncertainties of transport properties is also provided, and the effect of the uncertainty of tritium solubility is significant. Furthermore, as the FCI electric conductivity increases from 5 to 500 $\Omega^{-1}m^{-1}$, the tritium permeation rate decreases by 46% due to the increasing velocity in the gap. Lastly, the difference in tritium permeation rates between dual coolant lead lithium (DCLL) and helium-cooled lead lithium (HCLL) blanket concepts is quantified. The tritium permeation loss percentage from the HCLL concept is about one order of magnitude higher than from the DCLL concept (~ 17%. vs. 1.2%). This is mainly due to a much lower velocity and thus a much higher tritium partial pressure for the HCLL concept.

The computational models and results stated in this work provide guidance on the lead-lithium liquid metal blanket designs to comply tritium control requirements with regard to the reduction in tritium permeation and inventory and on planning the experiments for database evaluation.

Chapter 1
Introduction

It is essential to predict tritium transport in lead-lithium liquid metal blankets and to quantify permeation rate from the lead-lithium liquid metal breeder into the helium coolant for fusion reactors [1-3]. The key variables that have been identified that can strongly affect tritium transport and permeation, include the configurations of blanket concepts, the MHD flow distributions, and the material properties. Therefore, in the current phase of research and development, there is a strong incentive to develop comprehensive predictive capabilities (computational models) in order to plan the experiments and to provide necessary predictive tools for fusion blanket designs.

1.1 Background of the Problem

A tritium breeding blanket, as shown in Figure 1 [4], is a key component for sustainability of fusion energy. The blanket has several main functions: (1) it absorbs high energy neutrons, transforming their energy into heat that is transferred to the coolant, (2) it acts as a shield, preventing neutrons from reaching the superconducting magnets, and (3) it breeds tritium. Lithium in some form has been identified as the only element from which

adequate tritium breeding appears feasible. Liquid lithium, liquid lithium-lead alloys, molten lithium salts, and solid lithium compounds have been proposed as candidate tritium breeding materials in various blanket concepts [2].

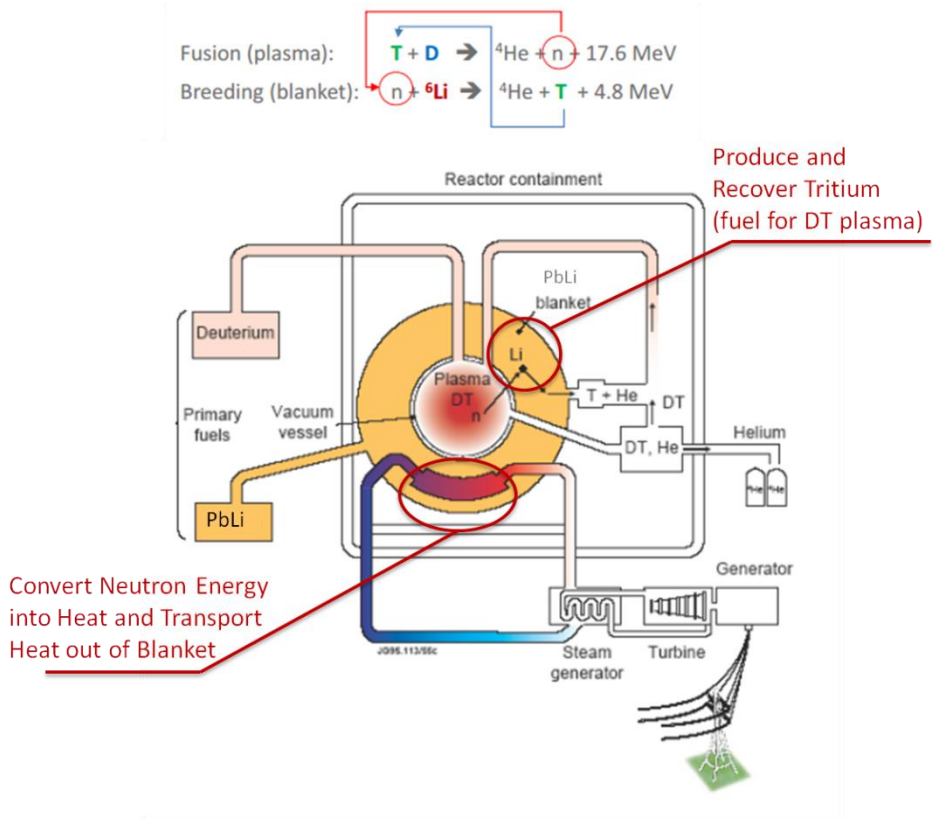

Figure 1. Tritium Breeding Blanket: A key component for sustainability of Fusion Energy [4]

Interest in using liquid lithium-lead alloys as tritium breeders for fusion blanket applications has grown considerably within the fusion community since the 1980's [2-4]. These alloys offer the following potentially attractive advantages: (1) a tritium breeder (Li) is combined with a neutron multiplier (Pb) in the same material, (2) low melting point (508K

for Li17Pb83 [10]), (3) good thermal conductivity compared with ceramic breeders, (4) more stability in terms of chemical reactions than pure lithium metal, and (5) the bright prospects for tritium recovery owing to low hydrogen solubility. However, there are still critical issues to address, such as the MHD effect, the corrosion of the blanket's structural materials, and tritium transport and permeation [6].

A number of blanket concepts utilizing the eutectic liquid metal alloy, Pb–17Li, have been developed with a range of performances and associated development risks [5]. Currently, two primary blanket concepts are the US Dual Coolant Lead Lithium (DCLL) concept and the European HCLL blanket concept (the DCLL is shown schematically in Figure 2; and the HCLL in Figure 3) [6-8].

The DCLL blanket has the potential to be a high-performance DEMO blanket design with a projected thermal efficiency of >40%. Reduced activation ferritic steel (RAFS) is used as the structural material. Helium is used to cool the first wall and blanket structure, and the self-cooled Pb-17Li breeder is circulated with velocities of the order of 0.05~0.1 m/s for power conversion and for tritium breeding and extraction. A SiC-based flow channel insert (FCI) is separated from the ferritic wall by a thin (~ 2 mm) gap also filled with PbLi. Both the gap flow and the flow inside the FCI box, known as the bulk flow, are driven by the same pressure head. The gap and the bulk flows can be connected through small openings

(either holes or a slot) in one of the FCI walls. The FCI acts as an electrical insulator for magnetohydrodynamic pressure drop reduction from the circulating Pb-17Li and as a thermal insulator to separate the high-temperature Pb-17Li (~650 ℃ to 700 ℃) from the RAF/M structure.

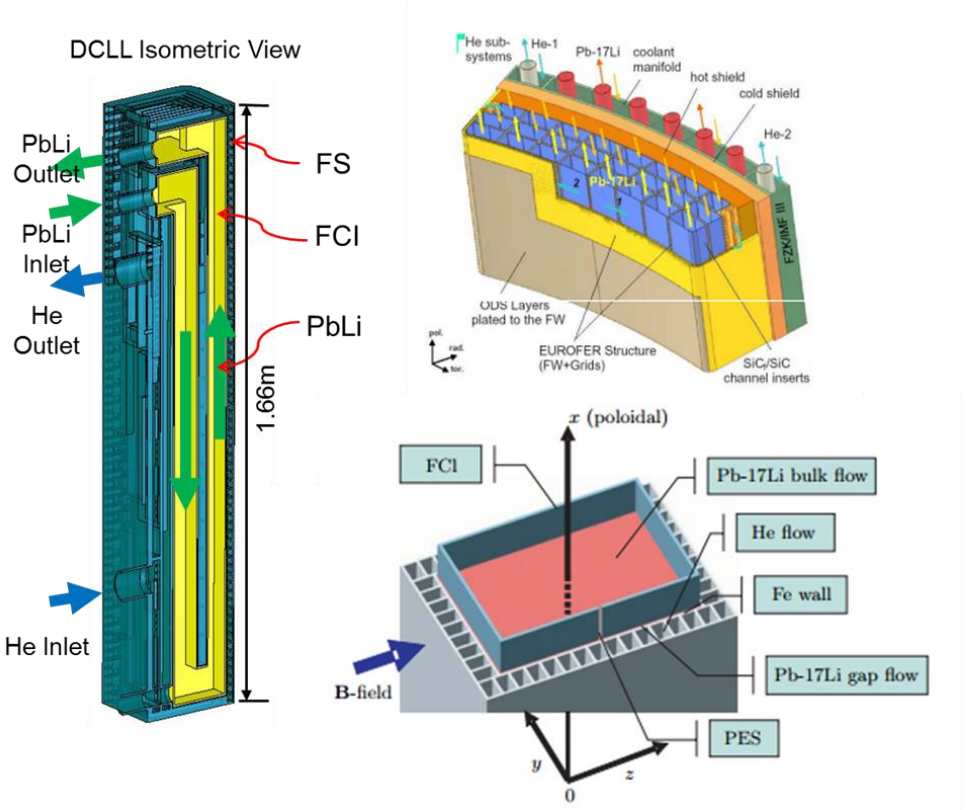

Figure 2. Reference DCLL blanket concept

A partial view of the current European HCLL blanket concept is shown in Figure 3. It is a modular design, where a number of rectangular boxes, the breeder units, are arranged in columns and combined to form a blanket module. Lead-lithium liquid metal feeds each column through a poloidal manifold, then the fluid enters the breeder units by flowing through narrow vertical gaps and expands in the sub-channels formed by the cooling plates. These fluid domains have a high aspect ratio (ratio of toroidal width to poloidal height) that can affect and modify the velocity distribution compared to the case of an almost square duct. The breeder units are connected two-by-two at the first wall by a small opening through which the supplied PbLi passes from one box to the adjacent one before being collected in a second poloidal manifold. The liquid metal in these channels flows very slowly, with velocities of the order of 1~1.5 mm/s. This is about 2 orders of magnitude lower than in the DCLL concepts, since the Pb–17Li is not used for heat extraction but only for tritium extraction.

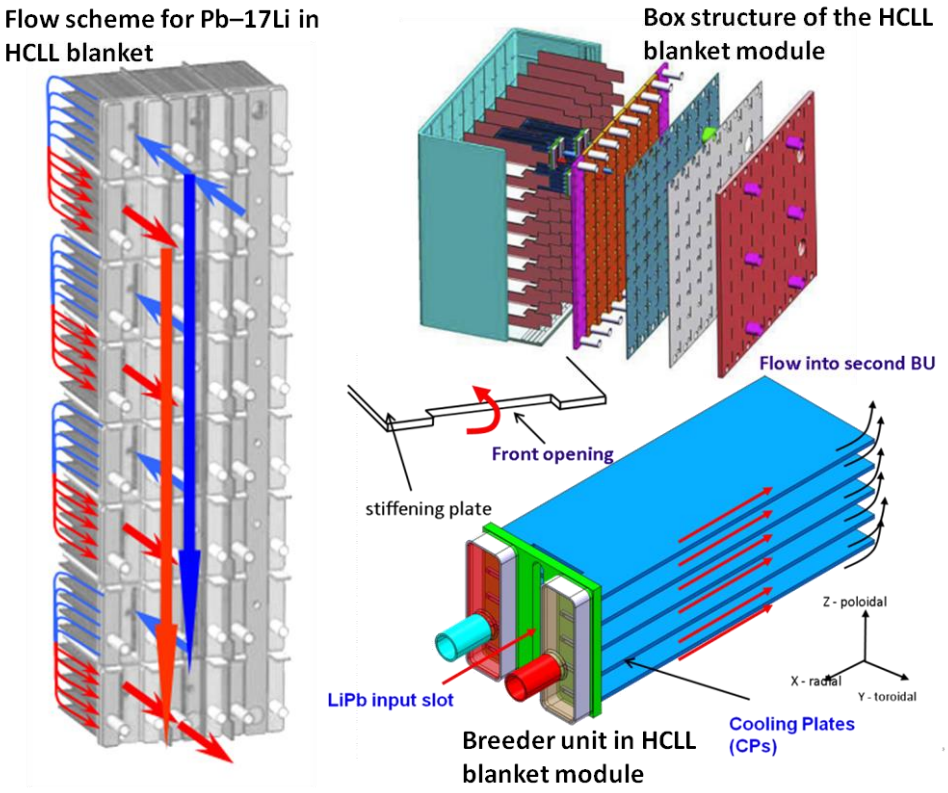

Figure 3. Reference HCLL blanket concept

For both the HCLL and DCLL concepts, tritium control is one of the key issues that has been studied for a long time. There are two main tritium control issues associated with lead-lithium liquid metal blanket designs. The first is to avoid excessive tritium concentrations for safety considerations. This requires a well-designed flow path with no "pockets" with stagnant PbLi in order to avoid excessive tritium concentrations there. The second goal is to control tritium permeation losses to an acceptable level. Because of its high tritium partial pressure due to the low solubility of tritium in PbLi, as seen in Figure 4, once tritium reaches a PbLi/metal interface, it would rather reside in almost any material other than PbLi. Thus tritium will permeate out through the structure walls and can be lost to the environment. ITER (International Thermonuclear Experimental Reactor) defines that the maximum allowable tritium inventory in an individual system to be less than 200g and the allowable tritium loss rate has been defined to be less than 10 Ci/FPD. An accurate predictive capability is needed to help achieving such stringent goal.

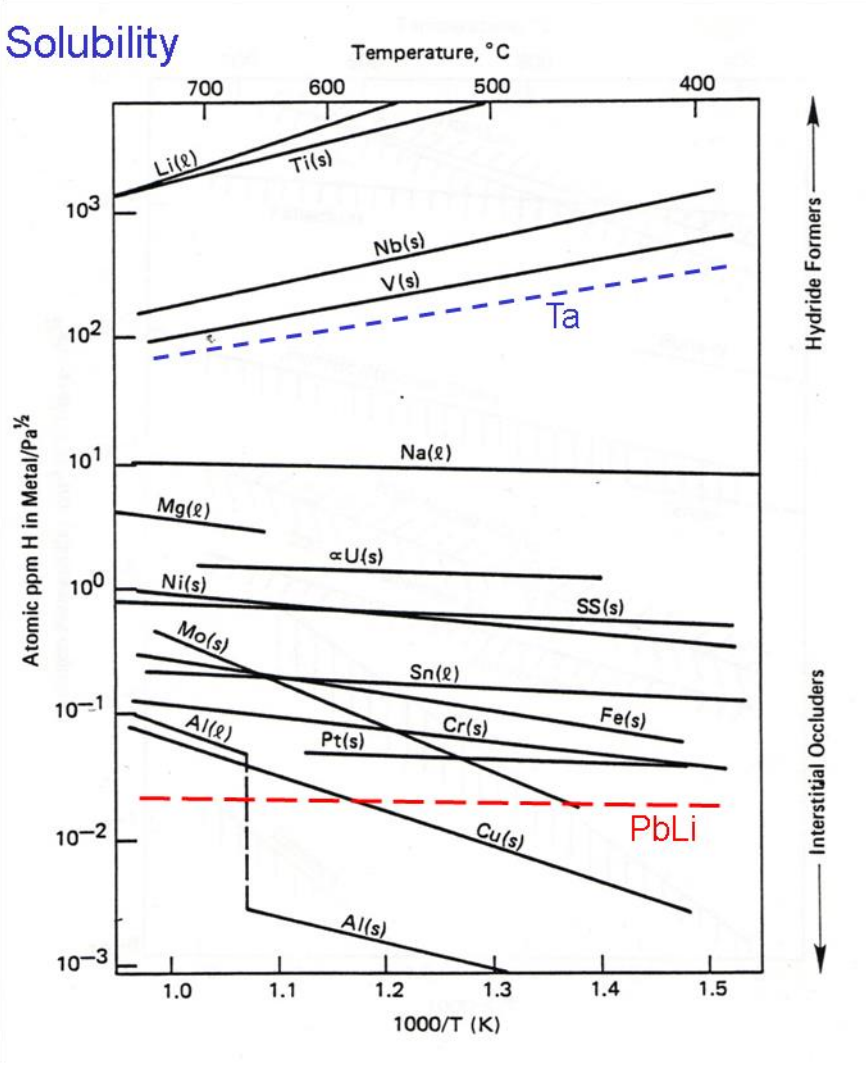

Figure 4. Tritium solubility in different materials

1.2 Problem Statement

Tritium is generated inside the breeder and moves via several mechanisms (e.g. diffusion, permeation, etc.) It potentially might reach the environment, giving a potential radiological hazard. Thus, the objective of this work is to evaluate the tritium distributions inside the blanket components and the tritium losses into the helium coolant, based on the complex blanket geometries and under realistic reactor-like conditions. In order to perform this study, development of mathematical models and computational codes for predicting tritium transport and permeation in lead-lithium liquid metal blankets is needed. As yet, no single fundamental method of calculating tritium transport has been universally accepted. There are numerous issues associated with this task that must be managed in order to calculate tritium transport in a lead-lithium liquid metal blanket. First, multiple tritium transport processes in multiple regions have to be considered simultaneously, such as tritium diffusion and convection through the liquid metal, transfer across the liquid metal/wall structure interface, and diffusion through the wall structure. A comprehensive model with the capability to include several tritium transport processes in each region and to couple the individual transfer mechanisms at material interfaces with an adequate set of boundary conditions is a fundamental task necessary for the modeling of tritium transport in liquid metal blanket. Second, flows of electrically conducting liquid metal will experience

complicated MHD effects in the magnetic fusion environment. MHD effects can have dramatic impacts on the flow distribution and cause complex velocity fields (e.g. Hartmann layer, side layer, reversed flow, stagnant flow, etc.) [3], thus affecting tritium transport and permeation rate. The geometric configurations of the blanket concepts are another key factor. For example, in the DCLL concept, a thin gap between the flow channel insert (FCI) and the structure will affect tritium transfer behavior and loss rate by changing the local MHD velocity distribution. A pressure equalization slot (PES), utilized at the FCI, will affect tritium transfer behavior and loss rate by providing a path for tritium to migrate between the core and the gap and also by changing the local MHD velocity distribution [9]. Furthermore, there are considerable uncertainties in the values for physical properties (e.g. tritium solubility, diffusion coefficients) of materials used in these systems [10], and modeling implementation and sensitivity analysis should be done in order to evaluate the impact of the different solubility and diffusivity values on the tritium permeation rate.

1.3 Previous Models and Deficiencies

At present, addressing tritium transport phenomena in LM blankets under fusion-relevant conditions is difficult due to their multi-physics, multi-material domains, and

complex blanket geometry. The experimental limitations are caused by requirements of magnetic fields and prototypic neutron sources, the conditions that can hardly be met at the same time in non-fusion devices. All these make studying phenomena in the blanket conditions very challenging. Therefore, modeling plays a key role in observing the overall tritium transport behavior for fusion blanket design. However, because a large number of variables that are likely to affect tritium behavior and the multi-physics processes have to be considered simultaneously, it is not surprising that a comprehensive model for tritium transport has not yet been fully developed. Numerical simulations are often limited to 1D or 2D simplifications and ignore some important factors (e.g. the MHD effect).

Currently, the Tritium Migration Analysis Program (TMAP) [11], developed by the Fusion Safety Program at INEL as a safety analysis code to analyze tritium retention and loss in fusion reactor structures, has also been used to analyze tritium permeation losses from the US Dual Coolant Lead Lithium (DCLL) ITER Test Blanket Module (TBM) with the use of mass transport correlations to estimate tritium transport in flowing PbLi. TMAP incorporates one-dimensional thermal- and mass-diffusive transport calculations through structures and zero dimensional fluid transport between enclosures and across the interface between enclosures and structures. Presently, TMAP is the reference tool for the simulation of the permeation phenomenon in ITER. Unfortunately it has an important disadvantage:

TMAP is only a 1D program. That makes it not completely adequate for the 3D blanket geometries and also makes it difficult to estimate tritium transport in the flowing liquid metal and to evaluate the impact of MHD effects.

1.4 Scope of Work

The primary purposes of this dissertation are: 1) to develop mathematical models and computational codes to quantify tritium distribution throughout the blanket and permeation rate from lead-lithium liquid metal to helium coolant, 2) to evaluate the important factors, such as geometric configuration of the blanket, MHD flow, uncertainties of transport properties that govern tritium permeation, and distributions. Specifically, this study differs and improves upon earlier works in several ways and key areas:

- Solving the problem in 3D multiple regions
- Including complex blanket geometry (e.g. PES, GAP) into analysis
- Coupling multiple tritium transfer processes
- Accounting for LM MHD velocity and temperature profiles
- Accounting for the tritium generation rate profile

In addition to this introductory chapter, the second chapter begins with a review of relevant physical phenomena and recent advances in tritium transport behavior in lead-lithium liquid metal blankets.

The theoretical formulation of the tritium transfer model and the numerical methodology are described in Chapter 3. The proposed model in this work includes multiple tritium transfer processes, adequately coupled, such as LM MHD flow, mass transfer at fluid-solid interfaces, and convection-diffusion in liquid metal. Numerical schemes have been developed and implemented into the computer code to link the different transport mechanisms for the different physical regions. The strategy taken here is to integrate thermal/fluid/MHD solver and mass transfer solver with developed utility for data mapping from MHD solver to mass transfer solver, benefiting from solving the MHD velocity and temperature profiles and handling the blankets' geometry complexity.

In order to evaluate the accuracy of the mathematical formulation that is implemented in the model and to generate confidence in the results provided by the computer code, I carried out three benchmark cases relevant for tritium transport assessment. Chapter 4 discusses the validations including: (1) permeation through solid media (validated with US-JA TITAN experiment [14]), (2) transport in flowing media (compared with an analytical solution for an absorption-convection-permeation problem [15]) and (3) release with tritium

generation source term (validated with in-reactor tritium release experiment from molten lithium-lead alloy $Li_{17}Pb_{83}$ [12, 13]).

Another major part of this study, presented in Chapter 5, explores the tritium transport and permeation behavior in the lead-lithium liquid metal blanket concepts. Several key issues are addressed in conjunction with the analysis, including:

- Parametric studies to identify the MHD effects and the buoyancy effects on tritium transport and permeation (section 5.3);
- Identification of the range of permeation rate change on the basis of uncertainties of the material properties (e.g. solubility and diffusivity);
- Tritium transport in a DCLL-type poloidal duct with a PES in the FCI to evaluate the PES effects on tritium concentration and permeation (section 5.4);
- Quantification of the tritium inventory and permeation rate in a DCLL U-shaped flow, which represent, the current US DCLL design (section 5.5);
- Tritium transport and permeation in the HCLL configuration and comparison with the case of the DCLL concept (section 5.6).

The last part of this study presents a tritium transport model considering helium bubbles existing in lead-lithium liquid metal (section 5.7). In this case, tritium may be absorbed into helium bubbles as the new forming phase T_2. Initial analysis is carried out as a future

reference on the importance of helium bubbles on tritium transport when the volume fraction of helium bubbles and the reference tritium partial pressure are changed.

1.5 References

1. M.A. Abdou, S.E. Berk, A. Ying, Y.K.M. Peng, S. Sharafat, et al., *Results of an international study on a high-volume plasma-based neutron source for fusion blanket development*, Fusion Technol. 29 (1) (1996) 1–57
2. M.A. Abdou, P.J. Gierszewski, M.S. Tillack, M. Nakagawa, J. Reimann, et al., *Technical issues and requirements of experiments and facilities for fusion nuclear technology*, Nucl. Fusion 27 (4) (1987) 619–688.
3. S. Malang, et al., *An example pathway to a fusion power plant system based on lead–lithium breeder: Comparison of the dual-coolant lead–lithium (DCLL) blanket with the helium-cooled lead–lithium (HCLL) concept as initial step*, Fusion Eng. Des. (2009).
4. P. Norajitra, L. Buhler, A. Uenaventura, E. Diegele, U. Fischer, E. Utter, R. Kruessmann, S. Malang, J. Reimann, A. Orden, D. Ward, G. Vieder, and F. Wasastjerna, *Conceptual Design of the dual-coolant blanket in the frame for the EU power plant conceptual study (TW2-TRP-PPCS12D9)*, Forschungszentrum Karlsruhe Report FZKA 6780 (2002).
5. L. Giancarli, V. Chuyanov, M. Abdou, M. Akiba, B.G. Hong, R. Lässer, C. Pan, Y. Strebkov, TBWG, *Breeding blanket modules testing in ITER: An international program on the way to DEMO*, Fusion Eng. Des. 81 (1–7) (2006) 393–405.

6. S. Smolentsev, N.B. Morley, M. Abdou, R. Munipalli, R. Moreau, C*urrent approaches to modeling MHD flows in the dual coolant lead lithium blanket*, Magnetohydrodynamics Vol. 42 (2006), No. 2-3, pp. 225–236.

7. L.V. Boccaccini, L. Giancarli, G. Janeschitz, S. Hermsmeyer, Y. Poitevin, A. Cardella, et al., *Materials and design of the European DEMO blankets*, J. Nucl. Mater. 329–333 (2004) 148–155.

8. Y. Poitevin, L.V. Boccaccini, A. Cardella, L. Giancarli, R. Meyder, E. Diegele, et al., *The European breeding blankets development and the test strategy in ITER*, Fusion Eng. Des. 75–79 (2005) 741–749.

9. S. Xu, N. Zhang and M. Ni, *Influence of Flow Channel Insert with Pressure Equalization Opening on MHD Flows in Liquid Metal Blanket*, To be appeared in Fusion Engineering and Design

10. E. Mas De Les Valls, L.A. Sedano, L. Batet, I. Ricapito, A. Aiello, O. Gastaldi and F. Gabriel, *Lead-lithium eutectic material database for nuclear fusion technology*, J. of Nuclear Materials 376 (2008) 353-357

11. G. R. Longhurst, *TMAP7 User Manual*, Idaho National Engineering and Environmental Laboratory Bechtel BWXT Idaho, LLC, 2004.

12. Takayuki Terai, Shin'ichi Nagai, Toshiaki Yoneoka and Yoichi Takahashi, *Mass transfer coefficient of tritium from molten lithium-lead alloy ($Li_{17}Pb_{83}$) to environmental gas under neutron irradiation*, Fusion Engineering and Design 17 (1991) 237-241.
13. Alexander PISAREV , Tetsuo TANABE , Takayuki TERAI , Gianluca BENAMATI & Mikhail MULLIN, *Modeling of In-Pile Experiments on Tritium Release from Molten Lithium-Lead*, Journal of Nuclear Science and Technology, 39:4, 377-381 (2002).
14. P. Fauvet and J. Sannier, *Hydrogen behavior in liquid LiPb alloy*, Journal of Nuclear Materials 155-157 (1988) 516 5l9
15. P. Ray, S. K. Bayen, B. K. Dutta, Calcutta, Indien and A. S. Gupta, Kharagpur, Indien, *Mass transfer with chemical reaction in a laminar falling film*, Wfirme and Stofffibertragung 22, 195-199 (1988).

Chapter 2

Physical Phenomena and Literature Review

Tritium transport analyses at blanket design levels provide important information for tritium control. Thus, this section is devoted to the review of:

1. The phenomena involved in tritium transport assessment in the DCLL blanket concept,
2. The main database needs for the assessment and the main sources for uncertainties,
3. The experimental support of the tritium transport in liquid metal blankets and,
4. The modeling of tritium transport in liquid metal blankets.

2.1 Tritium Transport Phenomena in the Liquid Metal Blanket Concepts

The individual physical processes that contribute to the behavior of tritium in liquid metal blankets can be summarized as:

1. Production of tritium within the liquid PbLi, primarily by Li(n,α)T reactions in the liquid lead-lithium (Pb-17Li):

$$n^1 + Li^6 = T^3 + He^4 \quad (1)$$

$$n^1 + Li^7 = T^3 + He^4 + n^1 \quad (2)$$

2. Migration of atomic tritium within the flowing PbLi according to its kinematic viscosity and its intrinsic diffusivity.
3. Tritium transfer across PbLi/helium-bubbles (if helium nano-bubbles exist in PbLi)
4. Adsorption, desorption and surface reaction of tritium at the PbLi/FCI interface.
5. Diffusion and trapping of tritium in the FCI.
6. Leakage through FCI cracks (if cracks exist in the FCI).
7. Adsorption, desorption and surface reaction of tritium at the LM/structure interface.
8. Interfacial phenomena between PbLi and the structure due to the formation of mass-resistive films of helium (if helium films exist between PbLi and the structure).
9. Diffusion of atomic tritium through the structure.
10. Dissolution-recombination and surface reaction at the structure/coolant interface and loss to the coolant stream.

Which of the above processes contributes the most to the tritium transport, permeation, and inventory within the lead-lithium breeder depends on the operating temperature range, the chemistry of the structure/liquid-phase, and the flow distribution.

More specifically, the variables that govern tritium transport may be summarized as follows:

- Material properties:

a. Tritium solubility

b. Tritium diffusivity

- Operating conditions:

a. MHD flow

b. Temperature

- Blanket design:

a. Geometric configurations of the blanket

b. The gap and the PES

2.1.1 Tritium Transport in MHD Flow

Tritium is bred together with He by $n(^{6}Li,^{3}{}_{1}H)^{4}{}_{2}He$ reaction in the PbLi flowing through channels. Once created as ions, tritons stop within a very short range (microns) and are transported in the breeding alloy according to the alloy kinematic viscosity and its intrinsic diffusivity. The ratio between both is called the Schmidt number, Sc. At 350~700 ℃, Sc ~ 200, i.e. the alloy velocity field is 200 times more effective at transporting tritium in solution than thermally-driven diffusivity. Then, in first instance a precise solution of hydrodynamic (MHD) equations providing reliable velocity field profiles in LM channels is essential for a reliable tritium assessment in the breeding blanket.

Current liquid metal blankets are complex MHD-sensitive designs involving complex phenomena [1]. In the recent past, several overviews of liquid metal MHD flows in fusion-relevant conditions were presented, focusing on the blanket issues common to all types of liquid metal blankets [14], such as the MHD pressure drop, flow distribution, electrical insulation, complex geometry flows, effects due to magnetic field non-uniformity, multi-channel effect, heat transfer, etc.

A few papers have overviewed specific issues associated with tritium transport with MHD flow. G. Sposito, et al. computed mixed MHD flow and tritium transport for a slender poloidal duct, representative of a DEMO HCLL blanket element, and observed that the spatial distribution of tritium concentration depended on the intensity and direction of the forced flow. Significant peak factors were obtained if the net flow rate was so low that re-circulation occurred [5]. F. Gabriel analyzed the 2D tritium permeation through the HCLL breeder unit cooling plates, and showed a developed concentration boundary layer acting as a mass transfer resistance which is equivalent to a PRF of 30 [6]. E. Mas de les Valls analyzed the flow near the gap region (close to the first wall) in the HCLL-TBM by simplified 2D C-shaped channels, and suggested that faster vortices appear in the gap region originate in high tritium concentration zones [3]. M.J. Pattison investigated the transport of tritium in the front unit of a DCLL US DEMO blanket duct numerically and showed that the

main losses arise from the presence of very slow moving fluid in the gaps between the FCI and the RAFS wall, while the tritium generated in the bulk flow inside the FCI remains there [7].

Currently, no model is available to solve the tritium transport problems under full MHD conditions. In most of the studies, the MHD effect was either ignored or considered in a relatively simple geometry.

2.1.2 Tritium Transfer across the Material Interface

The distribution and migration characteristics of tritium will be strongly affected by a number of physicochemical processes related to (1) solubility of tritium and tritium-containing species in the fluids and the structural materials and (2) transfer of tritium through interfaces. Although solution and diffusion are largely bulk phenomena, the observable permeation is often strongly dependent upon the properties and interactions at surfaces [8]. However, knowledge of the interface processes is much more limited. Only a few studies have been reported for in-situ and out-of-pile experiments [8-16] and agreed on phenomena (all chemical in origin) that are likely to have significant consequences in fusion equipment. One of these phenomena is the Langmuir isotherm (adsorption, desorption). A number of expressions have been deduced by different investigators to describe the adsorption of atomic and molecular species as a function of their concentration next to the adsorbing

substance. Langmuir was the first to develop a quantitative, no-empirical theory of surface adsorption processes [17]. This theory, based on molecular kinetic considerations, showed that the rates of adsorption and release of a species from a surface are strongly dependent upon the magnitude of the pressure of the species and the number of active sites available at the surface. Another phenomenon is the effect of surface impurities on adsorption and permeation of tritium. According to Langmuir theory, we can expect that the rate of any process occurring as a result of adsorption or release will also be dependent on the number of active sites available at the surface. In terms of the behavior of hydrogen isotopes in fusion devices, it is reasonable to assume that some of the impure species likely to be present together with the hydrogen (e.g. O, N, and C) either can permanently lodge on active sites making these sites unavailable to hydrogen or can compete with hydrogen for the active sites, thereby reducing the probability of occupation by hydrogen. A frequently observed consequence of this kind of passivation is the reduced permeability of metals with surface layers of chemically bound impurities. Experimental studies have shown that impurity layers on vanadium can reduce its hydrogen permeability by over three orders of magnitude [18]. The third important phenomenon is the effect due to isotopic dilution resulting from the presence of H and/or D at concentrations much larger than the tritium concentration. Chemical effects resulting from the appearance of one hydrogen isotope in the presence of

a large excess of either or both of the other two isotopes can have a significant impact on the migration of the diluted isotope [19]. Some of these surface effects could be important in determining the behavior of tritium in a fusion device. However, more reliable data are required to have a good database and to elucidate the mechanism.

2.1.3 He Bubble Effects on Tritium Transport Behavior

Breeding reaction by-products ($^{3}_{1}H$) and ($^{4}_{2}He$) are transported in the LM according to their respective state of solution. Helium production rates in breeder blankets are nearly mol-to-mol linked to the compulsory requirement of high T self-sufficiency of future deuterium–tritium (DT) fusion reactors. He concentration can modify heat/mass/electrical transfer interfacial exchange coefficients between the liquid metal breeder and the structural material. Thus, the study of the helium concentration profile in the blanket or any other fusion component becomes essential. The two transport values needed are the helium solubility (Henry's constant) and diffusion coefficient. The experimental data for Henry's constant in liquid metals are currently exotic and scarce. Measurements are not known of such magnitudes for PbLi eutectic. A first approximation of helium solubility in the eutectic was proposed in [20] based on values from the thermodynamic liquid hole model in liquid lithium and cohesion models.

Solubility of tritium atoms in PbLi is low but within the range of breeding rates and alloy residence times in segments, tritium concentrations are straightforward justified to keep well below sobresaturation limit. For helium atoms, the situation is much different. Solubility of helium in Pb-Li is so low that, at the ranges of the He-atoms breeding rates and alloy residence time in breeding material, the sobresaturation limit could be said to be surpassed naturally. When a solid solute surpasses the solubility limit in a liquid, it precipitates. If the solute is gaseous, its natural tendency (depending on external pressure) is to form bubbles. In LIBRETTO tests [21], bubble nucleation and interfacial nucleation between the liquid metal breeder and the structural material were observed. If these phenomena are confirmed and helium bubbles are finally formed, nucleating nano-bubbles could mean effective tritium sinks in liquid metal breeder channels. This would result in a net reduction of the tritium partial pressures in solution (and hence permeation fluxes) with some kind of additional 'natural' tritium extraction from the liquid metal channels. Therefore, depending on the bubble plume properties, in terms of bubble characteristics (size and stability) and then concentration, a plume of bubbles would impact tritium transport schemes in liquid metal channels. Until now, helium effects and their system design implications have not been considered in system designs. However, 2-phase dispersion models have been studied for quite a long time within the context of tritium recovery systems, i.e. bubble

columns. First efforts on determining the bubble diameter and behavior in helium-cooled lithium lead (HCLL) blankets have been advanced [21].

2.2 The Main Database and the Main Sources for Uncertainties

Material properties have potentially a determinant impact on tritium transport assessments (permeation rates, inventory build-up, extraction rates). These database include (1) the general materials and fluids thermophysical data, and (2) the tritium transport properties.

The PbLi thermophysical database for tritium transport assessments could be considered well-established. Main magnitudes are summarized in reference 22.The main sources of uncertainties for tritium transport in PbLi breeder blankets are coming from tritium transport properties: diffusion coefficient, solubility constant and recombination rate constant represent primary data with direct impact on tritium behavior in liquid metal blanket. Tritium solubility, defined as the function linking the concentration of dissolved tritium with its corresponding partial pressure at equilibrium over the liquid surface, is a fundamental design data need for all systems (magnetic or inertial confinement, hybrid systems, etc.) based on liquid breeders. The other main transport properties, the diffusion constant and the recombination rate constant, play a major role in the selection and optimization of tritium

extraction and coolant purification systems (in dual function blankets the two systems are acting on different fluids). However, to obtain precise and validated measurements of these properties is difficult, potentially full of parasitic effects and requiring a lot of database evaluation and collaboration.

Available databases on hydrogen solubility and transport properties are visualized in Figure 5, which shows considerable data scattering and discrepancies [23]. In the range of applicability (<500 C), Reiter data are verified by desorption experiments based on PVT measurements. However, among these data, high temperature data and low pressure regime data are still unreliable, and isotope effects among H-D-T, Li activities in PbLi, and impurity effects have not been clarified.

The measurements of the diffusion coefficient of hydrogen in the PbLi (Figure 6) show higher agreement and acceptable dispersion, with divergences caused by the experimental device, fitting models, surface effects, and control of convection [24].

These considerable uncertainties in the values for physical properties (e.g. solubility, diffusion coefficients) of materials make it necessary to examine how these would affect the results. Modeling implementation and a sensitivity analysis should be done in order to evaluate the impact of the different solubility and diffusivity values on the tritium permeation rate and to evaluate the urgency of further experiments to find reliable and agreed data.

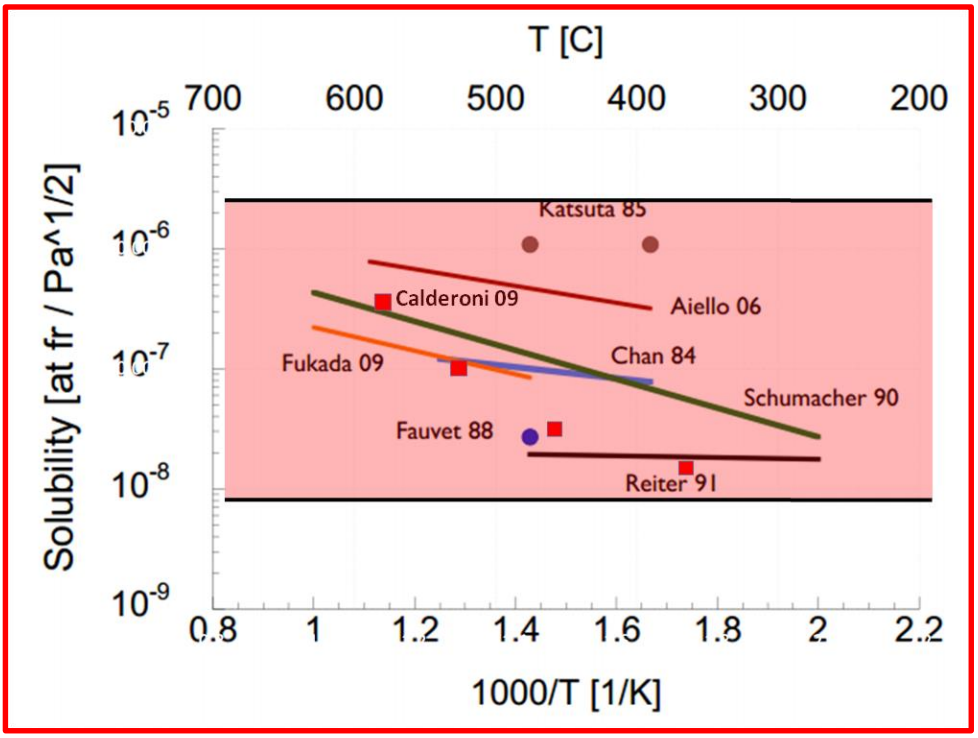

Figure 5. Different values of Sievert' solubility constant from different authors show considerable data scattering and discrepancies [23]

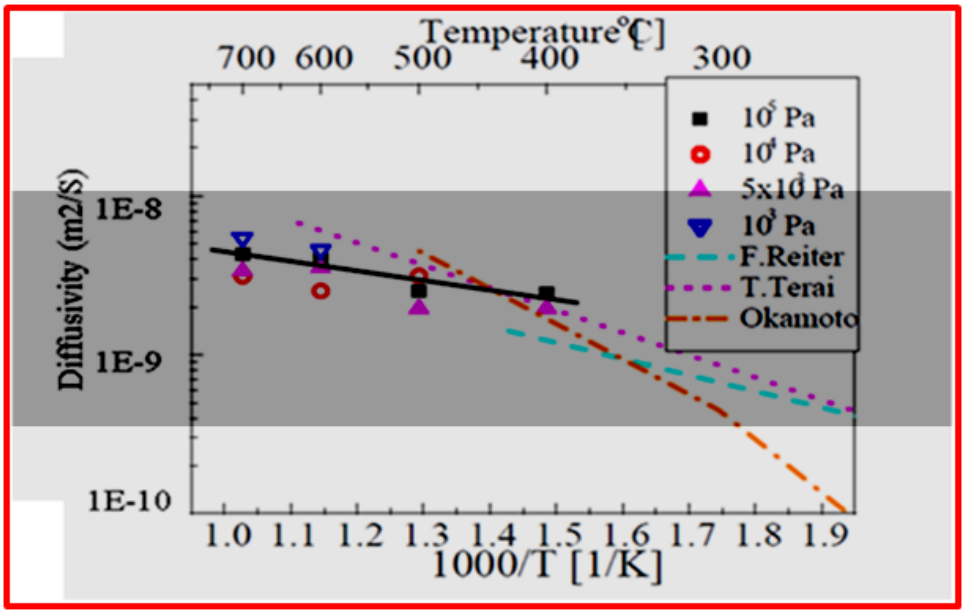

Figure 6. Comparison of the tritium diffusion coefficients obtained by different authors show higher agreement and acceptable dispersion [24]

2.3 Experimental Support of the Tritium Transport in Liquid Metal Blankets

The liquid lead-lithium breeder property database has been considerably extended in recent years, and a joint effort is currently underway in different countries to reduce the existing uncertainties and lack of experimental data. Indeed, a better experimental characterization of the properties of liquid breeders is strongly needed to ensure the best selection and the optimal operating conditions for liquid breeder blankets for experimental and commercial fusion reactors. The primary purpose of most experiments is to test tritium transport and permeation from a candidate liquid breeder material under conditions representing those expected in a fusion reactor blanket, and to provide tritium transport data from which models and computational analyses can be developed. Table 1 summarizes recent completed and on-going experiments done by various groups.

Table 1. Recent experiments related to tritium transport in LLB

Experiment	Group	Year	Description
H2 solubility experiments at INL, USA	INL, USA	08-09	Experimental determination of hydrogen isotopes transport properties in LLE
T2 experiments at INL, USA	INL, USA	10-11	
Forced convection liquid metal loop design at INL, USA	INL, USA	10-11	Current effort is mainly at program level and leveraged with activities related to advanced power plant concepts
PbLi Loop at UCLA, USA	UCLA, USA	09-11	PbLi technology experience, develop and test diagnostics for MHD, heat transfer and mass transfer
Libretto (Liquid Breeder Experiment with Tritium Transport Option) by NRG, Netherlands	NRG, Netherlands	09	To monitor online the in-pile tritium production and permeation through Eurofer in contact with lead lithium eutectic
Isotope effects on solubility and diffusivity of hydrogen isotopes in Li-Pb eutectic alloy at Japan	Kyushu University, Japan	09-10	Experimental clarification of T transfer and recovery in Li-15.8Pb-84.2 blanket

Tritium transport in PbLi breeder blankets is influenced by a fairly large number of factors such as material properties, temperature, and flow distribution. The purposes of the experiments are to determine the effects of these factors, to identify the most important transport mechanisms and finally to predict the performances of PbLi breeder blankets. In greater detail, the main objectives of these experiments can be delineated as follows:

- Database evaluation. Measure precise and validated tritium transport properties: diffusion coefficients, solubility constants, and recombination rate constants represent primary data with direct impact on tritium behavior in liquid metal blankets.
- Determine the effects of key operational factors upon tritium transport in liquid metal blankets. These factors include temperature, liquid metal flow rate, isotope effect, and impurities content. It is necessary to know how tritium transport is affected by operational factors so that understanding of tritium transport can be acquired.
- Measure tritium permeation through primary structure materials.
- Demonstrate PbLi thermal-fluid performance. The control of temperature and velocity profiles is regarded as a significant issue.

- In addition, transport data on other species which may provide some insights into transport of tritium will be obtained. Helium transport is potentially important for liquid metal blankets because it can cause bubbles, which may act as traps for tritium.

2.4 Modeling of Tritium Transport in Liquid Metal Blankets

Modeling plays a key role in observing the overall tritium transport behavior for fusion blanket design. A large number of variables that are likely to affect tritium behavior and the multi-physics processes have to be considered simultaneously, therefore it is not surprising that a comprehensive model for tritium transport has not yet been fully developed. Several codes, such as TMAP [25], BelFoam [21], and CATRIS [7] based on diffusive models, have been developed during the last few years.

The Tritium Migration Analysis Program (TMAP) was developed by the Fusion Safety Program at INEL as a safety analysis code to analyze tritium retention and loss in fusion reactor structures. TMAP has also been used to analyze tritium permeation losses from the US Dual Coolant Lead Lithium (DCLL) ITER Test Blanket Module (TBM), with the use of mass transport correlations to estimate tritium transport in flowing PbLi. TMAP incorporates one-dimensional thermal- and mass-diffusive transport and trapping calculations through structures and zero dimensional fluid transport between enclosures and across the interface

between enclosures and structures. Currently, TMAP is the reference tool for the simulation of the permeation phenomenon in ITER. Unfortunately it has some important disadvantages: (1) TMAP is only able to simulate permeation in 1D geometries; (2) it is difficult to estimate tritium transport in flowing LM; (3) it cannot be used to evaluate the impact of MHD; (4) it cannot include the temperature profile, which affects the transport properties. These limitations make it not completely adequate for the complex geometries present in the breeder blanket concepts.

BelFoam is another tritium transport solver developed by the Spanish Breeding Blanket Program. This code tries to add tritium transfer and helium transfer modeling capabilities to the existing CFD code OpenFOAM. These codes integrate a tritium transport solver with a CFD solver and try to provide a predictive tritium transport modeling for HCLL blankets [21]. However, BelFoam has limited capability to include multi-physics processes and to handle geometric complexity.

CATRIS is another mass transfer code developed by UCLA and has been used to simulate tritium transport in a poloidal duct with FCI, considering the MHD effect [7]. However, its deficiencies are: (1) it does not include the pressure equalization slot (PES) and back channel in the geometry, (2) it uses a fully developed velocity profile and (3) its tritium transport properties are constant, that is, it does not account for the temperature effect.

2.5 Improvements for This Work

A multi-physics predictive capability for tritium transport in liquid metal blankets has been developed in this thesis work. The developed model includes multiple tritium transport processes with appropriate boundary conditions for different material regions, such as diffusion and convection through the PbLi, transfer across the liquid/solid interface, diffusion of atomic tritium through the structure, and dissolution-recombination at the solid/gas interface.

The code differs and improves upon earlier works in several ways and key areas:

- Solving the problem in 3D multiple regions
- Including complex blanket geometry (e.g. PES, GAP) into analysis
- Coupling multiple tritium transfer processes
- Accounting for LM MHD velocity and temperature profiles
- Accounting for the tritium generation rate profile

Several key issues relevant to tritium transport and permeation in liquid metal blanket are addressed in conjunction with the analysis, such as:

- Quantifying the difference in tritium inventory and permeation rate between DCLL and HCLL blanket concepts.
- Identifying the PES effect on tritium transport and permeation in the DCLL concept.

- Evaluating the MHD effect and buoyancy effect as applied to tritium transport, inventory, and permeation.
- Identifying the range of permeation rate change on the basis of uncertainties of material properties (e.g. solubility and diffusivity).

2.6 References

1. N. Morley, S. Smolentsev, L. Barleon, I. Kirillov, M. Takahashi, *Liquid magnetohydrodynamics - recent progress and future directions for fusion*, Fusion Eng. Des. 51–52 (2000) 701–713.
2. N. Morley, S. Malang, I. Kirillov, *Thermofluid magnetohydrodynamic issues for liquid breeders*, Fusion Sci. Technol. 47 (2005) 488–501.
3. E. Mas de les Valls, *Flow Analysis in the HCLL-TBM ITER Channels including MHD and Heat Transfer,* V EU Conference on Computational Fluid Dynamics, 2010
4. I.R. Kirillov, C.B. Reed, L. Barleon, K. Miyazaki, *Present understanding of MHD and heat transfer phenomena for liquid metal blankets*, Fusion Eng. Des. 27(1995) 553–569.
5. G. Sposito, et al., *Mixed MHD convection and tritium transport in fusion-relevant configurations*, Fusion Engineering and Design, 75-79 (2005) 697-702.
6. F. Gabriel, *A 2D finite element modeling of tritium permeation for the HCLL DEMO blanket module*, Fusion Engineering and Design, 82 (2007) 2204-2211.
7. M.J. PATTISON, S. SMOLENTSEV, R. MUNIPALLI, M. A. ABDOU, *Tritium Transport in Poloidal Flows of a DCLL Blanket*, Fusion Sci. Technol., 60, 809 (2011).
8. G. Pierini et al. Nucl. Eng. Des. Fusion 1 (1984) 159.
9. A. Viola, P.L. Lolli-Ceroni and G. Pierini, Fusion Eng. Des. 8 (1989) 365.

10. G. Saibene, R. Sartori and F. Reiter, Fusion Technol. 14(1988) 808.

11. A.M. Polearo et aI., 1. Nucl. Mater. 119 (1983) 291.

12. H. Feuerstein et al., J. Nucl. Mater. 179-181 (1991) 882.

13. T. Terai et al., J. Nucl. Mater. 179-181 (1991) 871.

14. T. Terai et aI., Fusion Eng. Des. 17 (1991) 237.

15. T. Terai et al., Fusion Technol. 21 (1992) 781.

16. S. Tanaka and M. Yarnawaki, *Hydrogen transports through gas/liquid Li 17PbR3 interface and metal membrane contacting the alloy*, Journal of Nuclear Materials 191-194 (1992) 209-213.

17. J. Langmuir, J. Amer. Chem. Soc. 38 (1916) 2221; 39 (1917) 1848; 40 (1918) 1361.

18. R.R. Heinrich, C.E. Johnson and C.E. Crouthamel, J. Electrochem. Soc. 112 (1965) 1071.

19. R.G. Hickman, *Some problems Associated with Tritium in Fusion Reactors, Proc. Intern. Symp*. Technology of Controlled Thermonuclear Fusion Experiments and the Engineering Aspects of Fusion Reactors, 20-22 November 1972, Austin Texas, USAEC Report Conf-721111 (1973)

20. L.A. Sedano, CIEMAT Internal Report, 2007.

21. L.A. Sedano et al., IEA Meeting on Liquid Breeder for Fusion Application ANL, Chicago, US, April 1999.

22. H. Küchle., *Materials Database for Fusion Reactors Materials* (1987).

23. P. Calderoni, *Determination of hydrogen isotopes solubility in the eutectic PbLi alloy (LLE),*VLT November 2009 TeleCon.

24. S. FUKADA, *Isotope effects on solubility and diffusivity of hydrogen isotopes in PbLi eutectic alloy*, International Workshop on Liquid Metal Breeder Blankets September 23-24, 2010, CIEMAT, Madrid (Spain)

25. G. R. Longhurst, *TMAP7 User Manual*, Idaho National Engineering and Environmental Laboratory Bechtel BWXT Idaho, LLC, 2004

Chapter 3

Mathematical Formulation and Numerical Methodology

A fundamental objective of tritium transport modeling in LM blankets for fusion reactor applications is the development of a comprehensive model with the capability to include several transport mechanisms of the proposed phenomenological multiple processes by which tritium, once generated in the liquid breeder, migrates with the flowing liquid and permeates through the structure to the helium coolant. The aim of the theoretical model is to predict with sufficient accuracy the tritium transport, the concentration distribution, and the overall permeation and inventory. The first step consists of the identification of the sequence of relevant physical processes and the definition of the set of differential equations which govern the evolution of the phenomena under investigation. For tritium transport within a liquid metal blanket, the governing equations which describe the behavior of the tritium are essentially convection and diffusion equations in liquid, solid and gas phases, and rate equations or chemical equilibrium equations that govern the transfer at interfaces between different phases. To make the problem amenable to analysis, a number of simplifying assumptions, a set of initial and boundary conditions, and an efficient method of solution are

needed. Analytic solutions of problems are usually restricted to relatively simple, idealized geometries and boundary conditions, so that the corresponding results may not be fully applicable in realistic situations. In particular, tritium transport in PbLi blankets is too complex for analytic treatment, and a numerical solution of the governing partial differential equations is required.

3.1 Tritium Transport Model and Formulation

3.1.1 General Passive Scalar Transport Equation for the Concentration of Species

A general, passive, scalar transport equation for the concentration of species s, c_s (mol/m^3), can be expressed as [2]:

$$\partial c_s(\mathbf{x},t)/\partial t = -\nabla\cdot\mathbf{J}_s(\mathbf{x},t) + \dot{S}_s(\mathbf{x},t) - \sum_k(\partial c_s^{t_k}/\partial t + \nu_s c_s^{t_k}) - \nu_s c_s + \sum_m \nu_m^s (c_m + \sum_k c_m^{t_k}) \quad (3)$$

Where

c_s = mobile concentration of species "s" atoms (mol/m^3)
$\mathbf{J}_s$ = flux of species "s" atoms ($mol/m^2 s$)
$\dot{S}_s$ = local explicit source rate per unit volume of species "s" atoms ($mol/m^3 s$)
$c_s^{t_k}$ = concentration of atoms of species "s" in the "kth" trap (mol/m^3)
ν_s = radioactive decay frequency of species "s" atoms
ν_m^s = radioactive decay frequency of species "m" atoms that decay to species "s"

The flux of dissolved atoms $\mathbf{J}_s(x,y,z,t)$ is given by

$$\mathbf{J}_s = -D(T)\nabla c_s - (D(T)Q_s^* c_s / kT^2)\nabla T + c_s \mathbf{u} \tag{4}$$

Where D(T) is the diffusivity of species "s" in the material, Q_s* is the heat of transport or Soret coefficient, and T is the local temperature. The first term of the right hand side represents the flux of species "s" due to a gradient in the concentration of that species. The second term represents the flux of species "s" due to a temperature gradient and the third term is resulting from the bulk flow.

The inventory of solute atoms (or molecules) can be affected by trapping sites where the energy required for an atom to move to another nearby site is greater than that required for ordinary diffusion. Trapping sites can result from impurities and structural irregularities arising from cold work, precipitation of alternate phases including gas bubbles, or neutron displacement damage. Considering a solute particle (atom or molecule) concentration of species "s", c_s, the governing equations are written with respect to the "k^{th}" trap as

$$\frac{\partial c_s^{t_k}}{\partial t} = \alpha_{t_s} c_{t_k}^e \frac{1}{N} c_s - (\alpha_{r_k} + \nu_s) c_s^{t_k} \tag{5}$$

$$c_{t_k}^e = c_{t_k}^0 - \sum_s c_s^{t_k} \tag{6}$$

$$\alpha_{t_s} = \frac{D}{\lambda^2} \tag{7}$$

$$\alpha_{r_k} = \nu_0 \exp(-\frac{E_{t_k}}{kT}) \tag{8}$$

Here, in addition to previously defined quantities,

$c_s^{t_k}$ = concentration of atoms of species "s" in the "kth" trap

$c_{t_k}^{e}$ = concentration of empty traps of type "k"

$c_{t_k}^{0}$ = total concentration of traps of type "k" both filled and unfilled

E_{t_k} = trapping energy of the "kth" trap

α_{t_s} = trapping rate coefficient of species "s" atoms

α_{r_k} = release rate coefficient for trapped atoms of any species from trap "k"

For the term of tritium radioactive decay (rate of 5.5% per year), since generated tritium atoms are transferred to the extraction system, they stay in the blanket only for a short time. Thus, there is negligible radioactive decay of tritium in PbLi. The flux associated with temperature gradients is assumed to be much smaller compared to that due to concentration gradients and is therefore omitted. Traps result from irregularities in the structure, are not relevant to the liquid metal, and therefore are not included. Traps resulting from helium bubbles will be discussed in Chapter 5 and are therefore not included in this chapter.

3.1.2 Multi-Region Domains and the Selection of the Relevant Tritium Transport Mechanisms

Tritium transport through a liquid metal blanket and the relationships between materials are not easily delineated because of multiple materials and multiple regions. Figure 7 illuminates the model domains for a DCLL channel unit, which includes the flowing

domains: (1) the liquid metal (LM) domain, (2) the flow channel insert (FCI) domain, (3) the ferritic steel structure (FS) domain, and (4) the helium coolant (HC) domain. A system of differential equations governing the space and time evolution of tritium in each domain and an adequate set of boundary conditions coupling the individual transfer mechanisms in each region are hereafter outlined.

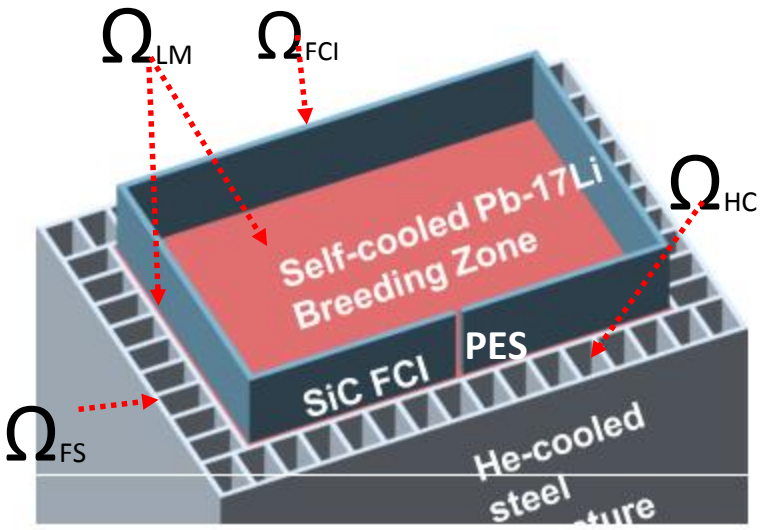

(1) liquid metal (LM) domain

(2) flow channel insert (FCI) domain

(3) ferritic steel structure (FS) domain

(4) helium coolant (HC) domain

Figure 7. Schematic diagram of the multiple domains of tritium transport in a DCLL breeder blanket unit

According to a typical DCLL blanket concept, the relevant tritium transport mechanisms presented in Figure 8 include the following multiple tritium transport processes:

- Tritium generation in the LM core and the gaps
- Tritium convection and diffusion in the flowing LM
- Tritium movement through the LM/FCI interface
- Diffusion of tritium in the FCI
- Tritium migration through the PES
- Tritium movement through the LM/ferritic steel (FS) structure interface
- Diffusion of tritium through the FS structure
- Tritium desorption and recombination at the FS/He coolant interface
- Tritium transfer and trapping into helium bubbles

In any given situation, the process that contributes the most to the tritium transport within the LM blanket depends on the specific material properties (e.g. tritium solubility and diffusivity), operating temperature range, and the flow distribution under consideration.

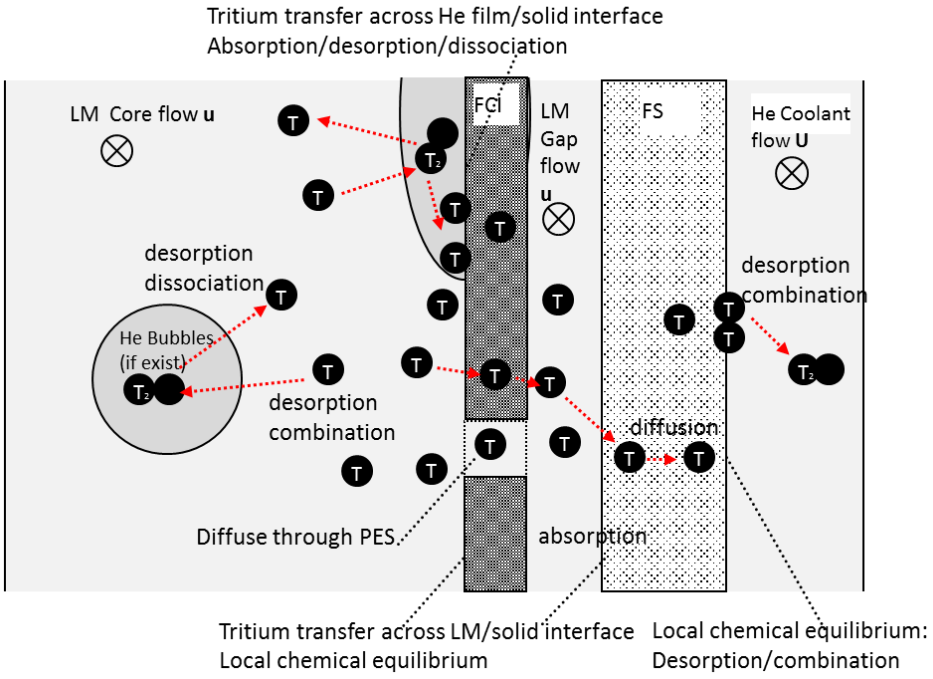

Figure 8. The schematic of the tritium transport model shows the sources and transportation modes of tritium in a DCLL breeder blanket unit

3.1.3 Governing Equations of Tritium Transport in the Individual Domains

Let's define c_{T_LM}, c_{T_FS}, c_{T_FCI} and c_{T2_HC} as the tritium concentrations in the LM, the FS structure, the FCI, and the helium coolant domains, respectively. In doing so, the following mass balance equations can be formulated in these domains.

- **Tritium convention and diffusion in the flowing liquid PbLi**

For tritium transport modeling in the liquid PbLi, we assume tritium does not affect liquid metal properties nor flow behavior, so that tritium can be represented as a passive scalar. Hydrodynamics are completely independent from tritium transport, as are the velocity boundary conditions. Hence, tritium is transported by diffusion and convection in the flowing liquid metal. We can formulate the following mass transport equation:

$$\frac{\partial c_{T\_LM}}{\partial t} = \nabla \cdot (D_{LM} \nabla c_{T\_LM}) - \mathbf{u}_{LM} \nabla c_{T\_LM} + \dot{S}_{T\_LM} \tag{9}$$

Where:

c_{T_LM} = tritium concentration within the liquid metal, $\left(\frac{mol}{m^3}\right)$;

D_{LM} = tritium diffusivity in the liquid metal as a function of temperature T, $\left(\frac{m^2}{s}\right)$;

$\mathbf{u}_{LM}$ = flowing velocity of the liquid metal, $\left(\frac{m}{s}\right)$;

$\dot{S}_{T\_LM}$ = volumetric tritium generation rate in the liquid metal, $\left(\frac{mol}{m^3 s}\right)$;

The diffusivity in liquid metal is given by:

$$D_{LM}(T) = D_{LM0} \cdot \exp(-\frac{E_{LM}(T)}{RT}) \tag{10}$$

Where:

D_{LM0} = pre-exponential factor for tritium diffusion in liquid metal, ($\frac{m^2}{s}$);

$E_{LM}(T)$ = tritium diffusion activation energy, ($\frac{J}{mol}$);

Calculating the tritium production rate source term inside the LM is very complicated. Fortunately, these values can be taken from neutronics codes or experiment results [7, 8]. The radial distributions of the tritium production rates for the DCLL-TBM and HCLL-TBM are reproduced in Figure 9 and Figure 10 and have been fitted by exponential decay:

For DCLL:

$$\begin{aligned}\dot{S}_{T\_DCLL} = 2.055\times10^{-6} + 5.702\times10^{-6}\times\exp(-\frac{x}{0.0061}) \\ + 2.247\times10^{-6}\times\exp(-\frac{x}{0.08276})\end{aligned} \tag{11}$$

For HCLL:

$$\begin{aligned}\dot{S}_{T\_HCLL} = 3.482\times10^{-7} + 1.898\times10^{-6}\times\exp(-\frac{x}{0.0084}) \\ + 1.625\times10^{-6}\times\exp(-\frac{x}{0.13})\end{aligned} \tag{12}$$

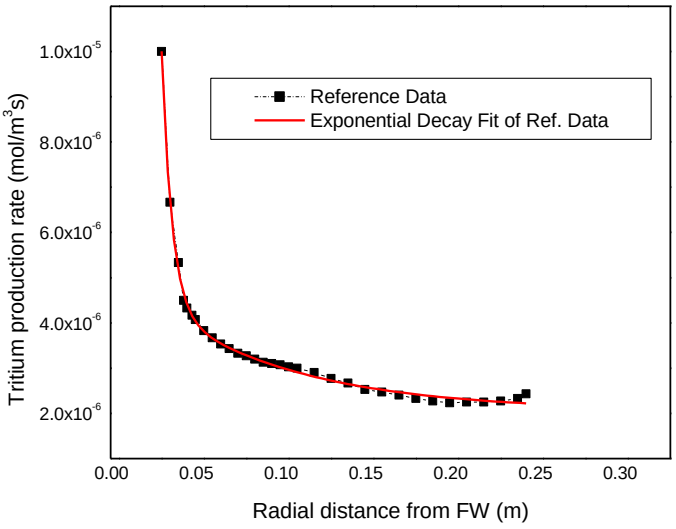

Figure 9. Radial variation of tritium production rate in PbLi (DCLL).

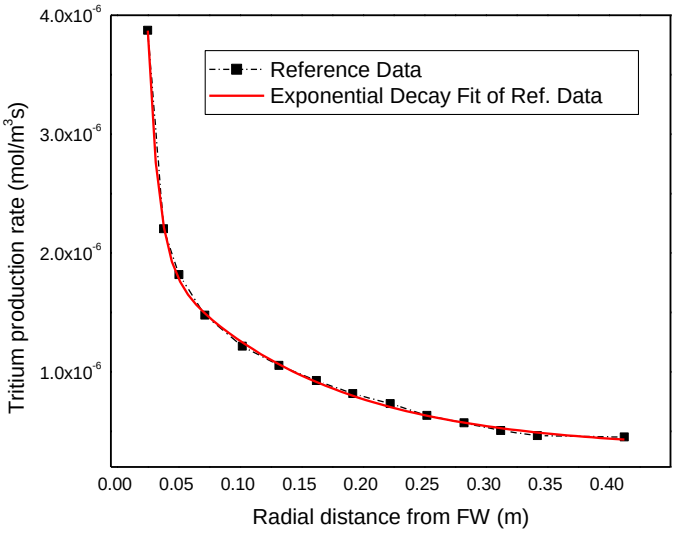

Figure 10. Radial profile of the tritium production in the PbLi (HCLL).

To obtain the convective part of the flux in the PbLi region, the equations for the steady state, laminar, incompressible, viscous, MHD flow are given by [4]:

$$\nabla \cdot \mathbf{u} = 0 \tag{13}$$

$$\frac{\partial \rho \mathbf{u}}{\partial t} + \mathbf{u}\nabla \rho \mathbf{u} = \mu \nabla^2 \mathbf{u} - \nabla p + \mathbf{j} \times \mathbf{B} \tag{14}$$

$$\nabla \cdot \mathbf{j} = 0 \tag{15}$$

$$\mathbf{j} = \sigma(-\nabla \phi + \mathbf{u} \times \mathbf{B}) \tag{16}$$

By combining equations (15) and (16), a Poisson equation for the electric potential is obtained:

$$\nabla \cdot (\sigma \nabla \phi) = \nabla \cdot (\sigma \mathbf{u} \times \mathbf{B}) \tag{17}$$

Where the variables B, j, ϕ, ρ, σ and μ denote the magnetic field, current density, electric potential, density, electric conductivity, and viscosity, respectively.

- **Diffusion of tritium through the FS structure**

After generating and migrating in the liquid metal, tritium reaches the LM/FS structure interface where it may be adsorbed into the solid structure. The adsorbed tritium is assumed

to migrate from the LM/FS interface to the FS/coolant interface by Fickian diffusion. The diffusion equation for the tritium concentration within the FS structure can be written as:

$$\frac{\partial c_{T\_FS}}{\partial t} = \nabla \cdot (D_{FS} \nabla c_{T\_FS} + (D_{FS} \frac{Q^*_{T\_FS} c_{T\_FS}}{kT^2}) \nabla T) \tag{18}$$

Where:

c_{T_FS} = tritium concentration within the FS structure, ($\frac{mol}{m^3}$);

D_{FS} = tritium diffusivity in the FS structure as a function of temperature T, ($\frac{m^2}{s}$);

$Q^*_{T\_FS}$ = the heat of transport or Soret coefficient, ($\frac{1}{K}$);

The diffusivity in FS structure is given by:

$$D_{FS}(T) = D_{FS0} \cdot \exp(-\frac{E_{FS}(T)}{RT}) \tag{19}$$

Where:

D_{FS0} = pre-exponential factor for tritium diffusion in FS structure, ($\frac{m^2}{s}$);

$E_{FS}(T)$ = tritium diffusion activation energy, ($\frac{J}{mol}$);

- **Diffusion of tritium through the FCI**

Similarly, after generating and migrating in the liquid metal, tritium reaches the LM/FCI interface where it may adsorbed into the FCI. The adsorbed tritium is assumed to migrate as atoms through FCI by Fickian diffusion. The diffusion equation for the tritium concentration within the FCI can be written as:

$$\frac{\partial c_{T\_FCI}}{\partial t} = \nabla \cdot (D_{FCI} \nabla c_{T\_FCI} + (D_{FCI} \frac{Q^*_{T\_FCI} c_{T\_FCI}}{kT^2}) \nabla T) \quad (20)$$

Where:

c_{T_FCI} = tritium concentration within the FCI, ($\frac{mol}{m^3}$);

D_{FCI} = tritium diffusivity in the FCI as a function of temperature T, ($\frac{m^2}{s}$);

$Q^*_{T\_FCI}$ = the heat of transport or Soret coefficient, ($\frac{1}{K}$);

The diffusivity of tritium in FCI material is given by:

$$D_{FCI}(T) = D_{FCI0} \cdot \exp(-\frac{E_{FCI}(T)}{RT}) \quad (21)$$

Where:

D_{FCI0} = pre-exponential factor for tritium diffusion in FCI, ($\frac{m^2}{s}$);

$E_{FCI}(T)$ = tritium diffusion activation energy, ($\frac{J}{mol}$);

- **Tritium transport in helium coolant**

In the channels of HAD-coated helium cooling system (HC), the mass transfer equation is defined as:

$$\frac{\partial c_{T2\_HC}}{\partial t} + \mathbf{U}_{HC} \nabla c_{T2\_HC} = \nabla \cdot (D_{HC}(T) \nabla c_{T2\_HC}) \quad (22)$$

Where:

c_{T2_HC} = tritium gas concentration ($\frac{mol}{m^3}$) within the helium coolant;

D_{HC} = tritium gas diffusion coefficient ($\frac{m^2}{s}$) in the helium coolant as a function of the temperature T;

$\mathbf{U}_{HC}$ = velocities ($\frac{m}{s}$) in the He coolant.

The diffusivity is given by:

$$D_{HC}(T) = D_{HC0} \cdot \exp(-E_{HC}(T)/RT) \tag{23}$$

Where:

D_{HC0} = the pre-exponential factor for tritium diffusion in helium coolant (m^2/s);

E_{HC} = tritium diffusion activation energy ($\frac{J}{mol}$);

3.1.4 Coupling through Material Interfaces

The distribution and migration characteristics of tritium will be strongly affected by a number of physicochemical processes related to:(1) solubility of tritium and tritium-containing species in the fluids and the structural materials, and (2) transfer of tritium through material interfaces. Although solution and diffusion are largely bulk phenomena, permeation is often strongly dependent upon the properties and interactions at interfaces such as the PbLi/FS, PbLi/FCI, and FS/HC interfaces. To supplement the transport equations in each domain, tritium transfer through these interfaces have to be modeled as a set of boundary conditions to complete the formulation of the problem.

Figure 11 shows the relevant notation used to define an appropriate set of boundary conditions.

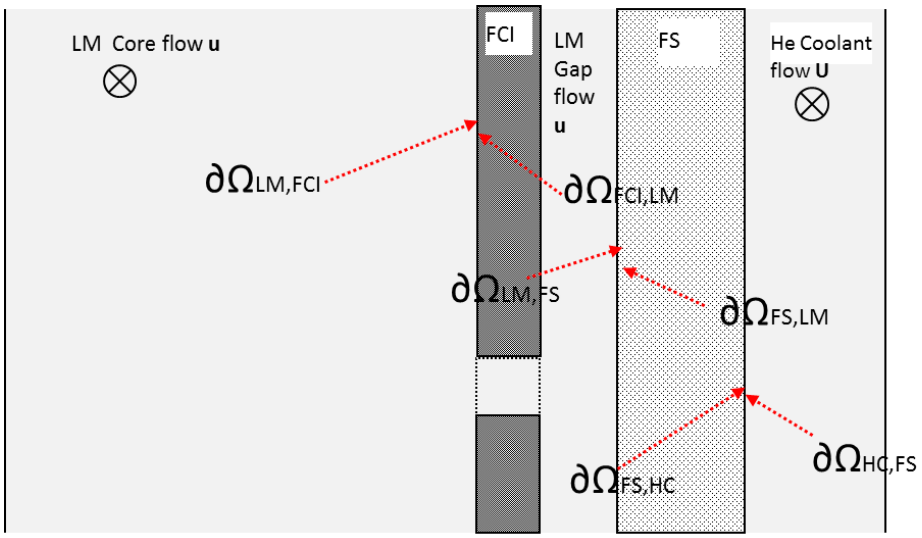

Figure 11. Boundaries and boundary labels for the modeled system.

- **Coupling at the LM/FS interface**

At the LM/FS interface, we apply Sievert's law and impose continuity of partial pressures, leading to the concentration discontinuities at interfaces.

$$\frac{c_{T\_FS}\big|_{\partial\Omega_{FS,LM}}}{c_{T\_LM}\big|_{\partial\Omega_{LM,FS}}} = \frac{K_{s\_FS}}{K_{s\_LM}} \tag{24}$$

Where

$c_{T\_FS}\big|_{\partial\Omega_{FS,LM}}$ = tritium concentration at boundary $\partial\Omega_{FS,LM}$

$c_{T\_LM}\big|_{\partial\Omega_{LM,FS}}$ = tritium concentration at boundary $\partial\Omega_{LM,FS}$

K_{S_LM} = the solubility of tritium in LM ($\frac{\text{mol}}{\text{m}^3 Pa^{0.5}}$)

K_{S_FS} = the solubility of tritium in FS ($\frac{\text{mol}}{\text{m}^3 Pa^{0.5}}$)

In addition to the chemical potential balance condition, we need to match the flux condition at the interface to ensure the flux continuity condition expressed as:

$$(-D_{LM}\nabla c_{T\_LM} + c_{T\_LM}\mathbf{u}_{LM})\cdot\mathbf{n}\big|_{\partial\Omega_{LM,FS}} = -(-D_{FS}\nabla c_{T\_FS})\cdot\mathbf{n}\big|_{\partial\Omega_{FS,LM}} \quad (25)$$

Here **n** is the normal unit vector to the respective boundary.

- **Coupling at the LM/FCI interface**

As for the LM/FS interface, the boundary conditions at the LM/FCI interface can be expressed as the species flux condition and the chemical potential balance condition.

The continuous flux condition can be expressed as:

$$(-D_{LM}\nabla c_{T\_LM} + c_{T\_LM}\mathbf{u}_{LM})\cdot\mathbf{n}\big|_{\partial\Omega_{LM,FCI}} = -(-D_{FCI}\nabla c_{T\_FCI})\cdot\mathbf{n}\big|_{\partial\Omega_{FCI,LM}} \quad (26)$$

The chemical potential balance condition by applying Sievert's law at the interface and imposing continuity of partial pressures can be expressed as:

$$\frac{c_{T\_FCI}\big|_{\partial\Omega_{FCI,LM}}}{c_{T\_LM}\big|_{\partial\Omega_{LM,FCI}}} = \frac{K_{s\_FCI}}{K_{s\_LM}} \quad (27)$$

Where

$c_{T\_FCI}\big|_{\partial\Omega_{FCI,LM}}$ = tritium concentration at boundary $\partial\Omega_{FCI,LM}$

$c_{T\_LM}\big|_{\partial\Omega_{LM,FCI}}$ = tritium concentration at boundary $\partial\Omega_{LM,FCI}$

K_{S_LM} = the solubility of tritium in LM ($\frac{\text{mol}}{\text{m}^3 Pa^{0.5}}$)

K_{S_FCI} = the solubility of tritium in FCI ($\frac{\text{mol}}{\text{m}^3 Pa^{0.5}}$)

- **Coupling at the FS/HC interface**

Since the FS/HC interface is a typical solid-gas interface, the tritium will undergo further dissociation and recombination once it is attached to the surface. This process can be expressed as

$$2T* \leftrightarrow T_2 + 2* \tag{28}$$

If the process of tritium dissociation and recombination governs, the net flow of tritium atoms through the surface is given by

$$J_{T_2} = K_{d_{T2}} P_{T2\_HC} - K_{r_{T_2}} c_{T\_FS}^2 \quad \text{at } \partial\Omega_{\text{HC,FS}} \tag{29}$$

$$J_T = 2J_{T_2} \quad \text{at } \partial\Omega_{\text{FS,HC}} \tag{30}$$

Where

P_{T2_HC} = molecular tritium partial pressure above the surface in HC, (Pa);

$K_{d_{T2}} = k_{d0} \cdot \exp(-E_d / RT)$ = the rate constant of tritium dissociation;

$K_{r_{T2}} = k_{r0} \cdot \exp(-E_r / RT)$ = the rate constant of tritium recombination;

Where

E_d = activation energy for dissociation, (J/mol);

k_{d0} = pre-exponential factor for dissociation, (m/s);

E_r = activation energy for recombination, (J/mol);

k_{r0} = pre-exponential factor for recombination, (m/s).

Under the typical liquid metal blanket configuration, helium coolant is flowing at a high mass flow rate, meaning that the tritium partial pressure in the helium coolant is low enough that the term of tritium dissociation from helium coolant back into FS structure is much smaller than the term of tritium recombination from FS structure into helium coolant. The boundary condition of tritium flux at the FS/HC interface can be written as:

$$(-D_{HC}\nabla c_{T_2\_HC} + c_{T_2\_HC}\mathbf{U}_{HC})\cdot\mathbf{n}\Big|_{\partial\Omega_{HC,FS}} = K_r c_{T\_FS}^2 \tag{31}$$

$$(-D_{FS}\nabla c_{T\_FS})\cdot\mathbf{n}\Big|_{\partial\Omega_{FS,HC}} = -2K_r c_{T\_FS}^2 \tag{32}$$

If the tritium movement by dissociation and recombination proceeds at a fast enough rate, such that there is effective equilibrium between gaseous and solid phases of the solute, Sievert's law applies:

$$c_{T\_FS} = K_{S\_FS}\sqrt{P_{T2\_HC}} \tag{33}$$

- **Boundary condition at the inlet of the PbLi domain**

At the inlet to the PbLi domain, we apply a concentration condition as:

$$c_{T\_LM} = c_{T\_LM,0} \tag{34}$$

- **Boundary condition at the outlet of the PbLi domain**

At the PbLi outlet, we assume that the convective contribution to the mass transport is much larger than the diffusive contribution. Thus the boundary condition of tritium flux can be written as:

$$(-D_{LM}\nabla c_{T\_LM} + c_{T\_LM}\mathbf{u}_{LM})\cdot\mathbf{n} = c_{T\_LM}\mathbf{u}_{LM}\cdot\mathbf{n} \tag{35}$$

3.2 Numerical Methodology

There is no single code that can calculate tritium transport in a PbLi blanket accurately. This is mainly because tritium transport is affected by the PbLi velocity profile and multiple tritium transport processes. First, to accurately quantify tritium behavior in a PbLi blanket, one needs to be able to predict the PbLi MHD velocity profile. Tritium is bred together with He by n(^{6}Li,$^{3}_{1}$H)$^{4}_{2}$He reactions in the PbLi flowing through channels. Once created as ions, tritium is transported in the breeding alloy according to the alloy kinematic viscosity and its

intrinsic diffusivity. The ratio between both is called the Schmidt number, Sc. At 350~700 ℃, Sc ~ 200, i.e. the alloy velocity field is 200 times more effective at transporting tritium in solution than thermally-driven diffusivity. Then, in first instance a precise solution of hydrodynamic (MHD) equations providing reliable velocity field profiles in LM channels are essential for a reliable tritium assessment in breeding blanket. Current liquid metal blankets are complex MHD-sensitive designs involving complex phenomena. Second, the code needs to be able to solve multiple tritium transport processes simultaneously, including diffusion and convection through the flowing PbLi under MHD conditions, diffusion of atomic tritium through the structure, and the coupling through the material interfaces, such as dissolution-recombination at the FS/coolant interface and transfer across the PbLi/FS interface. Currently, no single code is capable of solving the tritium transport problems in its full MHD conditions. In most of the studies, the MHD effect was either ignored or considered in a relatively simple geometry.

To solve the problem, the strategy taken here is to integrate different solvers for different phenomena, with a utility developed for passing data from one solver to the other solver, benefiting from solving the MHD velocity and temperature profiles and handling the blankets geometry complexity. Specifically, this approach includes three parts: (1) the

thermal/fluid and MHD solver, (2) the mass transfer solver, and (3) the utility for data mapping from MHD solver to mass transfer solver.

3.2.1 MHD Solver

The first stage is to compute the flow field. In the blanket, there is a very strong magnetic field, and the flow is dominated by the MHD effects. Two MHD solvers, HiMAG [5] and scSTREAM [3], were therefore adopted for this task. HiMAG, developed by HyPerComp Inc., in collaboration with the Fusion Science and Technology group at the University of California, Los Angeles, is a time-accurate magneto-hydrodynamics (MHD) solver for three-dimensional multiphase flows on structured or unstructured meshes. In the present form of HiMAG, the following capabilities are available: (1) three-dimensional incompressible flow solver (second-order accurate in space and time); (2) arbitrary mesh structure (structured/unstructured/hybrid); (3) parallel code environment; (4) computation of electromagnetic fields using the electric potential; (5) point implicit scheme, solved in an iterative manner; (6) multiple strategies to account for mesh skewness (non-orthogonality); and (7) modular addition of source terms. This solver has been validated using steady and unsteady canonical problems based on comparable analytical and numerical data. By use of appropriate meshes it has been possible to run cases at fairly large Hartmann numbers [5].

scSTREAM, a commercial thermal/fluid code developed by Software Cradle Co. Ltd., is able to compute three-dimensional MHD flows. It uses a structured mesh to provide extraordinary performance in both meshing and computation speed. The finite volume method is used for discretization which is common for fluid/thermal analysis. scSTREAM can solve a one million mesh model using less than 300 MB of RAM. Various useful functions, such as a VB interface and a user function with tabular input, are provided for customer user interfaces. In the current version of scSTREAM, the following features are available:

- CAD import, scSTREAM can import 3D CAD (e.g. Palasolid(X_T), STEP(.stp), STL, DXF and IDF) data to define model geometry;
- High-speed computing, High-speed computing enables scSTREAM to solve large-scale MHD analyses in an acceptable time;
- Parallel computing, scSTREAM's parallel solver is available for further reducing computation time.
- Multiple matrix solvers, such as JACOBI, SOR (Successive Over-Relaxation), MICCG (Modified Incomplete Cholesky Conjugate Gradient), ILUCR (Incomplete LU Conjugate Residual), ILUCGS (Incomplete LU Conjugate Gradient Squared);

- Various useful functions such as a VB interface and a user function with tabular input;
- Post-processor, used to visualize the data calculated by the solver.

scTREAM has been validated for MHD flow in 2D and 3D steady problems based on comparable analytical and numerical data. [5]

3.2.2 Mass Transfer Solver

After we compute the MHD flow field and/or temperature field, the next stage is to solve the mass transfer model. The approach taken in this research is to build and solve the proper tritium transport models within a framework of a thermal fluid code, ScTetra [6], taking advantage of solving the temperature profile and its effectiveness in handling the blankets geometry complexity. Sc/Tetra, a commercial code developed by Software Cradle Co. Ltd., is an all-in-one, general purpose CFD software, based on the finite volume method and using unstructured mesh (tetrahedron, pentahedron, and hexahedron). In addition to simulating the standard fluid flow and heat transfer applications, a module to solve the general mass transfer equations is included in this code. However, regarding the specific problem of the tritium transport in typical PbLi blanket configurations, we need to solve the mass transfer equations considering the following factors: (1) multiple domains, (2) coupling

through the material interfaces, (3) temperature-dependent transport properties, and (4) space-dependent tritium source terms. The standard settings of the analysis conditions of Sc/Tetra are not sufficient under these conditions. Therefore, new user-defined functions were developed to deal with such cases. User functions are written in C language and made as a DLL file. Sc/Tetra user functions can be classified into four groups:

1. Setting functions. They are called by the Sc/Tetra solver to do some special calculations, such as specifying the temperature dependent diffusivity. They are called for every node/element at every cycle.

2. Utility functions. They can be called from other user functions that users are programming. Users can obtain various information such as velocity, temperature, and concentration of elements, as well as coordinates, time, time steps, and nodes.

3. Timing functions. They are called at predetermined timing of Sc/Tetra. For example, usu_init() is called after completing initialization, or just before starting to process the first cycle. With this function, it is possible to initialize user-defined data in detail.

4. Notification functions. They are called from Sc/Tetra solver in accordance with the command setup, in order for the solver to notify the computation results to users.

In this work, the following user functions are developed: (1) user function for interface mass transfer, (2) user function for data mapping, (3) user function for temperature-dependent properties, and (4) user function for tritium or heat source term.

Figure 12 shows one example of a user--defined function to apply tritium transfer boundary conditions at the LM/FS structure interface.

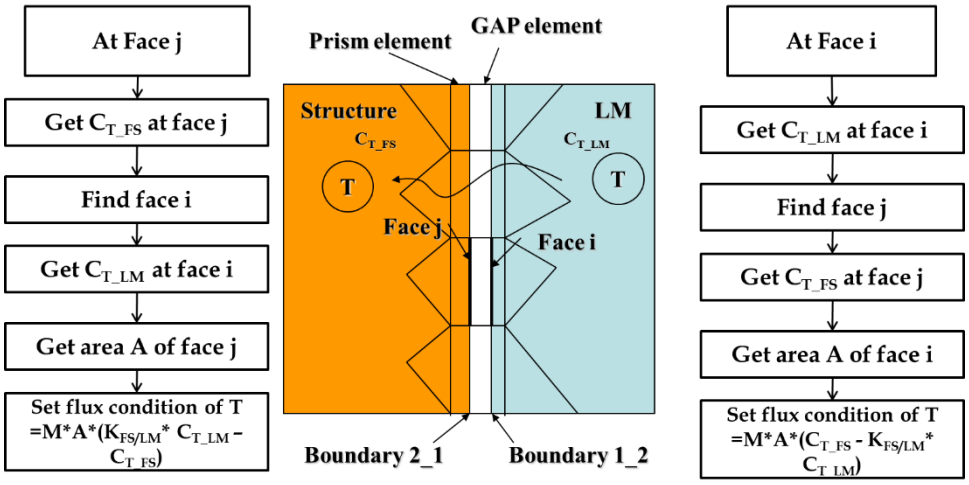

Figure 12. Example of user defined function to apply tritium transfer boundary condition at LM/FS structure interface.

Characterization of mass transfer at the material interface is a main concern. For example, for the LM/FS interface, tritium transfer has not yet been fully characterized from a phenomenological point of view. Assuming local chemical equilibrium for the system, the concentration of tritium at the interface is related by the equilibrium partition coefficient $K_{FS/LM}$. For the PbLi-structure interface, the tritium equilibrium can be defined as:

$$c_{T\_FS} = K_{FS/LM} c_{T\_LM} \tag{36}$$

Where $K_{FS/LM} = K_{S\_FS} / K_{S\_LM}$ is determined by the relative solubility of tritium in the LM, K_{S_LM}, and the FS structure, K_{S_FS}.

Additionally, we need to match flux conditions at the interfaces to ensure the flux continuity condition.

$$D_{LM} \frac{\partial c_{T\_LM}}{\partial n} = D_{FS} \frac{\partial c_{T\_FS}}{\partial n} \text{ at the LM/FS interface} \tag{37}$$

Where n is the normal direction of the interface.

There are discontinuities in the concentration profile and continuous flux at the boundaries between LM and FS phases. To get continuous flux over the phase boundaries, we apply a special type of boundary condition using the stiff-spring method. Instead of defining Dirichlet concentration conditions according to the partition coefficient $K_{SM/LM}$,

which would destroy the continuity of the flux, we define continuous flux conditions that, at the same time, force the concentrations to the desired values.

The flux boundary condition at the LM side can be expressed as:

$$\begin{aligned} J_{T\_LM-FS} &= (-D_{LM}\nabla c_{T\_LM} + c_{T\_LM}\mathbf{u}_{LM})\cdot\mathbf{n} \\ &= M\cdot(C_{T\_FS} - K_{FS/LM}C_{T\_LM}) \end{aligned} \quad \text{at } \partial\Omega_{LM,FS} \tag{38}$$

The flux boundary condition at the FS side can be expressed as:

$$\begin{aligned} J_{T\_FS-LM} &= (-D_{FS}\nabla c_{T\_FS})\cdot\mathbf{n} \\ &= M\cdot(K_{FS/LM}C_{T\_LM} - C_{T\_FS}) \end{aligned} \quad \text{at } \partial\Omega_{FS,LM} \tag{39}$$

Where

$\partial\Omega_{LM,FS}$ = the interface boundary belong to LM domain;

$\partial\Omega_{FS,LM}$ = the interface boundary belong to FS domain;

And M is a (nonphysical) velocity large enough to let the concentration differences in the brackets approach zero, thereby satisfying Equation 35. These boundary conditions also give a continuous flux across the interfaces provided that M is sufficiently large.

We apply this kind of boundary condition as a user-defined function, which is written in C++. The user function is shown in Figure 12. In the computer code, GAP elements are inserted between two materials. The GAP element has the shape of a prism. At face i, we first get the concentration of tritium, c_{LM}, and face area A, then we find face j on the other side of the element over the GAP element and get the concentration of tritium, c_{FS}, on face

j. Next we set a flux condition on face i as $M \cdot A \cdot (C_{T\_FS} - K_{FS/LM} C_{T\_LM})$. Similarly, we can set a flux condition on face j as $M \cdot A \cdot (K_{SM/LM} C_{T\_LM} - C_{T\_SM})$.

3.2.3 Data Mapping Utility

So far we have HiMAG and scSTREAM as the MHD solvers and Sc/Tetra as the mass transfer solver, so now a data mapping utility is needed to pass the velocity field from the MHD solver to the mass transfer solver. Since the MHD solver uses a structured mesh, a trilinear interpolation method is used in the data mapping utility. It approximates the value of an intermediate point (x, y, z) from destination data within the local axial rectangular prism linearly, using data on the lattice points shown in Figure 13.The procedure of trilinear interpolation can be described as follows:

- Find the eight corners of a cube that surrounds the point of interest. These corners have the values C_{000}, C_{100}, C_{010}, C_{110}, C_{001}, C_{101}, C_{011}, C_{111}.
- Perform linear interpolation between C_{000} and C_{100} to find C_{00}, C_{001} and C_{101} to find C_{01}, C_{011} and C_{111} to find C_{11}, C_{010} and C_{110} to find C_{10}.The linear interpolation can be expressed as $y = y_0 + (y_1 - y_0)\frac{x - x_0}{x_1 - x_0}$
- Do linear interpolation between C_{00} and C_{10} to find C_0, C_{01} and C_{11} to find C_1. Finally, we calculate the value C via linear interpolation of C_0 and C_1.

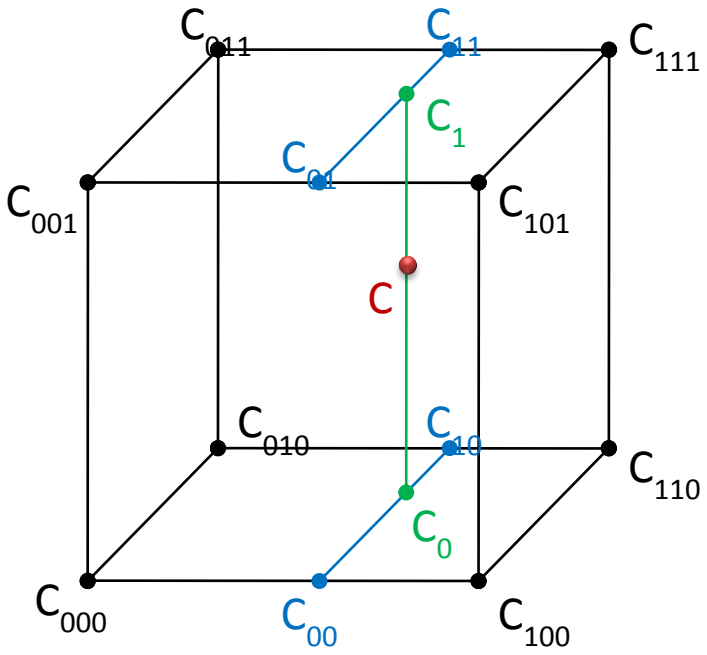

Figure 13. Depiction of 3D interpolation

The steps for mapping data from the MHD solver to the mass transfer solver are described in Figure 14. First, we load the source nodes, coordinates, field data and the destination nodes and coordinates data. Next, we do the coordinate transformation if the source and destination data are not in the same coordinate system. Then, we do the data mapping from source to destination using trilinear interpolation and write out the destination data with the field value. Finally, we read the mapped data into the Sc/Tetra solver using the user-defined function as discussed before.

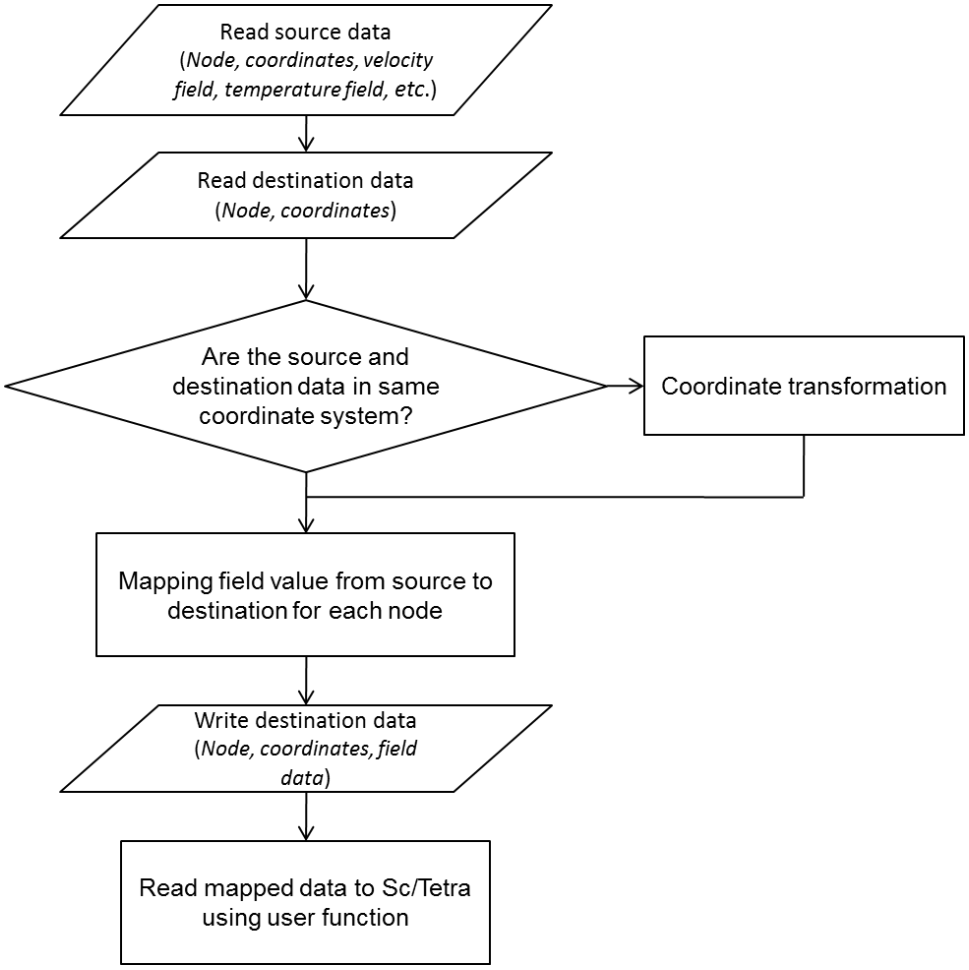

Figure 14. Steps for mapping data from MHD solver to mass transfer solver

3.2.4 Code Structure and Features of the Code

The overall structure of the computer code is shown in Figure 15. It includes three parts: (1) the thermal/fluid and MHD solver, (2) the mass transfer solver with user-defined functions, and (3) the utility for data mapping from MHD solver to mass transfer solver.

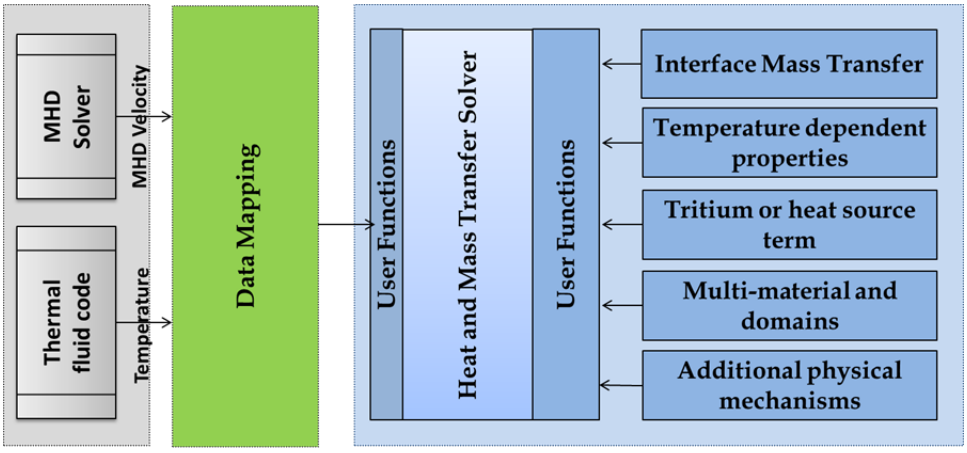

Figure 15. The structure of the tritium transfer code

The main features and advantages of this code include:

- Solving the tritium transport problems in MHD conditions by combining the MHD solver and the mass transfer solver.
- Extensive modeling capabilities by adopting user-defined functions.
- Solving the multiple tritium transfer processes coupled through boundary conditions at material interfaces.

- Solving the problem in 3D multiple regions and including complex blanket geometry (e.g. PES, GAP) into analysis.
- Advanced mesh generation for tetrahedron, pentahedron, and hexahedron elements. Prism layers can be inserted at walls to provide fine grid resolution in the boundary layer.
- Parallel solver for reducing computation time which is especially valuable for large scale models.
- Capability of CAD model import.
- Including pre- and post- processing.

By carrying out case studies using the proposed model and code, as discussed in Chapter 5, several key issues relevant to tritium transport and permeation in liquid metal blanket can be addressed, such as:

- Quantifying the difference of tritium inventory and permeation rate between DCLL and HCLL blanket concepts.
- Identifying the PES effect on tritium transport and permeation in DCLL concept.
- Evaluating the MHD effect and buoyancy effect on tritium transport and permeation.
- Identifying the range of permeation rate change on the basis of uncertainties of material properties (e.g. solubility and diffusivity).

3.5 References

1. M.A. Abdou, The APEX Team, *On the exploration of innovative concepts for fusion chamber technology*, APEX interim report overview, Fusion Eng. Des. 54 (2001) 181–247.
2. G. R. Longhurst, *TMAP7 User Manual*, Idaho National Engineering and Environmental Laboratory Bechtel BWXT Idaho, LLC, 2004.
3. scSTREAM, Software Cradle Co. Ltd., Japan.
4. R. Munipalli, V. Shankar, M.-J. Ni, N. Morley, *Development of a 3-D incompressible free surface MHD computational environment for arbitrary geometries: HIMAG DOE phase-II SBIR, period of performance*: June 2001–June 2003, Final Report, June 2003.
5. N. Morley, S. Smolentsev, N. Munipalli, M.-J. Ni, D. Gao, M. Abdou, *Progress on the modeling of liquid metal, free surface, MHD flows for fusion liquid walls*, Fusion Eng. Des. 72 (2004) 3–34.
6. Sc/Tetra, Software Cradle Co. Ltd., Japan.
7. P. NORAJITRA, L. BUHLER, A. UENAVENTURA, E. DIEGELE, U. FISCHER, E. UTTER, R. KRUESSMANN, S. MALANG, J. REIMANN, A. ORDEN, D. WARD, G. VIEDER, and F. WASASTJERNA, "Conceptual Design of the dual-coolant blanket

in the frame for the EU power plant conceptual study (TW2-TRP-PPCS12D)", Forschungszentrum Karlsruhe Report FZKA 6780 (2002).

8. C.P.C. Wong, M. Abdou, et.al., "Design Description Document for the U.S. Dual Coolant Pb-17Li (DCLL) Test Blanket Module", 2005

Chapter 4

Code Validations

In order to evaluate the accuracy of the mathematical formulation that is implemented in the model and to generate confidence in the results provided by the computer code, it is essential to compare its results with available experimental data and analytical solutions. Therefore the validation of the computer code is a very important phase, and it has been done in parallel with its development.

Three benchmark cases have been chosen for the analysis and the results will be hereafter presented and discussed. They have been selected for the validation as good examples of various features relevant for tritium transport assesses, such as permeation through solid media, transport in flowing media, and calculation of the tritium generation source term.

1. In-reactor tritium release experiment from molten lithium-lead alloy $Li_{17}Pb_{83}$, conducted in the fast neutron reactor "YAYOI" of the University of Tokyo, is relevant to evaluate the effects of temperature, sweep gas composition (adding of H_2) for PbLi sample with tritium generation source term [1, 2].

2. US-JA TITAN experiment, collaborated between INL and the University of Tokyo, is relevant to evaluate the effects of temperature transient on tritium/hydrogen permeation through α-Fe/PbLi sample [3].

3. Mass transfer in an absorption-convection-permeation problem [4].

4.1 In-Reactor Tritium Release Experiment from Molten Lithium-Lead (PbLi)

(1) Experimental apparatus

The tritium release experiment was performed by Terai [1] in an apparatus shown in Figure 16. This system consists of three parts; a sweep gas supply system, the in-reactor components, and a tritium monitoring and recovery system. The in-reactor components, filled with a PbLi sample (50 mm inner diameter, 20 mm depth), were irradiated by neutrons to generate tritium, at a rate of about 4 Bqs^{-1} gLi^{-1}, which is equivalent to a tritium generation rate $G=1.39\times10^{14}$ at s^{-1} m^{-3}. The tritium generated in the PbLi sample migrated in the sample and was released from the open surface of the sample. The released tritium was swept for counting by a He carrier gas including different concentrations of H_2. The tritium release rate was measured during irradiation as a function of time. The release rate $j_T(t)$ increased up to a steady state level equal to the tritium generation rate G.

(2) Modeling with Generation, Diffusion and Recombination

It was suggested in the experiment that tritium release was limited by recombination of H and T atoms at low hydrogen pressure and by diffusion at high hydrogen pressure. Therefore, we constructed a model, duplicating the experimental setup, and considering tritium generation in the volume, diffusion in the bulk, and recombination on the surface. Mass transfer equations were solved using our developed model and code. The recombination flux condition at the PbLi open surface was computed using user-defined functions.

The material properties and parameters used for the analysis are listed in Table 2.

Table 2 Properties Data Used for the Analysis [Ref. 1]

Property and parameter	Expression
Experiment	Terai
Temperature	873K
Sample material	PbLi
Thickness	20mm
Diameter	50mm
Diffusivity	$4.97\times10^{-7}m^2\ s^{-1}$
Solubility	$6.5\times10^{20}m^{-3}\ Pa^{-1/2}$
Recombination coefficient	$2.03\times10^{-27}m^4\cdot s-1$
Tritium generation rate	1.39×10^{14} at $s^{-1}\ m^{-3}$
Sweep gas composition	helium + hydrogen (33, 43, 1000, 10000Pa)

The principal observation in the experiment was that the tritium release rate increased if hydrogen gas was added to the He sweeping flow due to H-T recombination. As hydrogen started to be swept about 12 hours before irradiation, one can suggest that its concentration in the eutectics reached the equilibrium value [2], which is determined by the Sievert's law $C_H=K_S(P_{H2})^{1/2}$, where K_S is the tritium solubility in PbLi.

The fluxes of tritium atoms, which desorb from the surface being combined in either T_2 or HT molecules, can be defined as [2]

$$j_T = j_T(T_2) + j_T(HT) = K_r \cdot C_T(C_T + C_H) \tag{40}$$

The calculated build-up curves of the tritium release rate, normalized to the tritium generation rate, are plotted for comparison with the experimental data in Figure 17. One can see that the model results show a very good agreement with the experimental observations with different sweep gas composition. The calibration analysis indicates that the developed model and computer code have a good predictive capability of various features relevant for tritium transport assesses, such as the bulk diffusion, surface recombination, and volumetric source term.

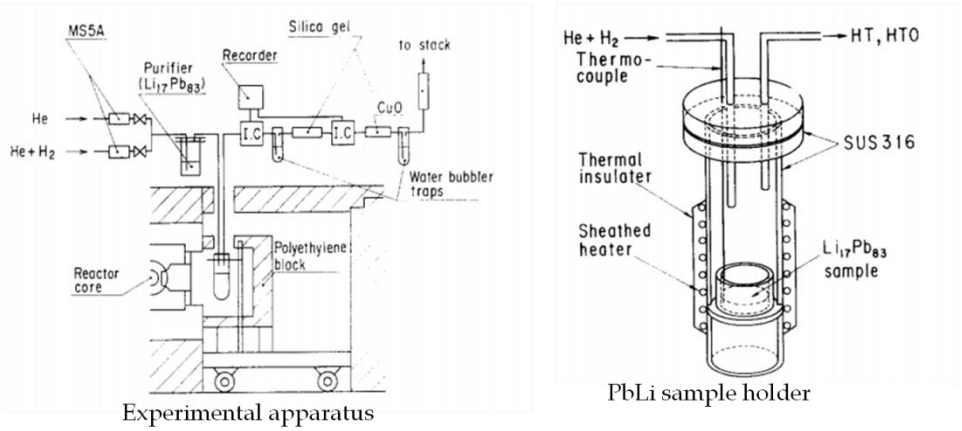

Figure 16. Schematic diagram of the in-situ tritium release experiment from molten PbLi [ref. 1]

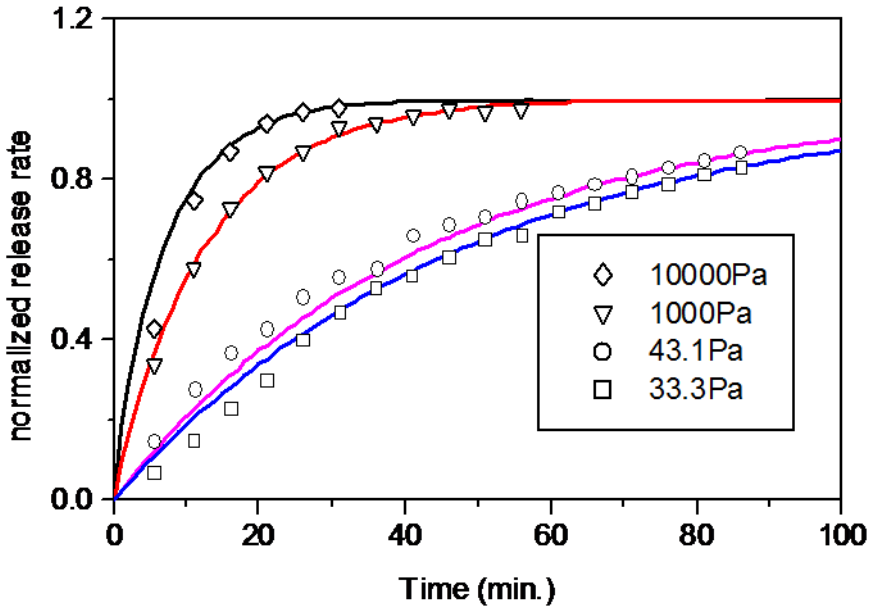

Figure 17. Tritium release rate calculated in suggestion of bulk diffusion and surface recombination

4.2 US-JA TITAN Experiment of Transient Hydrogen Transport through α-Fe/PbLi System

As another benchmark example, the US-JA TITAN experiment [3] has been selected for the calibration of the accuracy of the mathematical formulation and the boundary conditions that were implemented in the model. In the experimental campaign, the time history of hydrogen and deuterium permeation through a series of media, including α-Fe film and PbLi film, was studied. A 3D model duplicating the experimental setup was created, and solubility and diffusivity data from literature were used for hydrogen isotopes transient analysis.

In this experiment, H and D are determined by using a permeation pot. The experimental apparatus and the details of the pot are shown in Figure 18. The Li-Pb pot, made of α-Fe, the eutectic alloy composed of Li and Pb with the molar ratio of 17:83, was inserted in the center position on the α -Fe plate in the vessel. A constant concentration of a gas mixture of H_2 or D_2 and Ar was introduced into the bottom section separated by the α-Fe plate. After they permeate through the α-Fe plates, the H_2 or D_2 molecules are purged by Ar gas, and the H_2 or D_2 concentration in the purge gas is detected by gas-chromatography.

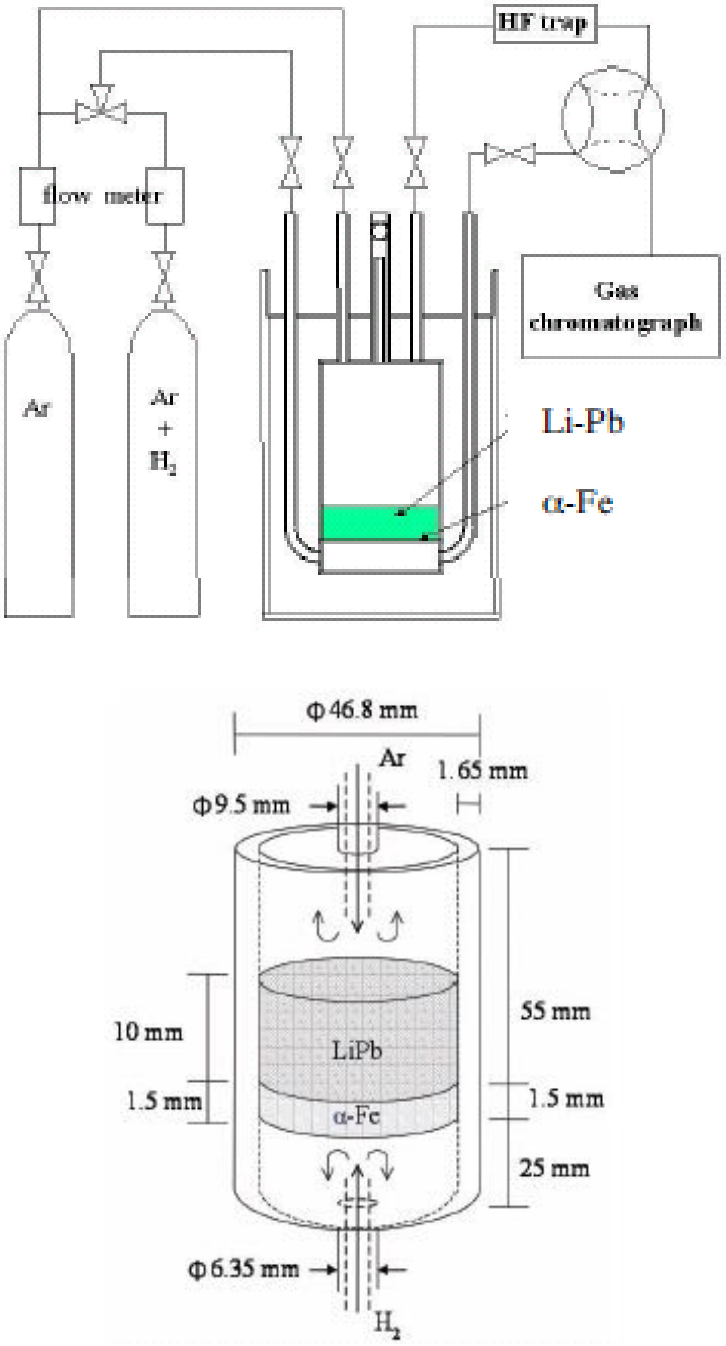

Figure 18. US-JA TITAN experiment apparatus of transient hydrogen transport through α-Fe/PbLi system [Ref. 3].

Next, we constructed a model duplicating the experimental setup as shown in Figure 19. H_2 or D_2 molecules in the gas mixture dissociate on the Fe plate. Dissociated H atoms permeate through the Fe plate, H atoms arrive at the LiPb-Fe interface, and they dissolve in a form of H or D atoms in Li-Pb. Then they permeate through the Li-Pb eutectic alloy. On another surface of Li-Pb, two H or D atoms combine and form a H_2 or D_2 molecule. The H_2 or D_2 molecules are purged by Ar gas. The solubility and diffusivity data from literature were used for hydrogen isotopes transient analysis.

3D mass transfer equations were solved using Sc/Tetra. The species equilibrium condition at Fe/PbLi interface, recombination flux condition at PbLi/downstream-side interface, and Sievert's law at Fe/upstream-side interface were computed using user-defined functions. Figure 20 shows examples of the build-up curves of H permeation through the LiPb layer. The benchmark results showed good agreement with the experimental observations for hydrogen permeation through the α-Fe/PbLi pot at different temperatures. The calibration analysis indicates that the governing equations and the boundary conditions that have been selected to link the different mass transport mechanisms for the different regions are correct.

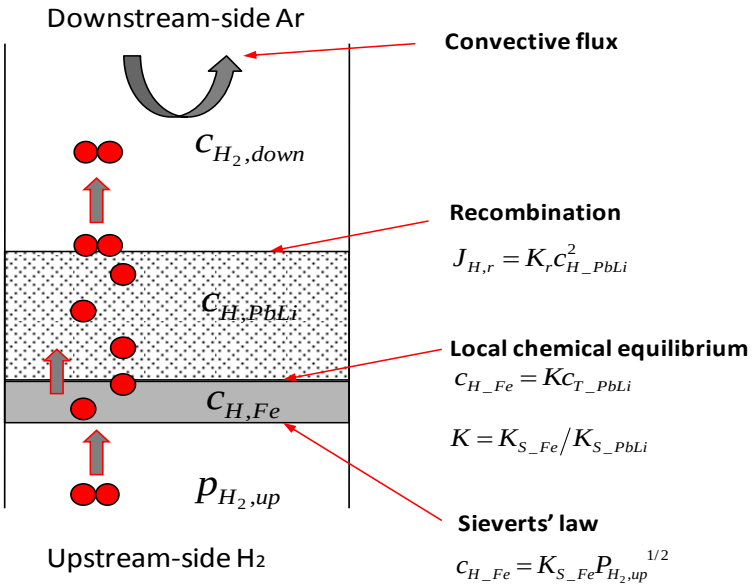

Figure 19. Numerical model duplicating the experimental of transient hydrogen transport through α-Fe/PbLi system

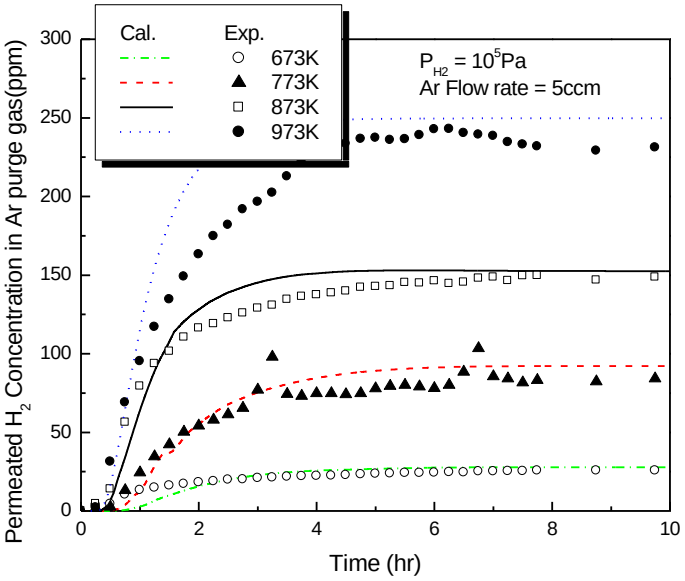

Figure 20. Permeated H_2 concentration in Ar purge gas

4.3 Mass Transfer in a Absorption-Convection-Permeation Problem

This problem is defined for gas absorption in a laminar falling film with homogeneous and heterogeneous chemical reactions and external gas-phase mass transfer resistance as shown in Figure 21. The film is in contact with the gas phase containing the solute at a concentration of c_0. The wall is a permeable wall.

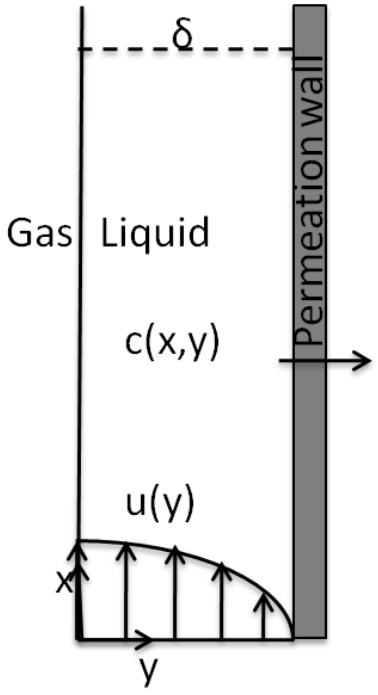

Figure 21. Sketch of absorption-convection-permeation problem

The equation governing the concentration of the dissolved gas in the presence of a homogeneous zero-order reaction in the liquid phase is given by [4]

$$u_i(1-(\frac{\bar{y}}{\delta})^2)\frac{\partial \bar{c}}{\partial \bar{x}} = \frac{\partial^2 \bar{c}}{\partial \bar{y}^2} + k \tag{41}$$

The boundary conditions are

$$\bar{c}\big|_{x=0} = 0,\ \left.\frac{\partial \bar{c}}{\partial \bar{y}}\right|_{\bar{y}=0} = -k_g(c_0 - \bar{c}),\ \left.\frac{\partial \bar{c}}{\partial \bar{y}}\right|_{\bar{y}=\delta} = -k_s\bar{c} \tag{42}$$

The dimensionless equation and boundary conditions are

$$\begin{aligned} &(1-y^2)\frac{\partial c}{\partial x} = \frac{\partial^2 c}{\partial y^2} + \alpha \\ &c\big|_{x=0} = 0,\ \left.\frac{\partial c}{\partial y}\right|_{y=0} = -Bi(1-c),\ \left.\frac{\partial c}{\partial y}\right|_{y=1} = -\beta c \end{aligned} \tag{43}$$

Where $x = \bar{x}/\delta \cdot Pe,\ y = \bar{y}/\delta,\ c = \bar{c}/\bar{c}_0,\ \alpha = k\delta^2/D,\ \beta = k_s\delta/D,\ Bi = k_g\delta/D$

For α=0 and Bi= ∞, the absorption-convection-permeation case results in an eigenvalue problem, with the solution [4]

$$\begin{aligned} &c(x,y) = 1 - \frac{\beta y}{\beta+1} + \sum_{n=1}^{\infty} A_n Y_n(y) e^{-\lambda_n^2 x} \\ &Y_n(y) = e^{-\lambda_n^2 y^2/2}\lambda_n^{1/2}\,{}_1F_1(b-a+1;2-a;\lambda_n y^2) \end{aligned} \tag{44}$$

Where, ${}_1F_1$ is hypergeometric function. λ_n and Y_n are the eigenvalues and eigen functions.

(2) Modeling with absorption-convection-permeation

We construct a model considering the same problem with surface absorption, convection in the film, and permeation through the wall. Mass transfer equations were solved using our developed model. The calculated development of the concentration profile for α=0 and Bi=∞ is plotted for comparison with the analytical solution in Figure 22. One can see

that the model results showed a very good agreement with the analytical results. The calibration analysis indicates that the developed model and computer code have good accuracy under the condition of species transporting in flowing fluid with a permeable wall.

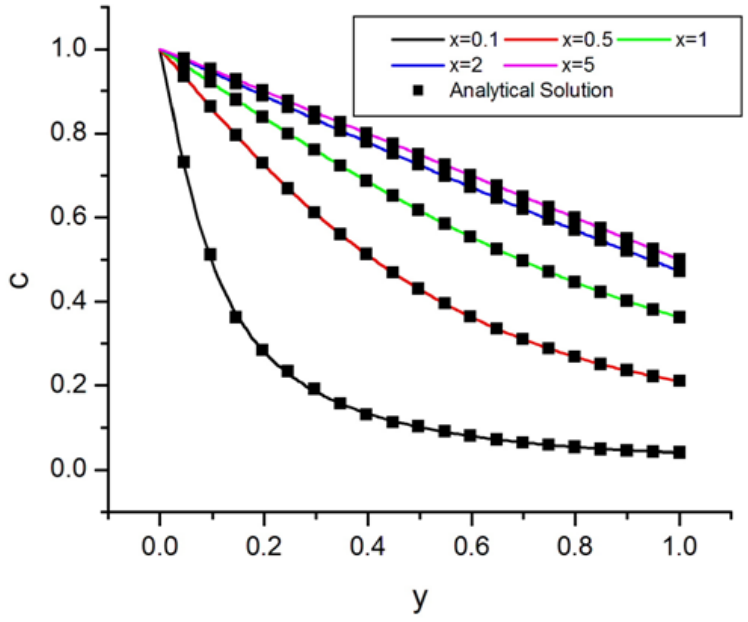

Figure 22. Development of the concentration profile for α=0 and Bi=∞.

4.4 References

1. Takayuki Terai, Shin'ichi Nagai, Toshiaki Yoneoka and Yoichi Takahashi, *Mass transfer coefficient of tritium from molten lithium-lead alloy ($Li_{17}Pb_{83}$) to environmental gas under neutron irradiation*, Fusion Engineering and Design 17 (1991) 237-241.
2. Alexander PISAREV , Tetsuo TANABE , Takayuki TERAI , Gianluca BENAMATI & Mikhail MULLIN, *Modeling of In-Pile Experiments on Tritium Release from Molten Lithium-Lead*, Journal of Nuclear Science and Technology, 39:4, 377-381 (2002).
3. P. Fauvet and J. Sannier, *Hydrogen behavior in liquid LiPb alloy*, Journal of Nuclear Materials 155-157 (1988) 516 5l9
4. P. Ray, S. K. Bayen, B. K. Dutta, Calcutta, Indien and A. S. Gupta, Kharagpur, Indien, *Mass transfer with chemical reaction in a laminar falling film*, Wfirme- und Stofffibertragung 22, 195-199 (1988)

Chapter 5

Cases Studied and Results

5.1 Introduction

In this section the results of the mathematical model described in the previous sections will be reported. The tritium assessment is affected by different factors, as highlighted during the description of the model. Thus the objective is first to show the relevance of the different factors (the MHD effect, material properties (e.g. solubility, diffusivity), the buoyancy effect and the helium bubble effect) by a parametric study (Section 5.3 and section 5.7) in which the main parameters for the tritium transport system will vary in a reasonable range, and the solution in terms of steady state tritium losses and inventories will be visualized. Then followed by the following case studies considering the reference blanket configurations were analyzed:

1. Tritium transport is analyzed in a poloidal duct with a pressure equalization slot (PES) in the flow channel insert (FCI) (Section 5.4). In the DCLL concept, a thin gap between the FCI and the structure will affect tritium transfer behavior and loss rate by changing the local MHD velocity distribution. A PES, utilized at the FCI, will also affect tritium transfer behavior and loss rate by providing a path for tritium to migrate between the core and the

gap and by changing the local MHD velocity distribution. Thus the objective is to evaluate the impact of a PES on tritium transport and permeation.

2. Tritium transport is analyzed in a DCLL U-shaped flow channel (Section 5.5). The aim of this study is to estimate the tritium concentration and the permeation losses in the reference DCLL geometry, which represents the current US DCLL design. In this design, three U-shaped ducts with the FCI and the structure wall, connected through the inlet/outlet manifolds. PbLi starts in the feeding circular pipe, then it expands in the manifold and distributes into three channels. The liquid metal flows among three back channels and into the front channels by passing through the U-turns. After distributing into the front channels, the fluid is collected in the outlet manifold. Since the configurations for all three channels are similar, simulations were only done for the center channel as representative of the three channels.

3. Tritium transport in the HCLL configuration was analyzed and compared with the case of the DCLL concept (Section 5.6). The HCLL blanket concept is characterized by a low velocity of the liquid metal breeder, which is about 2 orders of magnitude lower than in the DCLL concepts since the Pb–17Li is used only for tritium extraction, not for heat extraction. This means that tritium inventory and permeation for the HCLL concept will be much higher than for the DCLL concept.

5.2 Properties Data Used for the Analysis

Table 3 reports the main material properties database adopted in this research. In general, tritium transport properties might be affected by large uncertainties. As an example, the tritium solubility in PbLi determined by Reiter (and adopted for this study in most cases) looks quite far from the one reported by different authors. The plot of Figure 23 was meant to show that it is important to bear in mind that tritium properties in materials might be quite different between several experimenters.

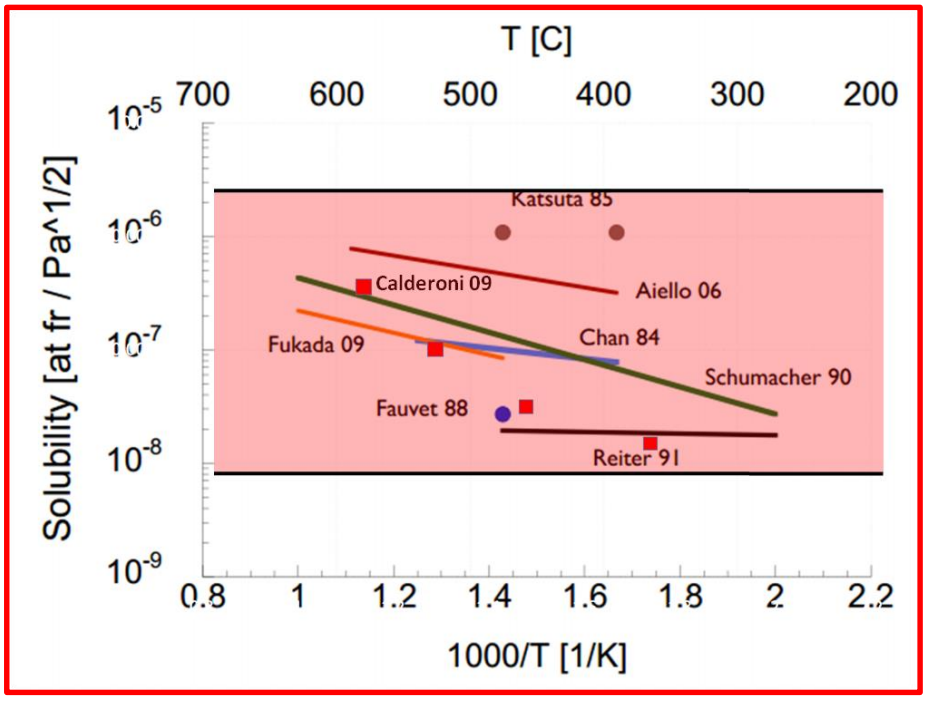

Figure 23. Different tritium solubility in PbLi by different authors

Table 3. Properties data used for the case analysis

Property	Expression	Reference
Liquid metal Pb-17Li		
Density (kg/m^3)	$\rho = 10.52 \times 10^{-3}(1 - 113 \times 10^{-6} T)$	[1]
Dyn. viscosity (Pa s)	$\mu = 1.87 \times 10^{-4}(11640 / RT)$	[2]
Specific heat (J/kg K)	$C_p = 195 - 9.116 \times 10^{-3} T$	[2]
Thermal conductivity (W/K m)	$\lambda = 1.95 \times 10^{-2} + 19.6 \times 10^{-5} T$	[2]
Electric resistivity (Ω m)	$\rho_{el} = 102.3 \times 10^{-6} + 4.26 \times 10^{-8} T$	[2]
Diffusivity (m^2/s)	$D = 4.03 \times 10^{-8}(-19500(J / mol) / RT)$	[3]
Solubility (mol m^{-3} Pa$^{-0.5}$)	$K_s = 1.31 \times 10^{-3}(-1350(J / mol) / RT)$	[3]
Recombination coefficient (m^4/at s)	$K_r = 1.01 \times 10^{-25}(-29350(J / mol) / RT)$	[4]
Ferritic steel		
Solubility (mol m^{-3} Pa$^{-0.5}$)	$K_s = 0.1(-23810(J / mol) / RT)$	[5]
Diffusivity (m^2/s)	$D = 1.22 \times 10^{-7}(-14470(J / mol) / RT)$	[5]
SiC		
Diffusivity (m^2/s)	$D = 9.8 \times 10^{-8}(-1.89(eV) / kT)$	[6]
Solubility (atoms cm^{-3}atm$^{-0.5}$)	$K_s = 8.29.8 \times 10^{15}(0.61(eV) / kT)$	[6]

5.3 Parametric Studies

As discussed in Chapter 2 and Chapter 3, the tritium transport and permeation are supposed to be affected by many factors. In order to show the importance and the impacts of these factors on the results, we will report tritium losses and distributions, while considering the following factors inside this tritium transport study:

- The MHD effect (varying MHD velocity profiles and Hartmann numbers);
- The effect of uncertainties of tritium solubility;
- The effect of uncertainties of tritium diffusivity;
- The buoyancy effect (considering an upward flow and a downward flow).

The parametric studies do not consider the effects of adding an FCI or PES. The effects of FCI and PES configurations are presented in next section.

5.3.1 MHD Effect

Flows of electrically conducting liquid metal will experience complicated MHD effects in the magnetic fusion environment. MHD effects can have dramatic impacts on the flow distribution and cause complex velocity fields (e.g. Hartmann layer, side layer, reversed flow, stagnant flow, etc.), thus affecting the tritium transport and permeation rate. In this section,

with the aim of showing the effect of the MHD sensitivity of tritium behavior in the liquid metal, two parametric analyses were carried out: (1) the velocity profile effect on tritium transport, and (2) the effect of the Hartmann number on tritium transport.

5.3.1.1 Velocity Profile Effect on Tritium Transport

In order to more clearly see how the MHD flow affects the tritium distribution, three typical velocity profiles are imposed according to various conditions:

1. Parabolic velocity profile as it would be obtained if no MHD effects were involved.
2. Hartmann layer velocity profile (flat) as it would be obtained on a Hartmann wall in MHD flow.
3. Side layer velocity profile (M-shape) as it would be obtained on a side wall in MHD flow.

The 2D problem is defined in two regions as shown in Figure 24: the liquid PbLi region (1m ×0.035m), and the structure region (4mm thickness ferritic steel).

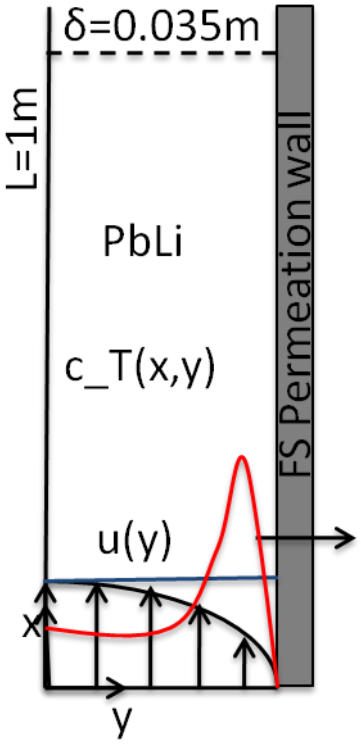

Figure 24. Diagram of the 2D geometry: the liquid region (1m×0.035m) and the 4mm structure region.

Figure 25 and Figure 26 show the three velocity profiles and the corresponding tritium concentration along the y-direction at x=0.8m at the same mass flow rates (average velocity at 0.0675m/s). Tritium accumulates near the wall region for the parabolic velocity profile, which results in a high tritium permeation flux (Figure 28) and consequently a high tritium leakage rate. On the contrary, for the MHD-type velocity profiles (side layer and Hartmann

layer velocity profiles), the tritium concentration increase near the wall region is no more present. This means that a lower tritium permeation flux can be maintained because of higher convection effects near the wall. A full two dimensional plot of the concentrations for three velocity profiles is also given in Figure 27 for clarity. The side layer velocity profile keeps tritium in the center region, the Hartmann layer velocity profile keeps tritium uniform; meanwhile, the parabolic velocity profile keeps tritium near the wall region.

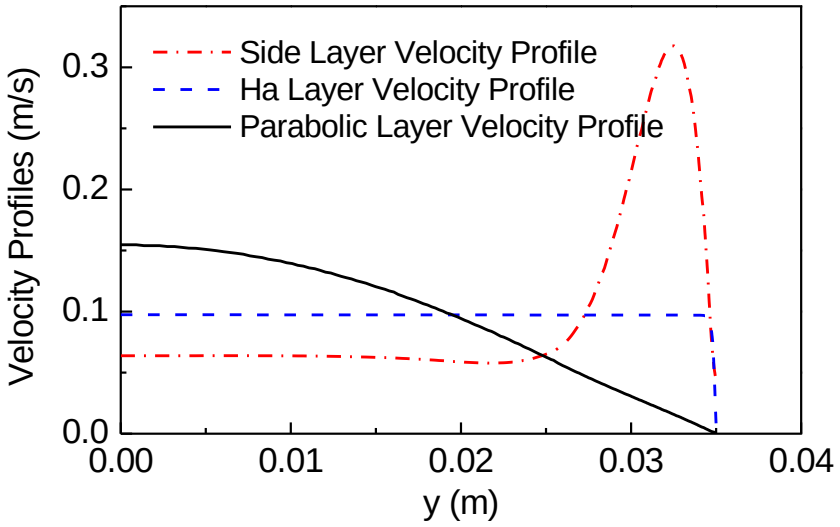

Figure 25. Parabolic, side layer and Hartman layer velocity profiles along y-direction at same mass flow rates.

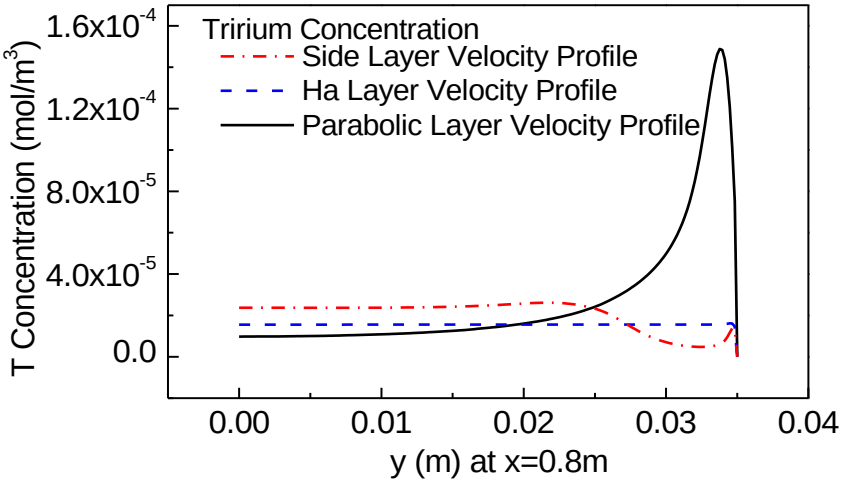

Figure 26. Tritium concentrations along y-direction at x=0.8m for parabolic, side and Hartman layer velocity profiles.

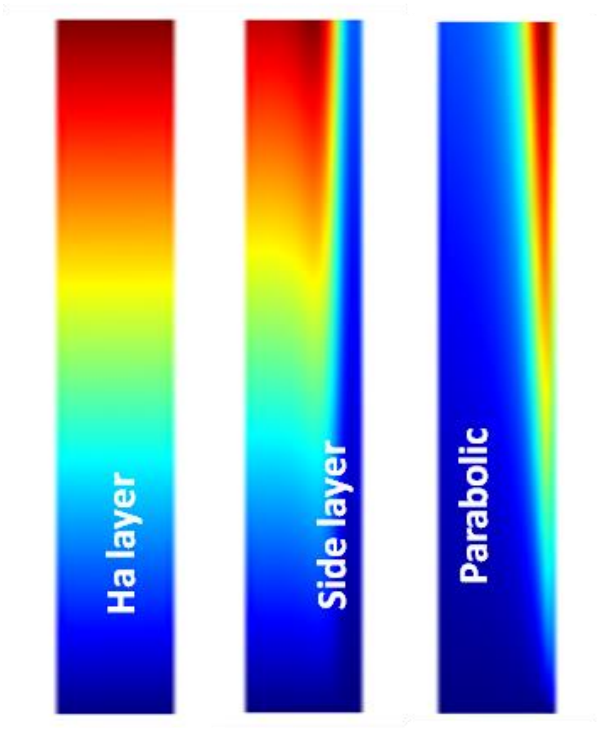

Figure 27. Tritium concentration in PbLi for various velocity profiles

The permeation flux (Figure 28) shows a significant reduction for MHD type velocity profiles. This is reasonable since the velocity distribution close to the wall governs the tritium permeation. Side layer velocity profile is the best for representing the tritium distribution. It provides a higher convective effect due to its higher velocity near the wall and consequently keeps most of the tritium in the PbLi bulk, reducing tritium permeation through the wall.

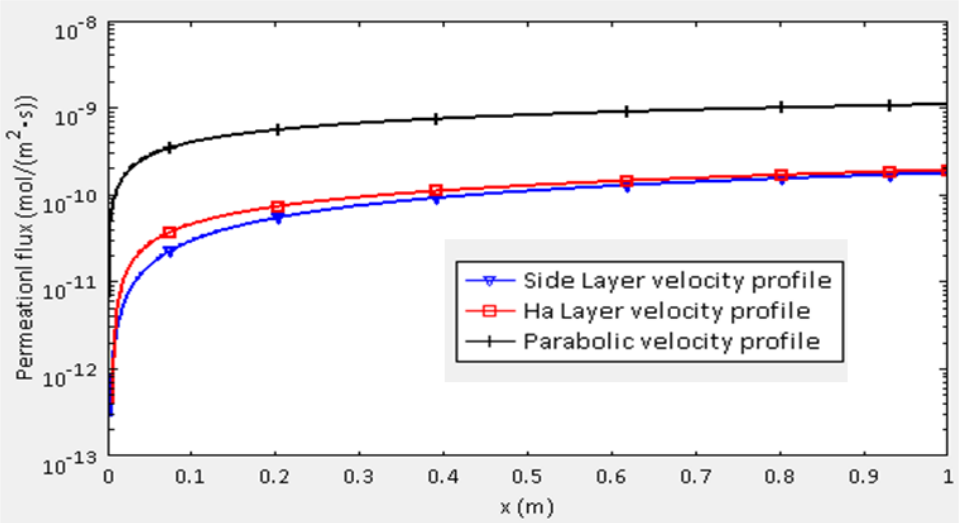

Figure 28. Tritium permeation flux along wall for parabolic, side layer and Hartman layer velocity profiles shows a reduction for MHD type velocity profiles.

5.3.1.2 The Hartmann Number Effect on Tritium Transport

Tritium permeation is controlled by the near wall velocities, as discussed in previous analysis. The Hartmann number is the main parameter that affects the side layer and Hartmann layer velocities. A sensitivity analysis was carried out for the PbLi flow in a duct with 1m length, 60mm*60mm cross-section, and 2mm conducting wall. The following five Hartmann numbers were selected for the analysis: Ha=0, Ha=100, Ha=1000, Ha=1440, Ha=3175, together with an inlet velocity of 0.0675m/s and a reference temperature of 773K. The reference material property data set was summarized in Section 5.2. The results of this analysis are hereafter presented and discussed.

Figure 29 shows how tritium concentrations at the outlet of PbLi flow are markedly affected by changing the Hartmann number from Ha=0 to Ha=1000. Tritium concentration peaks close to the walls at a low Hartmann number, while it becomes more concentrated in the center as the Hartmann number increases. As a result of less tritium moving near the wall, the permeation rate through the wall is reduced.

Figure 30 shows that the total permeation rate decreases as the Hartmann number increases. By changing the Hartmann number from Ha=10 to Ha=1000, the permeation rate dropped from 2.98e-10 mol/s by 60% to 1.25e-10 mol/s. However, the rate of decrease due to the increase of Hartmann number becomes slower as the Hartmann number increases. For example, permeation rate dropped by only about 10% from 1.25e-10 mol/s to 1.1e-10 mol/s as the Hartmann number increased from Ha=1000 to Ha=3175.

Summarizing the obtained results regarding the impact of the MHD effect on the tritium transport, it is immediately clear that the MHD effect will bring certain benefits in terms of reducing the tritium permeation rate.

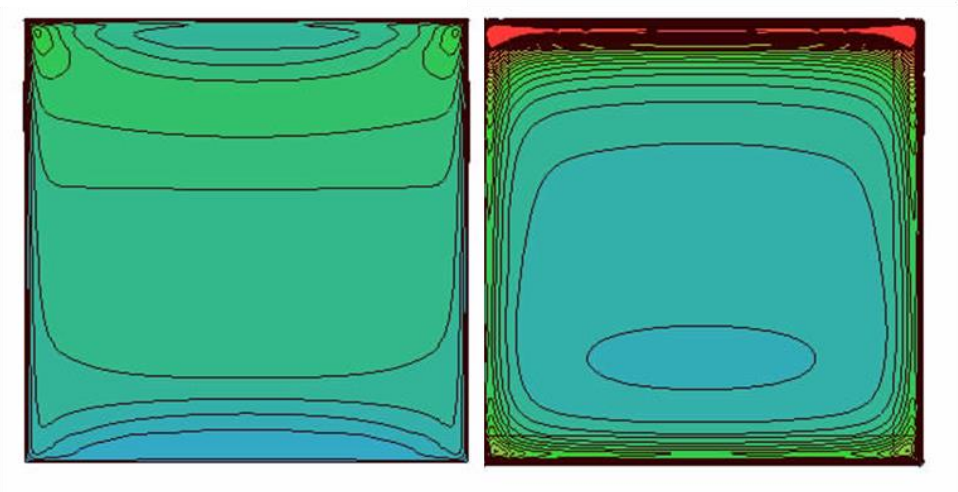

Figure 29. Tritium concentration in outlet (left: Ha=1000, right: Ha=10), it is peaked close to the walls at low Ha, while it becomes more concentrated in the center as Ha increases.

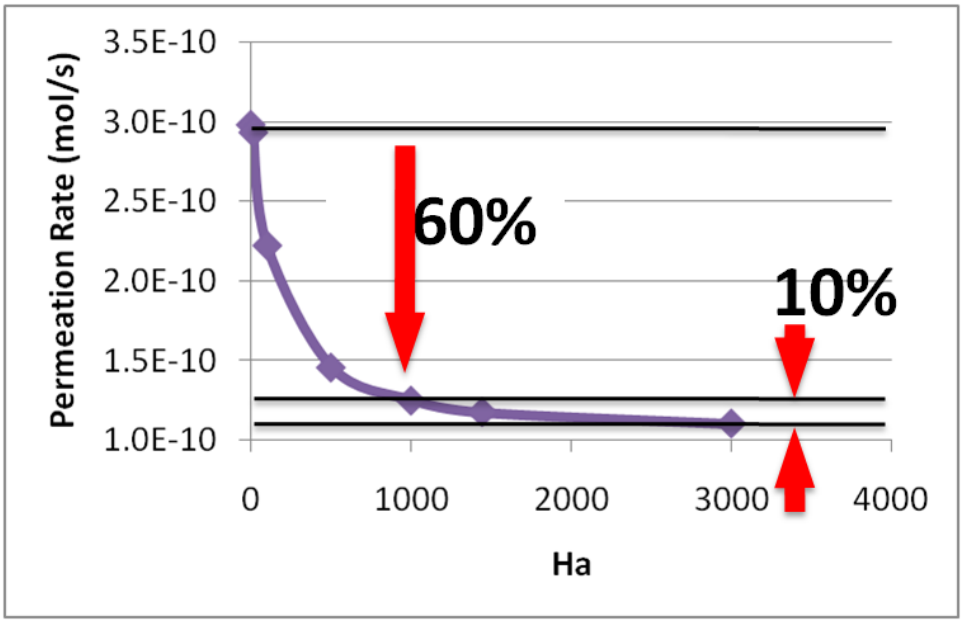

Figure 30. Tritium permeation rate decreases as Hartmann number increases, but it becomes slower at high Ha.

5.3.2 Effect of the Tritium Solubility

Tritium solubility, the function linking the tritium concentration solubilized in liquid metal with the corresponding tritium partial pressure at equilibrium, is one of the basic factors for the liquid metal breeder blanket concepts because of its strong impact on tritium permeation rate from the blanket into the helium cooling system. Available database on tritium solubility is visualized in Figure 5, which shows considerable data scattering and discrepancies. Therefore, a sensitivity analysis should be done in order to evaluate the impact of the different solubility values on the tritium permeation rate and to evaluate the urgency of further experiments to find reliable and agreed data.

With the aim of showing the range of permeation rate change on the basis of uncertainties of the tritium solubility, a parametric study was carried out in a duct flow with 1m length, 60mm*60mm cross-section, and 2mm conducting wall. Figure 31 shows the steady state tritium permeation rate obtained by varying the tritium solubility over a range of reference values from 1e-8 at·fr/$Pa^{0.5}$ to 1e-6 at·fr/$Pa^{0.5}$ (from 5e-4 to 1e-2 mol·m^{-3}·$Pa^{-1/2}$ in SI unit) obtained by different authors.

As shown in the results, higher tritium solubility provides a smaller tritium permeation rate. This is mostly due to the tritium partial pressure decreasing at a high tritium solubility. Over the range of reference tritium solubility, tritium permeation rate decrease from 1.5e-10

mol/s by about 80% to 2.4e-11 mol/s. The effect of the uncertainty in the values for tritium solubility on tritium permeation is quite marked, especially for the reference range (as marked by a rectangle in Figure 31), in which the tritium permeation rate is most sensitive with the values of tritium solubility.

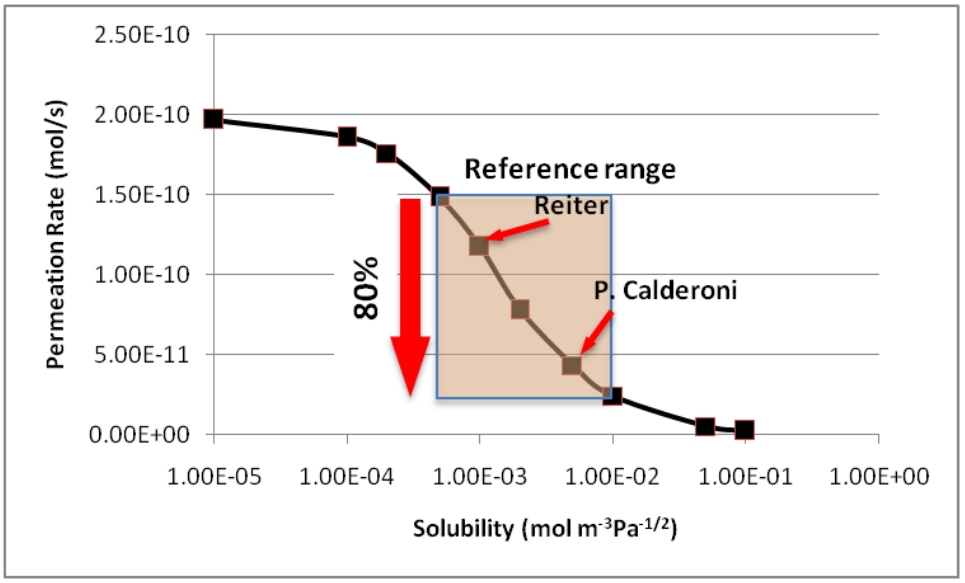

Figure 31. Effect of tritium solubility on permeation rate

5.3.3 Effect of the Tritium Diffusivity

Tritium diffusivity is another basic property that plays a major role in tritium transport in the liquid metal breeder blanket concept. Available database on tritium diffusivity in PbLi, visualized in Figure 6, are spread in about one order of magnitude. Therefore, a sensitivity analysis should also be done to evaluate the impact of the different diffusivity values on the

tritium permeation rate and to evaluate the urgency of further experiments to find reliable and agreed data.

Figure 32 shows the effect of a change in the tritium diffusivity in PbLi on the tritium permeation rate. Four cases were investigated in the range of reference values of tritium diffusivity from 1e-9 m^2/s to 1e-8 m^2/s: (1) D=1e-9m^2/s, (2) D=3e-9m^2/s, (3) D=6e-9m^2/s, and (4) D=1e-8m^2/s. As shown in the figure, the diffusion coefficient clearly affects the tritium permeation rate by controlling the amount of tritium diffusing from the PbLi to the PbLi/FS interface. Higher tritium diffusivity provides a higher tritium permeation rate. Over the range of reference tritium diffusivity, tritium permeation rate increase from 1.41e-10 mol/s by 18% to 1.67e-10 mol/s.

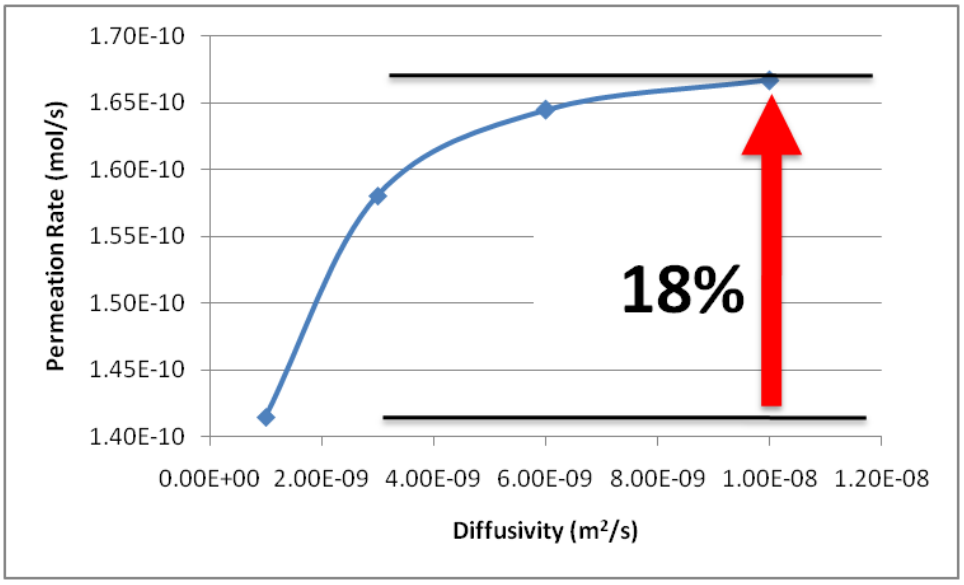

Figure 32. Effect of tritium diffusivity on permeation rate

5.3.4 Buoyancy Effect

A magnetic field causes flow redistribution, changing the velocity profile near the channel walls, thus affecting the tritium transfer efficiency and the permeation rate. Meanwhile, buoyancy effects due to non-uniform volumetric heating may cause a reverse flow and an associated high tritium concentration in some conditions, which can be a concern to the breeder blankets.

This analysis models a piece of the poloidal duct through which the PbLi flows associated with the buoyancy effects (in Figure 33). The flowing liquid is PbLi at 500°C in the inlet. The vertical duct is a square steel duct with the cross-sectional dimensions 20 cm by 20 cm, 1cm wall thickness (a=b=10 cm), and length L=2 m from top to bottom. Dimension "b" is the Hartmann length (i.e. b is taken along the magnetic field). Dimension "a" is half of the duct width across the magnetic field. Two radial ducts have cross-sectional dimensions 20 cm (along the magnetic field) by 10 cm (across the magnetic field) and length 40 cm. The volumetric heating that drives buoyant flow in the vertical duct changes exponentially with the radial distance as: $q'''(y) = q_0 e^{m(y/a-1)}$. Parameter q_0 is the maximum volumetric heating at the interface between the wall and the flowing liquid, W/m^3. The velocity profiles are obtained using the HiMAG solution for parameters Gr = 1E8, Re = 1E5, and Ha = 400.

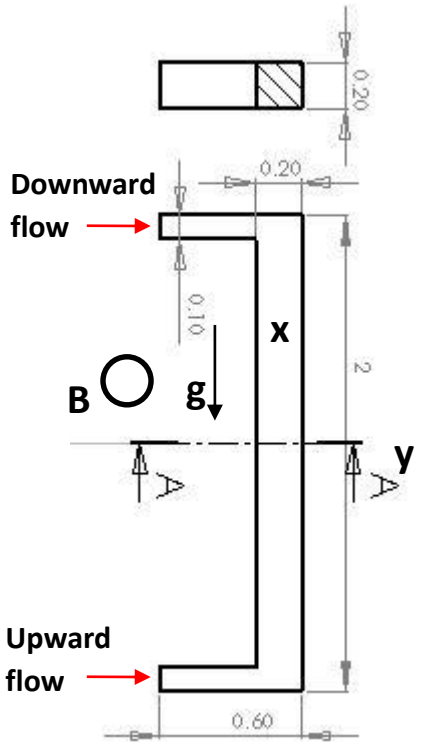

Figure 33. Tritium transport in the poloidal duct through which the PbLi flows associated with the buoyancy effects

With the aim of investigating the influence of buoyancy effects on the tritium transport and permeation, both the downward flow case and upward flow case were carried out. Figure 34 shows the velocity profiles and the corresponding tritium concentration distribution for the case of downward flow. It can be seen that there exists a strong shear layer at the center of the channel and there is a region of buoyancy-induced reverse flow near the front wall. As a result, high tritium concentration is observed in the circulated flow area.

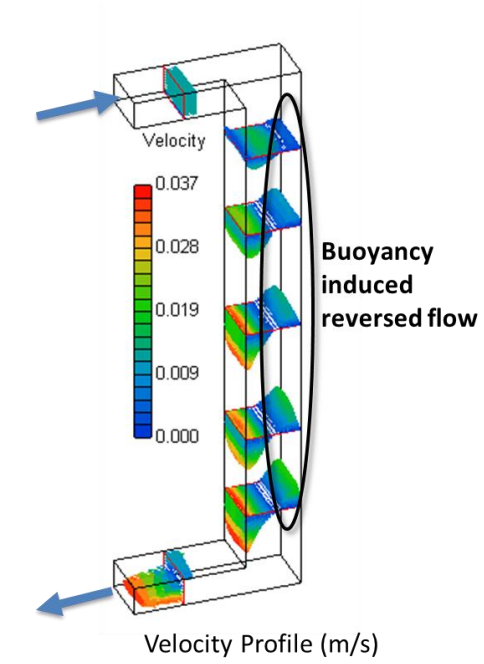

Figure 34. The downward flow velocity profiles (left) with a region of Buoyancy induced reverse flow near the front wall. The tritium distribution (right), high tritium concentration is observed in the region of reversed flow.

Figure 35 shows the velocity profiles and the corresponding tritium concentration distribution for the case of upward flow. This case used the same parameter values as for downward flow. The velocity profile is much different from downward flow, as there is no a strong shear layer at the center of the channel and no reverse flow near the front wall. As a result, we can see a rough uniform tritium distribution, and there are no high local tritium concentrations except a peak in the front-top corner due to low velocity in that area.

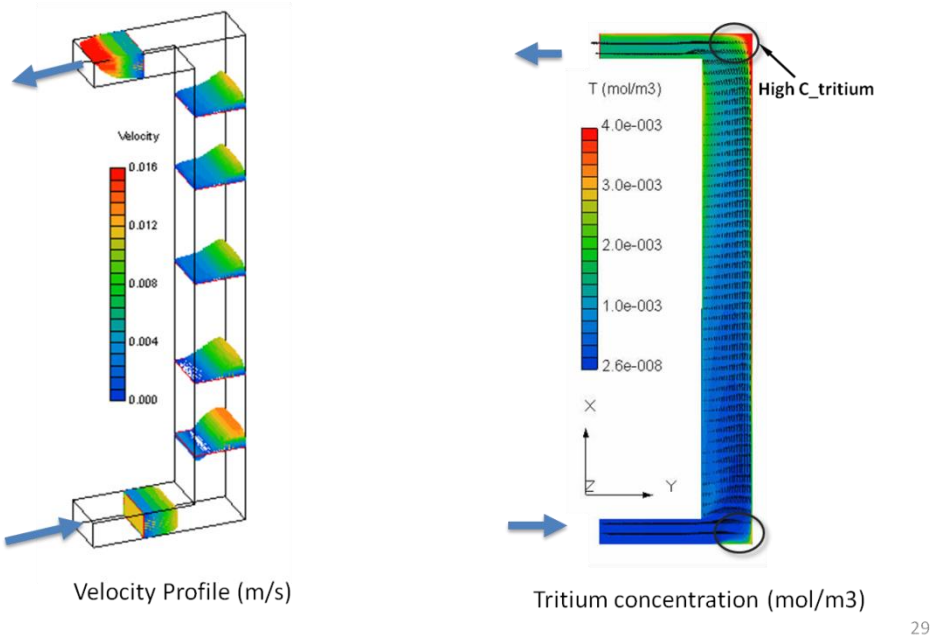

Figure 35. The velocity profiles and the corresponding tritium concentration distribution for the case of upward flow.

Figure 36 shows the tritium distribution along the side layer and Hartmann layer at different locations of x= -0.5m, 0, and 0.5m. It can be seen that tritium concentration is much lower for the case of upward flow than for the case of downward flow. This means that a much lower tritium inventory is expected for the case of upward flow.

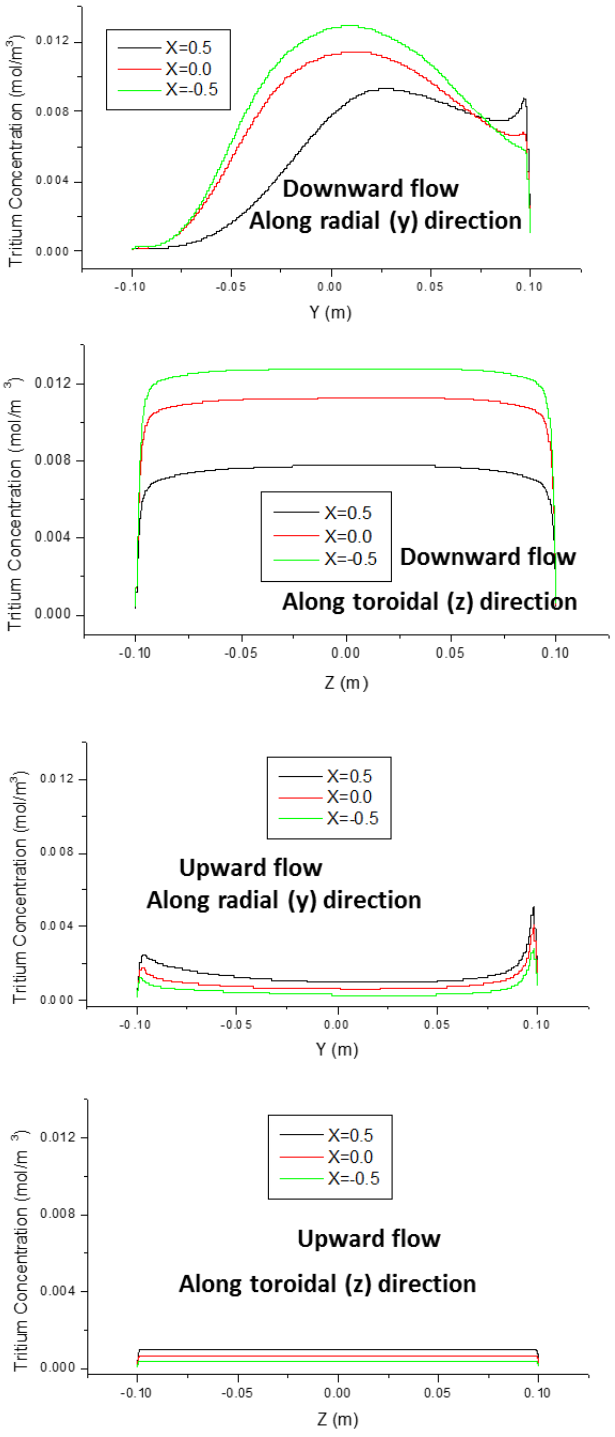

Figure 36. Tritium distribution along the side layer and Hartmann layer at different locations of x=-0.5m, 0, and 0.5m

To evaluate the influence of the buoyancy effect of the liquid flow between the cases of downward flow and upward flow, tritium permeation rate and inventory are summarized in Table 4. Based on the geometry, flow conditions, and material properties, the calculated permeation loss is about 5% of production for the case of downward flow. It is about 20% higher than the permeation loss for the case of upward flow, in which about 4% of produced tritium will permeate out through the wall. Meanwhile, tritium inventory for the case of upward flow dropped by nearly 80% compared to the case of downward flow.

Table 4. Tritium inventory and losses for the Buoyancy affected PbLi MHD flows

	Downward flow	Upward flow
Tritium generation rate (mol/s)	3.78e-7	3.78e-7
Tritium permeation rate (mol/s)	1.88e-8	1.55e-8
Losses percentage (%)	5%	4% (↓18%)
Tritium inventory (mol)	4.71e-4	9.53e-5 (↓80%)

5.3.5 Discussion of the Results based on the Parametric Studies

Parametric studies on the effect of the following key variables on the behavior of the tritium distribution, as well as on its permeation rate, were investigated: (1) the effect of the velocity profile, (2) the effect of the Hartmann number, (3) the effect of the tritium solubility, (4) the effect of the tritium diffusivity, and (5) the buoyancy effect. The principal features of the predicted tritium transport may be summarized as follows:

1. MHD effects will bring certain benefits in terms of reducing the tritium permeation rate due to the aspect of higher velocity near the wall region under the considered MHD conditions. Tritium concentration peaks close to the walls without MHD, while it becomes more concentrated in the center as the Hartmann number increases. As a result of lower tritium partial pressure near the wall, the permeation rate through the wall will be reduced. However, the rate of decrease due to the increase of Hartmann number becomes slower as the Hartmann number increases.

2. The calculation results indicated that the effect of the uncertainty in the values for tritium solubility in PbLi on tritium permeation is quite strong, especially for the reference range, in which the tritium permeation rate is most sensitive to the values of tritium solubility. Higher tritium solubility provides a lower tritium permeation rate.

3. The diffusion coefficient markedly affects the tritium permeation rate by controlling the amount of tritium diffusing from the PbLi to the PbLi/FS interface. Higher tritium diffusivity provides a higher tritium permeation rate.

4. In the buoyancy affected PbLi MHD flows under analyzed, there exists a strong shear layer at the center of the channel, and there is a region of buoyancy-induced reverse flow near the front wall for case of the downward flow. As a result, the calculated permeation loss is about 20% higher than the permeation loss for the case of upward flow. Tritium inventory for the case of upward flow dropped by nearly 80% compared to the case of downward flow.

5.4 Tritium Transport in a Poloidal Duct with FCI and PES

5.4.1 Introduction

In the DCLL blanket, the self-cooled breeder, PbLi, circulates for power conversion and tritium breeding, experiencing MHD effects. Reduced activation ferritic steel is used as a structural material. Helium is used to cool the first wall and the blanket structure. A key element of the DCLL concept is the flow channel insert (FCI) made of a silicon carbide composite (SiCf/SiC), which is used as an electric insulator to reduce the impact from the MHD pressure drop, and as a thermal insulator to separate the high temperature PbLi from the ferritic structure. The FCI is separated from the wall by a thin gap filled with the same

liquid metal. The same pressure head drives the liquid metal through the channel and the gap. There can be openings in one of the walls of the FCI, such as a pressure equalization slot (PES), to equalize the pressure on both sides of the FCI, thus resulting in almost no primary stresses in the insert. However, the FCI and PES affect the tritium transfer behavior and loss rate. First, they change the local MHD velocity distribution, which in turn affects tritium diffusion and convection. Secondly, the PES provides a path for tritium to migrate between the core and the gap. Therefore, the objective of this case study is to evaluate the impact of the PES on tritium transport and permeation.

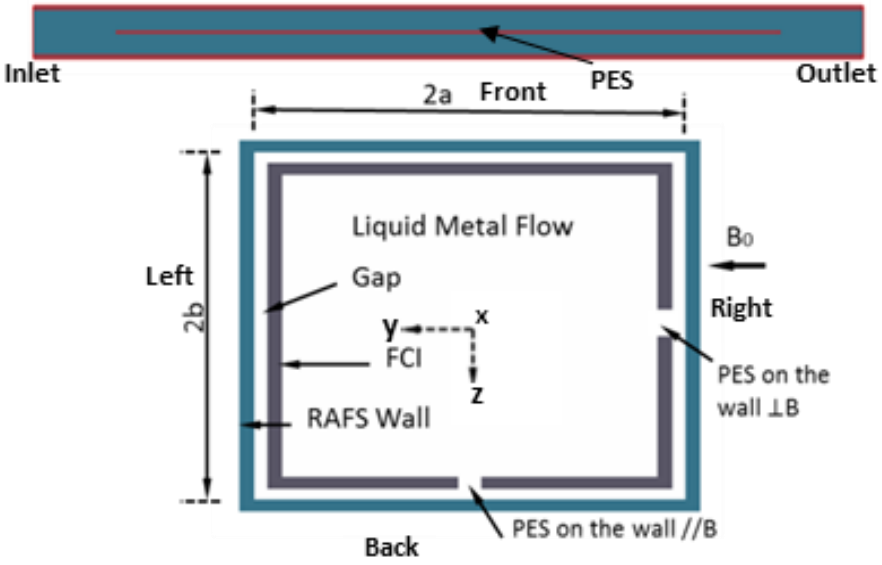

Figure 37. The cross-section drawing of the blanket duct shows the PES openings. Here the PES is opened from x=0.1m to 0.9m and with 2a=0.06m, 2b=0.06m, RAFS wall 0.002m, FCI 0.002m, PES 0.003m, Gap 0.002m

5.4.2 PES Effect on Tritium Concentration and Permeation

In this study, we formulate the problem in 3D and numerically solve the complete set of governing equations with appropriate boundary conditions at various interfaces. The tritium transport is analyzed in a front duct in a DCLL-type outboard blanket where PbLi moves poloidally. Three types of poloidal ducts have been investigated: one without the PES, one with the PES in the wall parallel to the magnetic field, and one with the PES in the wall perpendicular to the field. A sketch of the cross-sectional area of the liquid metal blanket channel with FCI is shown in Figure 37.

The velocity field is obtained by performing a 3D simulation with magnetic field strength of 1.852T. The electrical conductivities are $\sigma_{LM}=7\times10^{5}\Omega^{-1}m^{-1}$, $\sigma_{FS}=1.46\times10^{6}\Omega^{-1}m^{-1}$, $\sigma_{FCI}=5\times10^{2}\Omega^{-1}m^{-1}$. Non-uniform meshes with dimensions 216×195×164 are used to discretize the geometry with 216 non-uniformly distributed meshes in the x-direction. We assume that the inlet velocities are same over gap and core, a uniform velocity of U0=0.0675m/s is given as an inlet boundary condition, the pressure at the outlet is specified as zero, and non-slip boundary conditions are applied on the solid walls.

Velocity distributions at the cross-section of x=0.5m are plotted in Figure 38. In Figure 38(a) for the case of no PES, when we set y=0, we see the velocity profile has a relatively

high velocity in the gaps parallel to the magnetic field and a very low velocity in the gaps perpendicular to the field. When any PES is introduced, the high velocities in the front and back gaps disappear. Figure 38 also shows that when a PES is opened parallel to the field, we see a strong reversed flow at the location of the PES due to a large component of Lorentz force along the negative main flow direction. In Figure 38(b), we have set z=0. In the figure we see flat-shaped velocity profiles in the core and very low velocities in the left and right gaps. For the case of a PES opening perpendicular to the field, the velocity is not symmetric. It is higher in the right gap than left gap, and a velocity drop in the core near the location of the PES is observed. These velocity profiles match earlier observations for various FCI flows reported in [8]. A full three dimensional plot of the results from the cross-section at x=0.5 is also given in Figure 39 for clarity.

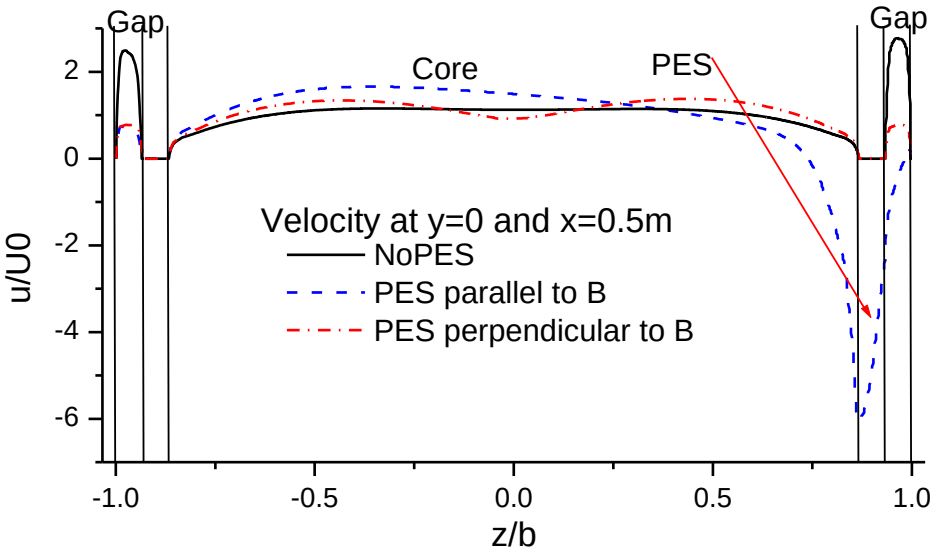

(a) along y=0

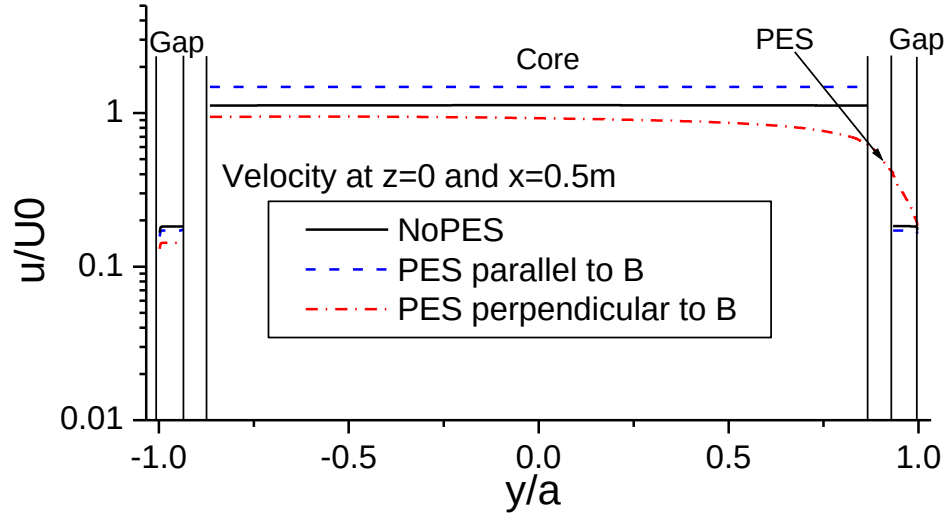

(b) along z=0

Figure 38. Velocities at the cross-section of x=0.5m. (a) Along y=0, it shows a strong reversed flow near the insert for the case of PES is opened parallel to the field. (b) Along z=0, it shows flat-shaped velocity profiles in the core and very low velocities in the left and right gaps.

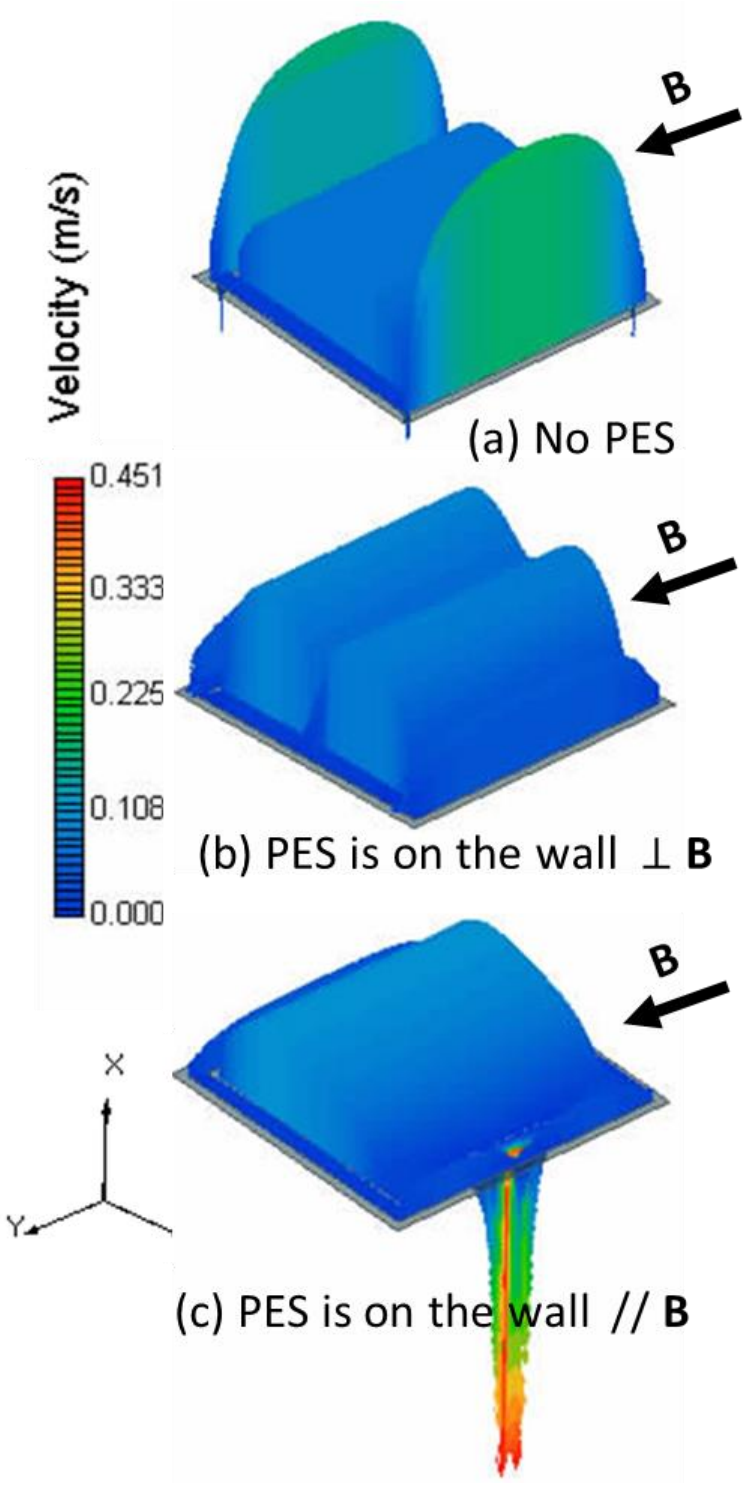

Figure 39. Velocity profiles at a cross section of x=0.5m for various PES configurations.

The computer code to solve the FCI flow field has been validated by solving Ming-Jiu Ni's case [8]. In Ni's case, a PES is opened parallel to the magnetic field, and GaInSn was selected as the liquid metal with 2a = 34mm and 2b = 40mm. The velocity profile at the cross-section of x=0.5m as seen in Figure 40 shows good agreement with Ni's solution.

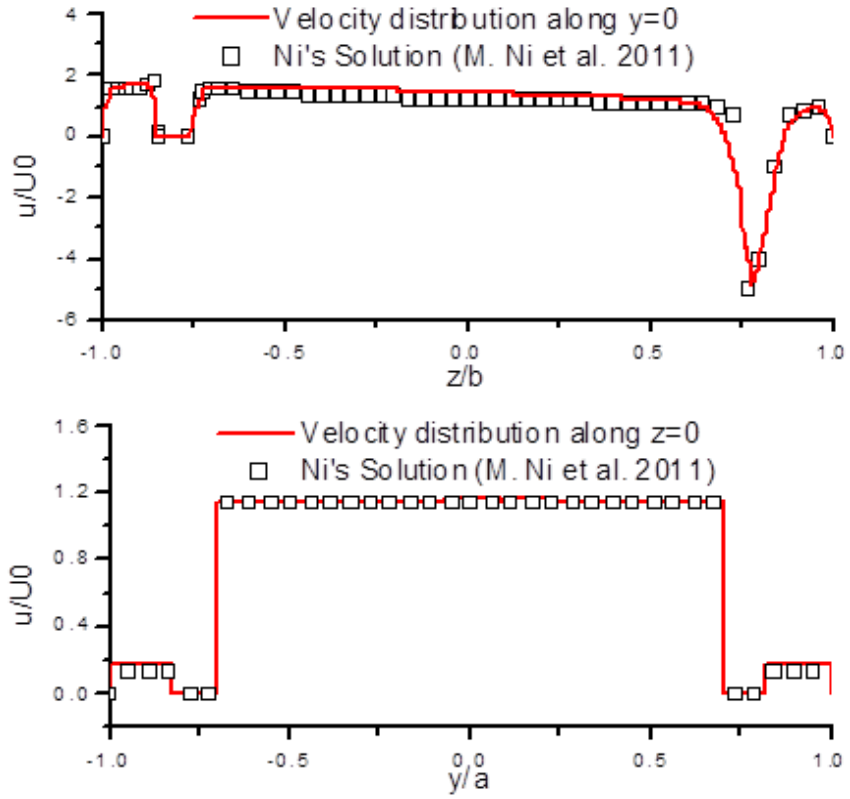

Figure 40. Comparison of velocity at y-z cross-section.

Tritium concentration fields are obtained by solving a fully 3-D problem with the aforementioned boundary conditions at various interfaces. Additionally, zero concentration

is given at the inlet and a convective flux boundary condition is given at the outlet. The tritium generation rate is plotted in Figure 9.

Figure 41 shows the tritium concentration profiles at the cross-section of x=0.5m for the three different PES configurations. Without a PES opening in an FCI, the tritium concentrations in the gaps aligned perpendicular to the magnetic field are higher than in the other two gaps and in the core, as seen in Figure 41(a). Tritium concentration increases in the positive z-direction of the gaps, reflecting the decreased tritium generation rate away from the front wall. Also, because of the high velocity jet found in the front and back gaps, tritium concentration near the front wall is reduced. With a PES in a wall perpendicular to the magnetic field, the concentrations in the right gap became lower than in the left gap, which reflects the non-symmetric velocity profile described in Figure 38(b). Also, a weak concentration jump was formed around the PES as seen in Figure 41(b). With a PES in a wall parallel to the magnetic field, such as in Figure 41(c), we see a high tritium concentration in the bulk area near the location of the PES, which is due to the reversed flow at that location.

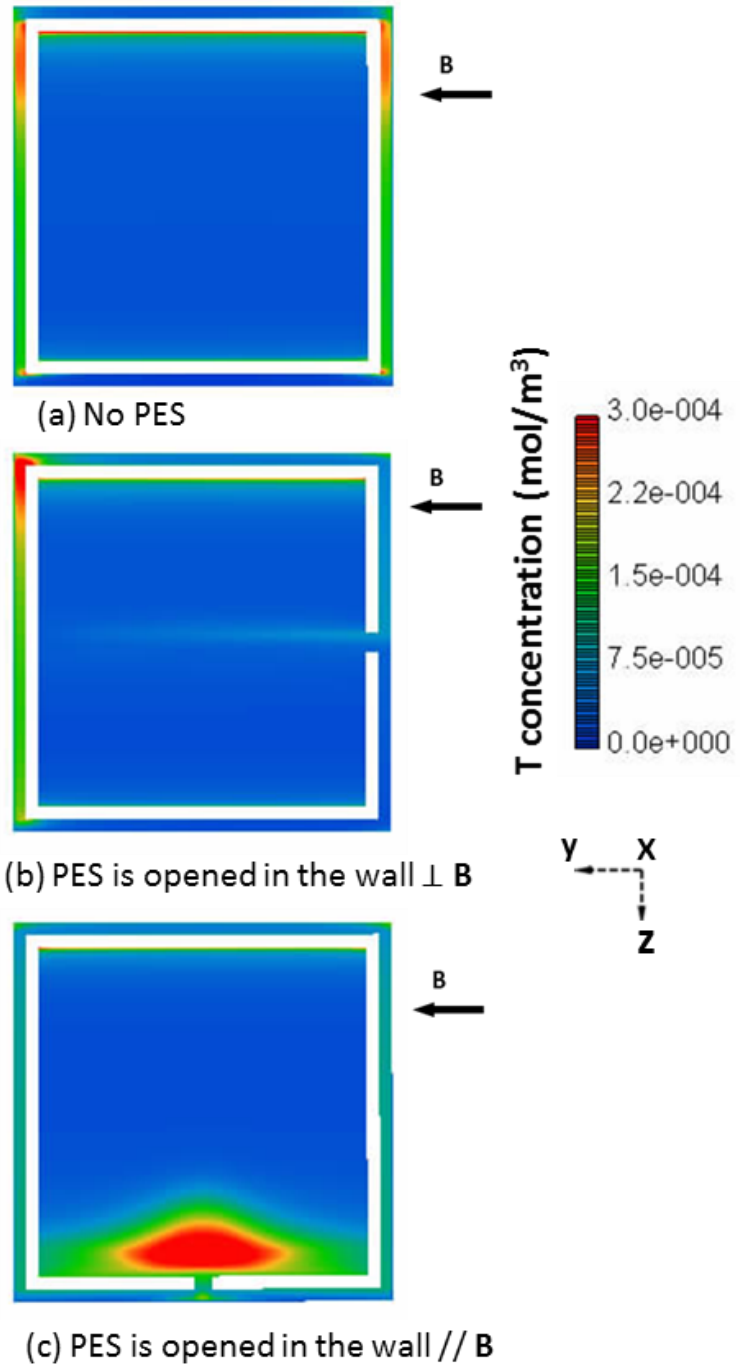

Figure 41. Tritium concentrations at a cross section of x=0.5m for various PES configurations.

Figure 42 also demonstrates the features seen in Figure 41(c). In Figure 42, we are seeing the tritium distribution at the cross-section of y=0 along the flow direction. Tritium accumulates in the core area above the PES. It is also interesting to notice that tritium accumulates near the back wall behind the PES end, as marked by the cycle region and resulting in a local tritium permeation jump, as shown in Figure 45(c). This is due to very low velocities in that area, as shown by the arrow plot of velocity in Figure 42.

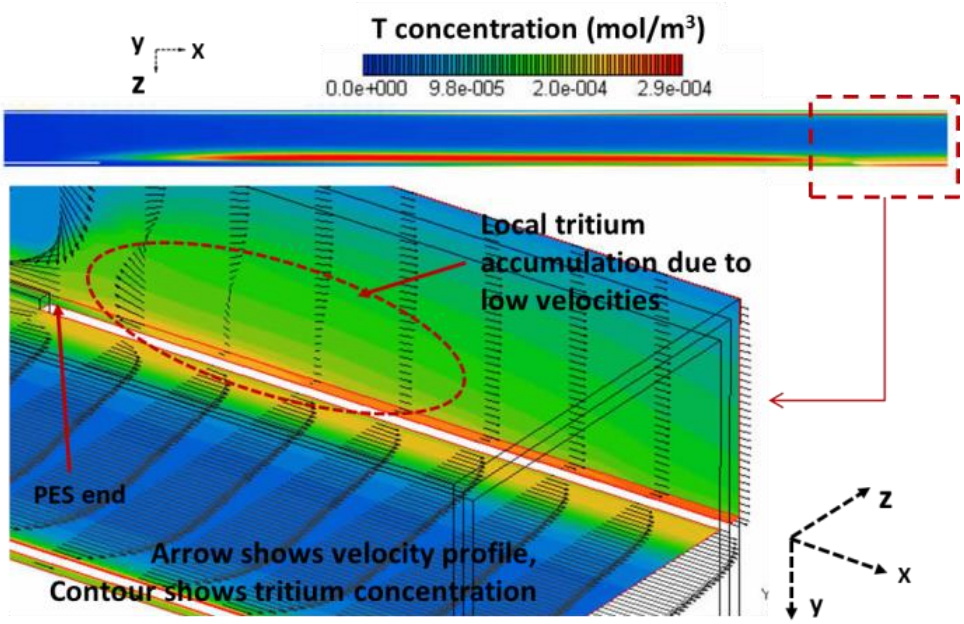

Figure 42. Tritium concentration near the outlet (bottom) and at the cross-section of y=0 (top) with PES wall parallel to the field. Here Tritium accumulated in the core area above the PES and in the back gap behind the PES end.

When we plot the tritium concentrations at the same cross-sections as in Figure 38, we see the interesting coupling between velocity and tritium concentration. This is done in Figure 43 and Figure 44, where the tritium concentrations at the cross-section of x=0.5m are plotted along y=0 and z=0, respectively. These tritium concentration curves correspond to the velocity profiles seen above. The important conclusion is that high tritium concentrations are always associated with low-speed velocities. For example, in the front and back gaps, as seen in Figure 43, the case of no PES (which has a relatively high velocity profile) gives the lowest tritium concentrations. The highest concentrations are observed when the PES is opened parallel to the field and occurs complementary to the velocity decrease shown in Figure 38.

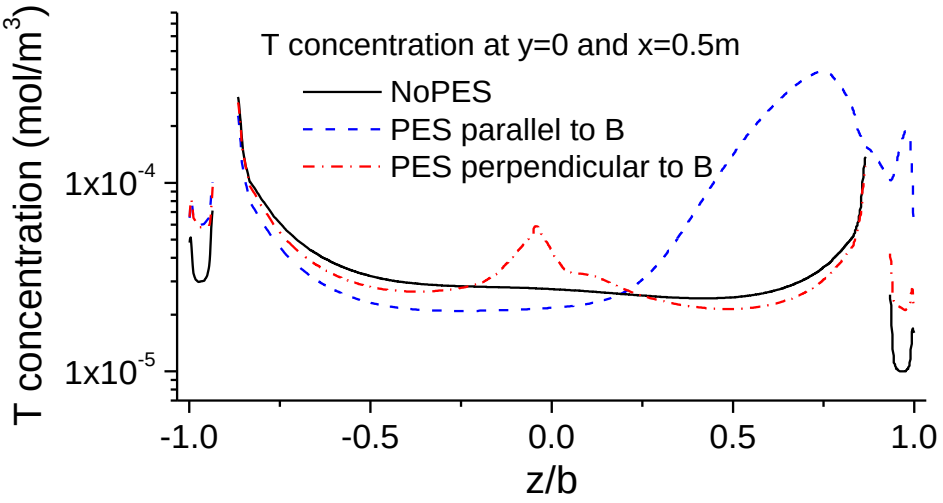

Figure 43. Tritium concentrations along the line of y=0m at the cross-section of x=0.5m shows a high tritium concentration in the bulk area near the location of the PES for the case of PES is opened parallel to the field

Along z=0, as shown in Figure 44, tritium concentrations in the left and right gaps are higher than in the core for all three cases. The case of no PES gives a higher tritium concentration, and the case of the PES opening parallel to the field gives a lower concentration. When the PES is opened perpendicular to the field, it results in the highest tritium concentration in the left gap and the lowest concentration in the right gap compared to other two cases. Figure 43 and Figure 44 show that the tritium transport across the PbLi is not only governed by diffusion, but can be dominated by the advective movement of the bulk PbLi.

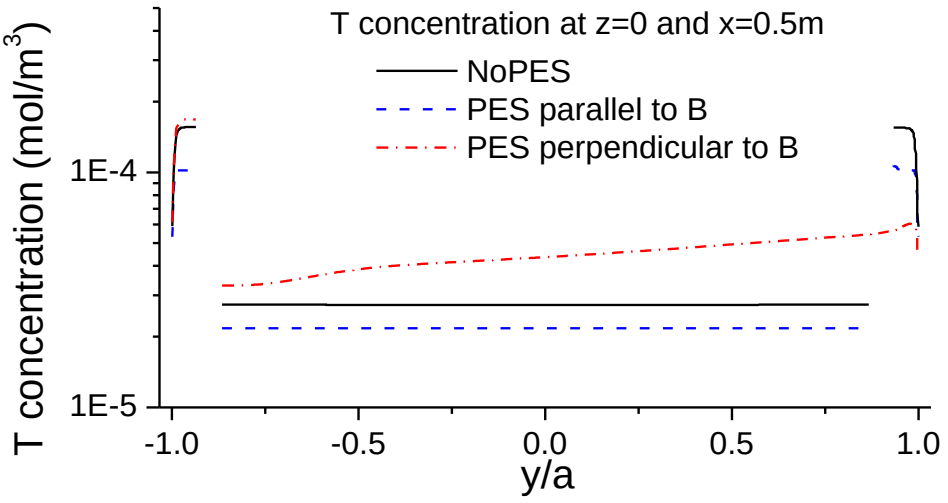

Figure 44. Tritium concentrations along the line of z=0m at the cross-section of x=0.5m shows higher concentrations in the gaps than in the core

Figure 45 shows the tritium permeation per unit length through the front, back, left, and right LM/FS wall. For the case of no PES in the FCI, tritium permeation is higher through the left and right walls than the front and back walls, due to high concentrations in the left and right gaps, as highlighted in Figure 41(a). Tritium permeation through front wall is higher than the back wall, because of the high tritium generation rate in the front gap. With a PES opening in the right wall, which is perpendicular to the magnetic field (Figure 45(b)) the front wall has the highest permeation flux, and the back wall has the lowest value. There is also a difference between the left wall and right wall. Tritium permeation is lower through the wall on the PES side, as seen in Figure 45(b), because of lower tritium concentration in

the right gap. With a PES opening in the back wall parallel to the magnetic field, tritium permeation is higher through the front wall, as seen in Figure 45(c), while the permeation through the back wall (where the PES is located) increases compared to the other two cases. It is also interesting to notice that there is a tritium permeation jump through back wall behind the end of the PES. This is attributed to high tritium concentration in that area due to low velocities, as described with Figure 42.

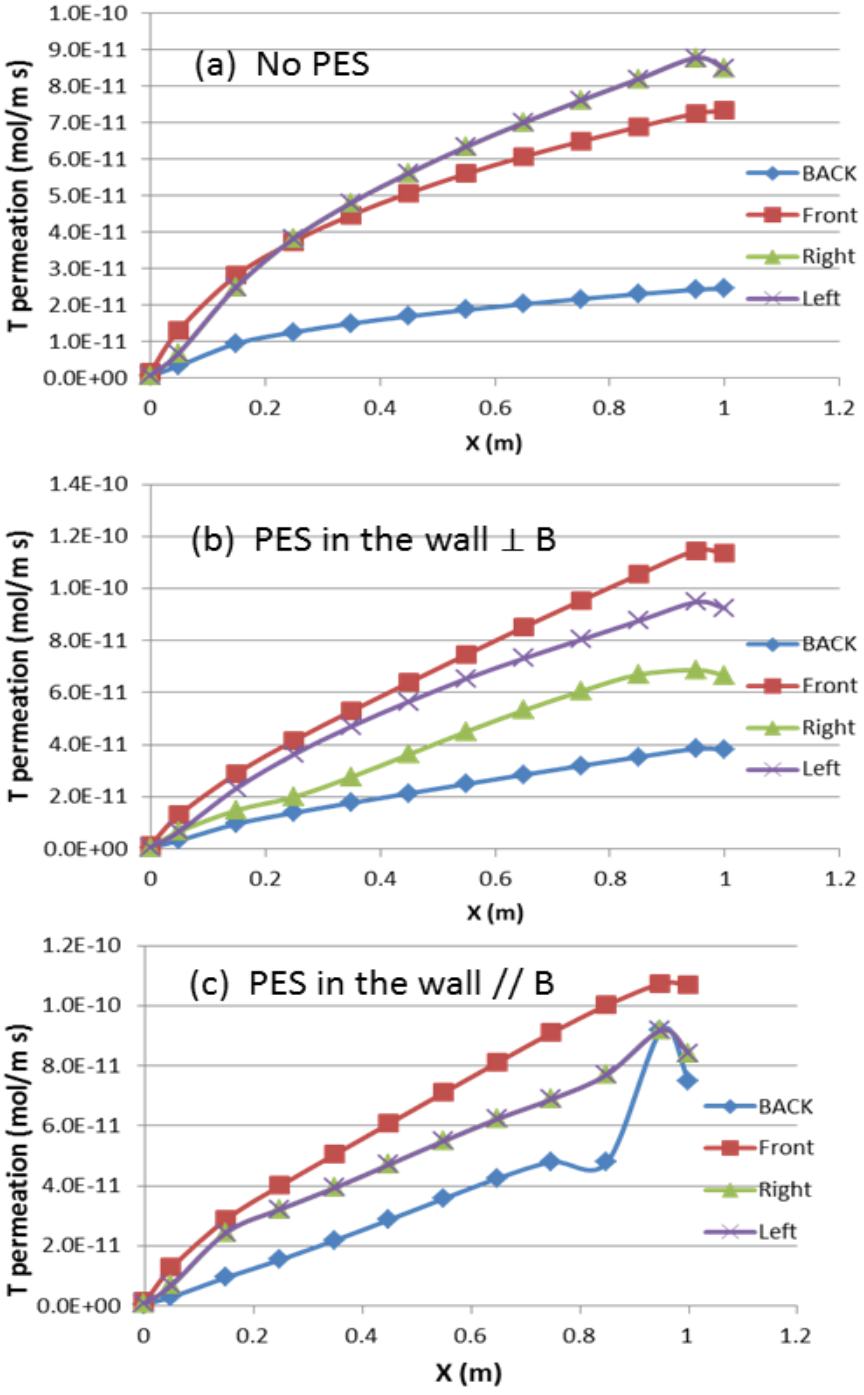

Figure 45. Tritium permeation per unit length through the LM_FS walls (the front, back, left and right walls).

Figure 46 shows the total tritium permeation through the four LM/FS walls. It can be seen that tritium permeation is higher when the PES is opened in the wall parallel to the magnetic field. The overall permeation losses for the three different PES configurations are summarized in Table 5. For the case without a PES under the given conditions, tritium loss is 1.25% of the tritium production, which confirms earlier results (tritium permeation loss is less than 2% of the total tritium production [11]) for a DCLL duct flow without PES. When the PES is opened perpendicular to the magnetic field, it results in a higher tritium loss of 1.32% of the tritium production. The case of the PES opening parallel to the field gives the highest tritium loss of 1.41% of tritium production. The amount of increase in tritium permeation is minimized because the PES is located in the back wall where tritium generation rate is lower.

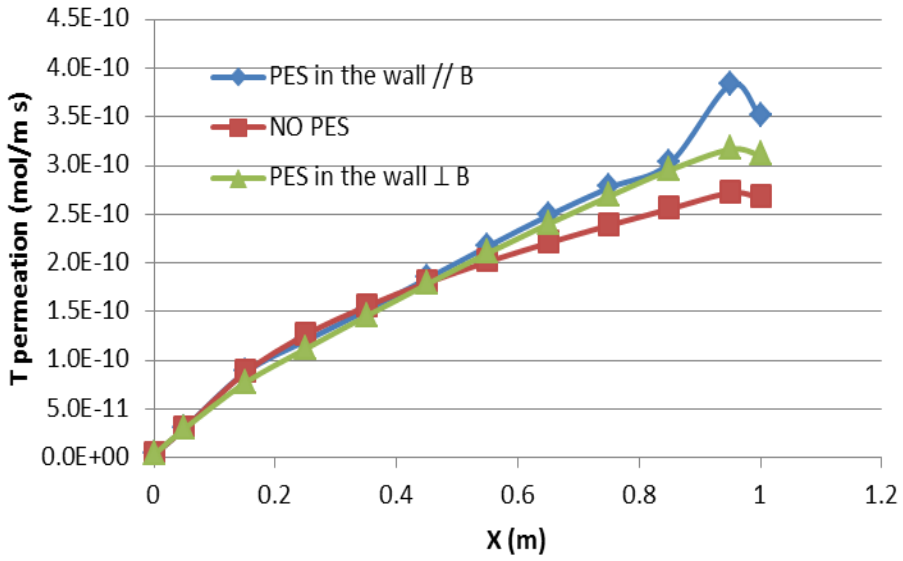

Figure 46. Total tritium permeation per unit length through LM-FS walls

Table 5. Tritium Losses for Three PES Configurations

	No PES	PES in the wall // B	PES in the wall ⊥ B
Tritium generation rate (mol/s)	1.406e-8	1.410e-8	1.412e-8
Tritium permeation rate (mol/s)	1.76e-10	1.99e-10	1.87e-10
Losses percentage (%)	1.25%	1.42%	1.32%

5.4.3 Effect of the FCI Electric Conductivity

The electric conductivity of the FCI affects the electromagnetic coupling between the flow in the gap and the bulk and thus changes the velocities in the gap and the bulk. As the electric conductivity of the silicon carbide composite decreases, the effect of electromagnetic coupling between the flow in the gap and the bulk flow reduces; thus the velocity in the gap drops [11].

Figure 47 shows the effect of a change in the electric conductivity of the FCI on the tritium permeation rate for the case of the PES opened on a side wall away from the FW. Five cases were investigated in the range of reference values of electric conductivity of the FCI from 5 to 500 $\Omega^{-1}m^{-1}$. As shown in the figure, the electric conductivity of the FCI clearly affects the tritium permeation rate by changing the velocity in the gaps. A higher electric conductivity of the FCI provides a higher velocity in the gap and thus a lower tritium permeation rate. Over the range of reference electric conductivity of the FCI from 5 to 500 $\Omega^{-1}m^{-1}$, tritium permeation rate decreased by about 46%.

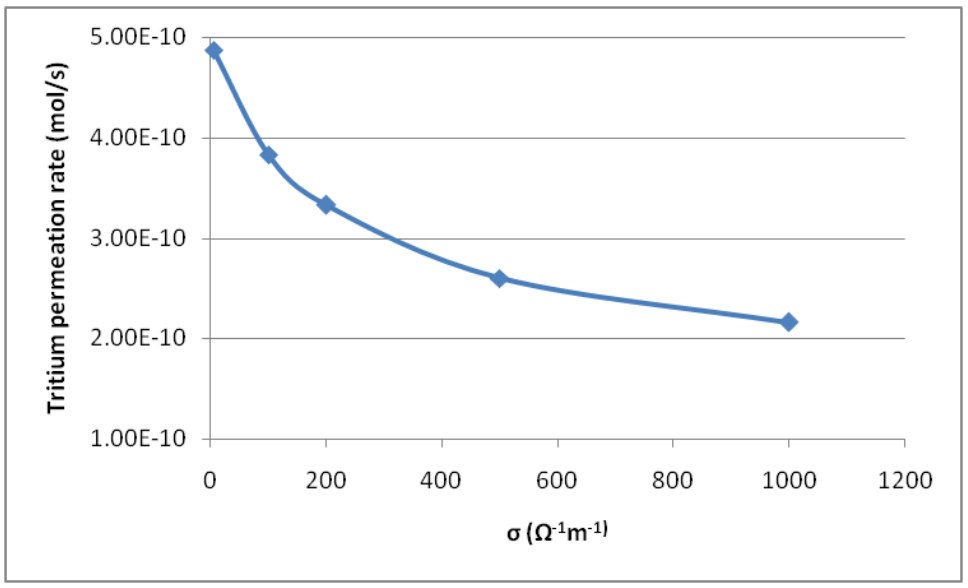

Figure 47. Tritium loss rate as a function of FCI conductivity

5.4.4 Discussion of the Results

In this case study, we analyzed tritium transport and quantified the tritium loss rate in a front duct of the DCLL-type outboard blanket where PbLi moves poloidally. Three types of poloidal ducts have been considered: one without the PES, one with the PES in the wall parallel to the magnetic field, and one with the PES in the wall perpendicular to the magnetic field.

As a result of the analysis, the following remarks can be made:

1. A PES in the FCI changed the velocity profiles and thus changed the tritium concentrations in the core and gaps. High tritium concentrations are always associated with low-speed velocities.

2. In the case without the PES in the FCI, high tritium concentration is observed in the Hartmann gaps because of the low velocities there. Tritium concentration is low in the back gap (the side gap away from the first wall) because of relatively high velocities and a low tritium generation rate there. Tritium concentration is higher in front gap (the side gap near the first wall) than in the back gap because of the higher tritium generation rate there. As a result, tritium permeation flux is higher through the Hartmann walls due to the higher tritium concentration in the Hartmann gaps, and tritium permeation flux is higher through the front wall than the back wall.

3. In the case with the PES in the side wall away from the FW, in the slot, the electric current flows perpendicular to the magnetic field lines, resulting in a strong flow-opposing Lorentz force, which turns the flow in the slot region in the opposite direction. The slot also affects the flow jet in the side gaps, which is reduced in comparison to the case of no slot. As a result of the change in velocity profile due to the PES, a lower mass flow rate in the front gap provides a higher tritium concentration and thus increases the tritium permeation

rate through front gap. We see a high tritium concentration in the bulk area near the location of the PES, which is due to the reversed flow at that location.

4. In the case with the PES in the Hartmann wall, all major flow features observed in the case with no openings, such as near-wall jets, are essentially the same, but the magnitude of the velocity in the side gaps is reduced. Another difference occurs within a narrow area adjacent to the slot. In this area, the velocity profile exhibits a velocity deficit zone, stretching from the wall with the slot to the opposite Hartmann wall. As a result of the change in velocity profile, the concentrations in the Hartmann gap near the slot became lower than in the opposite gap, which reflected the non-symmetric velocity profile. Also, a weak concentration jump was formed around the velocity deficit zone.

5. Under the given conditions, the case of a non-PES duct gives the lowest tritium loss of 1.25% of the tritium production, while tritium loss increased nearly 15% to 1.42 % for the case of PES opening parallel to the magnetic field. This is mostly because of the increasing of the permeation through the front wall due to the velocity is reduced when the PES is introduced.

6. The electric conductivity of the FCI clearly affects the tritium permeation rate by changing the velocity in the gaps. A higher electric conductivity of the FCI provides a higher velocity in the gap and thus a lower tritium permeation rate.

5.5 Tritium Transport in a DCLL U-shaped Flow

5.5.1 Background Information

In the previous section, we analyzed tritium transport in a DCLL-type duct flow. To provide the realistic prediction regarding the tritium transport and permeation in the DCLL blanket concept, a DCLL U-shaped flow which represented the current US DCLL design was constructed, and the results are presented and discussed in this section.

The reference DCLL design is illustrated in Figure 48. Three U-shaped ducts with FCI and FS walls connect through inlet/outlet with manifolds. PbLi starts in the feeding circular pipe, then the PbLi expands in the manifolds and distributes into three channels. The liquid metal flows among three back channels and then into the front channels by passing through the U-turns. After distributing into the front channels, the fluid is collected in the outlet manifold. A detailed description of DCLL blanket design specifications is reported in reference [9]. Since the configurations for all three channels are similar, simulations were only done for the center channel as representative of the three channels (Figure 49).

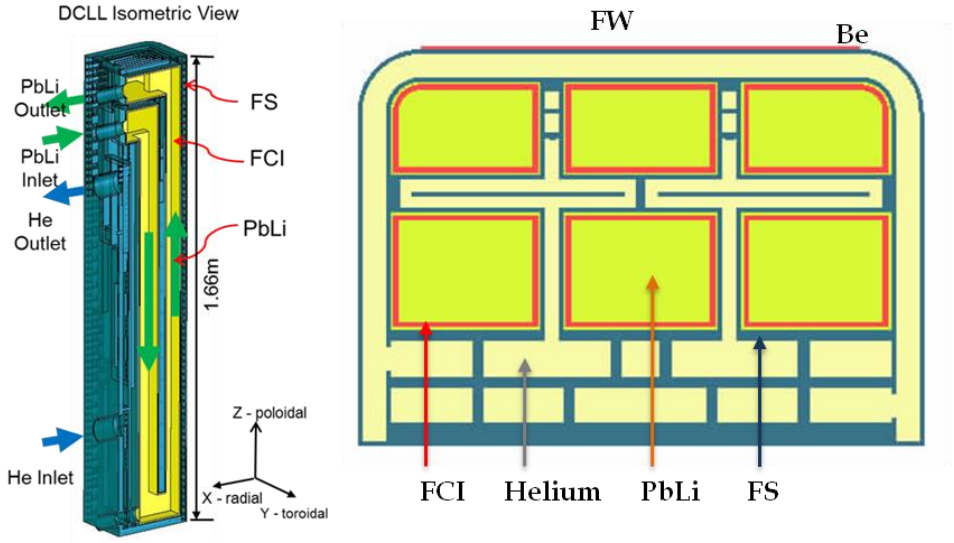

Figure 48. The reference DCLL design: Three U-shaped duct flow with FCI and FS walls connected through inlet/outlet with manifolds

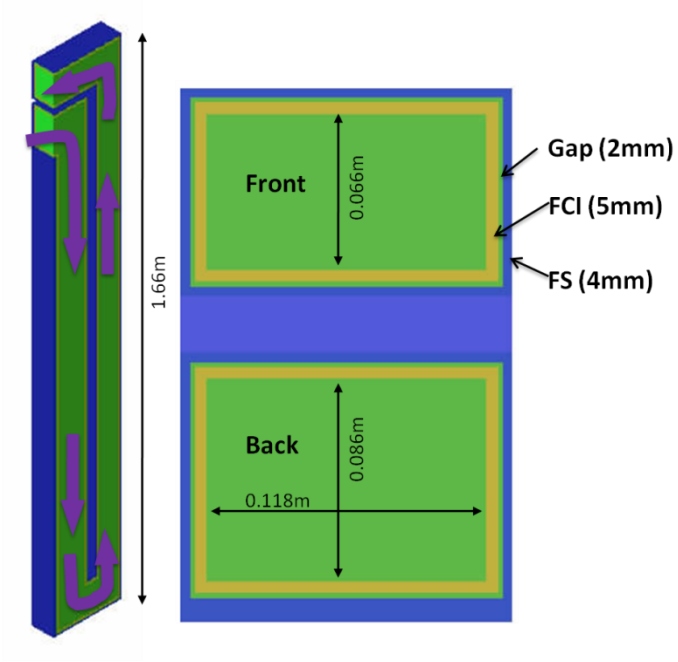

Figure 49. The analyzed DCLL central U-shape channel as representative of the three channels

5.5.2 Estimation of Tritium Permeation in a DCLL U-shaped Flow

The velocity field is obtained by performing a 3D simulation with a magnetic field strength of 1.8T and with an inlet velocity of liquid metal of 0.049 m/s. With these values, the liquid metal velocity will be about 0.7m/s in the front channel and 0.09m/s in the back channel. Figure 50 shows the velocity profiles due to MHD effects in the channels and 3D effects near the bends and manifolds. There are similar velocity profiles in the front and back channels (as discussed in Section 5.4 Tritium Transport in a Poloidal Duct with FCI and PES), i.e. higher velocities in side gaps and very low velocities in Hartmann gaps. Local circulated flows are observed in the bend areas as marked in the figure.

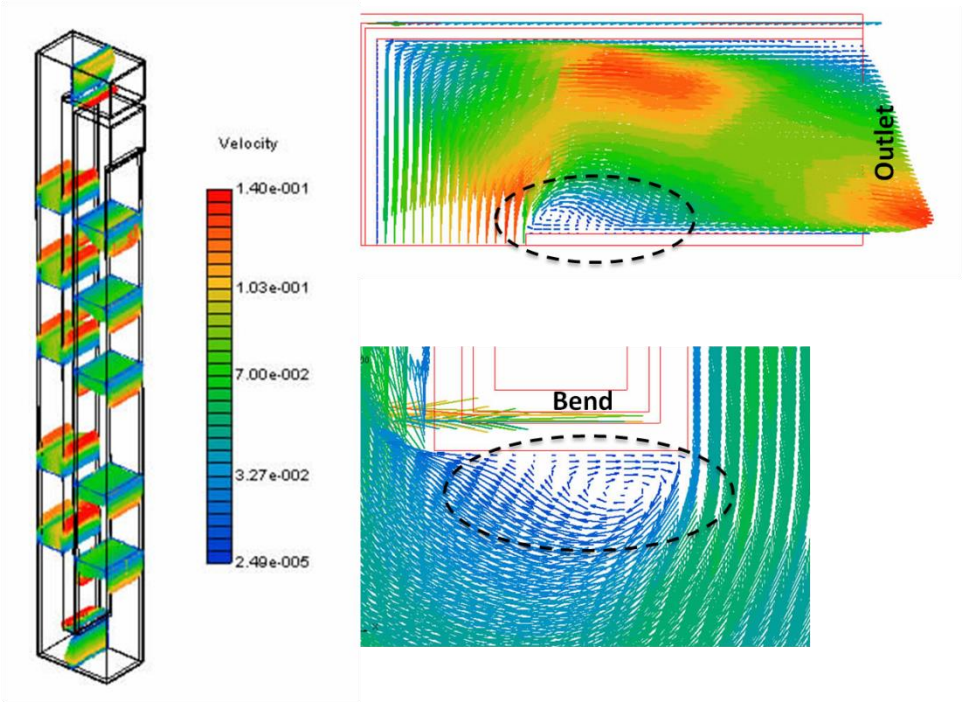

Figure 50. Velocity profile shows higher velocities in side gaps and very low velocities in Hartmann gaps and local circulated flow near the bend areas.

The tritium transport calculation is performed by solving a fully 3-D mass transfer problem with appropriate boundary conditions at various interfaces, as discussed in Chapter 3. Additionally, zero concentration is given at the inlet and a convective flux boundary condition is given at the outlet. The tritium generation rate is plotted in Figure 9.

Tritium diffusion coefficients and Sievert's constants are dependent on temperature and activation energy. There is a dramatic discrepancy between the values computed and presented in various references. The values used in this study are listed in Section 5.2.

Figure 51 displays the contour plots of the tritium concentrations along the channel, showing lower values in the back channels and accumulation along the PbLi pathway. Tritium concentrations in the channel, reflecting the velocity profile effect, are well-described by Figure 51, where the detailed tritium concentration is plotted on the central cross-section of the channel. There is high tritium concentration in the Hartmann gaps because of the low velocities, and low tritium concentration in the side gaps because of relatively high velocities there. Tritium concentration decreasing in the radial direction of the gaps reflects the decreased tritium generation rate away from the front wall. The detailed tritium concentration near the bend areas, as plotted in Figure 52, shows relatively high local tritium concentration near the local circulated flow area.

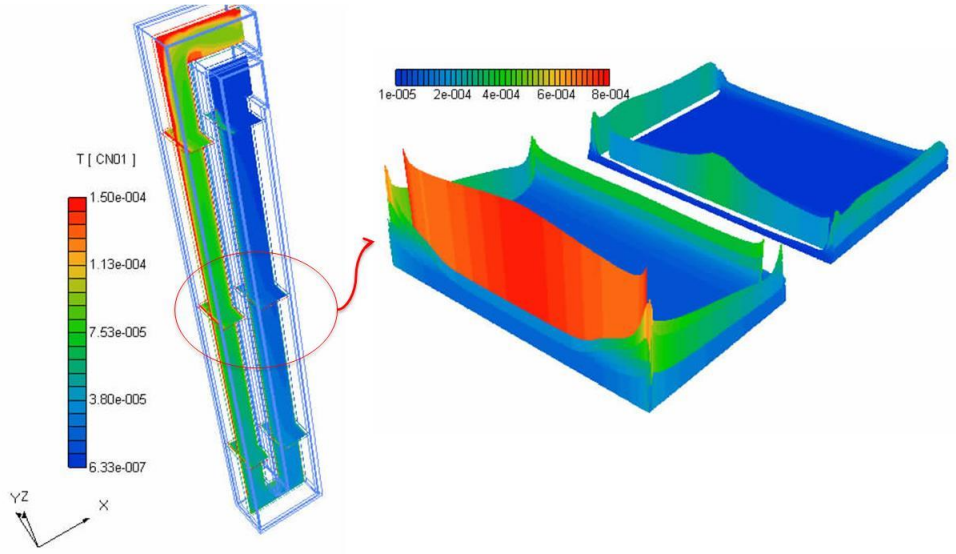

Figure 51. Tritium concentrations (mol/m^3) in DCLL channel with toroidal magnetic field and radial distributed tritium production.

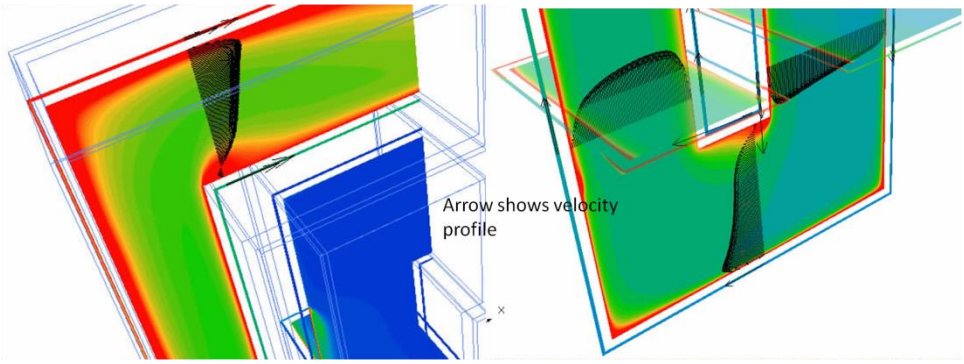

Figure 52. Tritium concentrations (mol/m^3) near the bend areas shows relatively high local tritium concentration near the local circulated flow area

Figure 53 shows the tritium permeation flux through the FS wall, showing lower values in the back channels and increasing along the PbLi pathway. Tritium permeation flux is higher through the Hartmann walls due to higher tritium concentration in the Hartmann gaps, as discussed before. Tritium permeation through the front wall is higher than the back wall because of the high tritium generation rate in the front gap.

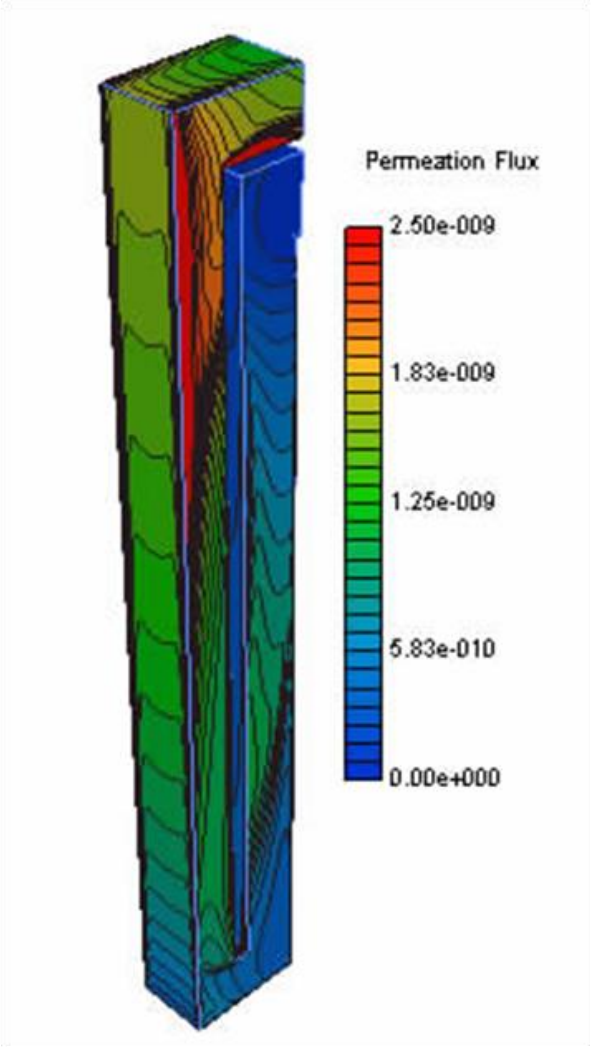

Figure 53. Tritium permeation flux (mol/m^{2}s) through FS wall shows relatively higher values through the Hartmann walls than side walls.

The overall tritium generation, inventory, and permeation for the analyzed DCLL channel are summarized in Table 6. Under the given conditions, 1.2% of generated tritium permeates through the FS wall to the helium coolant.

Table 6. Summary of tritium generation, inventory and permeation for the analyzed DCLL channel

	DCLL U-shaped Channel
Tritium generation rate in PbLi (mol/s)	9.72e-8
Tritium inventory (mol)	2.64e-6
Tritium exit rate from outlet (mol/s)	9.60e-8
Tritium permeation rate (mol/s)	1.16e-9
Losses percentage (%)	1.2%

5.5.3 Influence of the Gap Flow Rate due to the Inlet Manifold

In previous analysis, we assumed that the inlet velocities are same over gap and core, however, one important issue which needs to be addressed is associated with the contribution of the inlet manifold. The inlet manifold design will enhance the fraction of liquid flow in the gap, or in the other hand increase mass flow rate in the core, and the resulting effect on the tritium permeation from the gap to the coolant might be important. Since the manifold

design for DCLL is not finalized, a sensitivity analysis for the influence of the gap flow rate due to the inlet manifold design has been carried out and used to help understand and predict the tritium permeation.

With the aim of investigating the influence of a change in the fraction of the liquid flow between the gap and the core, the ratio of inlet velocity of the gap over the inlet velocity of the core $\frac{\mathbf{U}_{\mathbf{inlet\_gap}}}{\mathbf{U}_{\mathbf{inlet\_}core}} = 1$ was replaced by $\frac{\mathbf{U}_{\mathbf{inlet\_gap}}}{\mathbf{U}_{\mathbf{inlet\_}core}} = 0.1$. As a result of the change, a large increase of tritium concentration in the gap was observed (see observed tritium concentration profile in Figure 54). The resulting effect on tritium permeation rate and inventory is summarized in Table 7. A lower mass flow rate in the gap provides a higher tritium concentration in the gap and thus increases the tritium permeation rate. Over the range of the ratio of inlet velocity of the gap over the inlet velocity of the core from 1 to 0.1, tritium permeation rate increases from 1.16e-9 mol/s by 140% to 2.81e-9 mol/s.

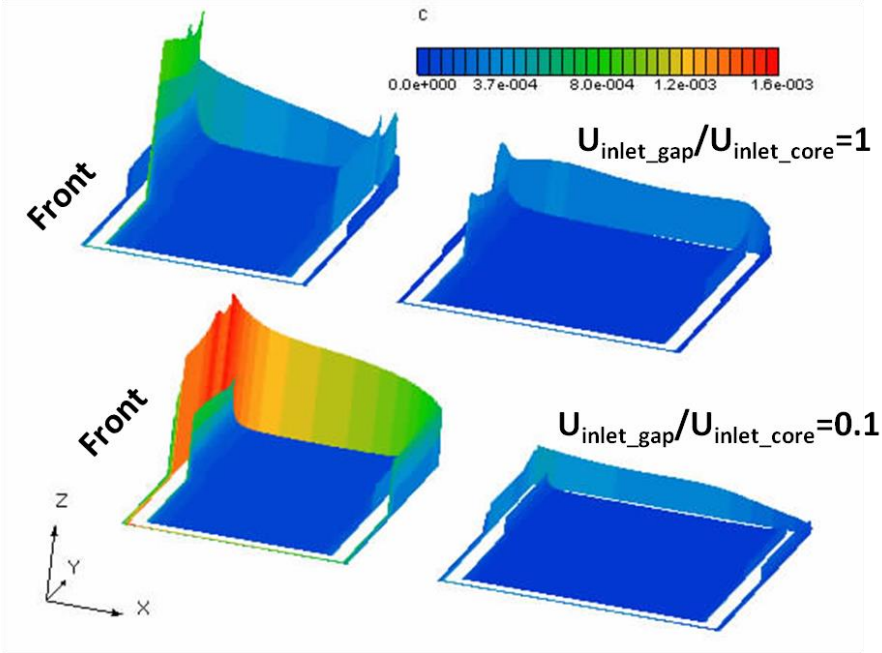

Figure 54. Comparison of tritium concentrations (mol/m^3) in DCLL channel with a change of the ratio of gap inlet velocity over the core inlet velocity from 1 to 0.1.

Table 7. Summary of tritium generation, inventory and permeation for the analyzed DCLL channel with a change of the ratio of gap inlet velocity over the core inlet velocity from 1 to 0.1.

DCLL U-shaped Channel	$\frac{\mathbf{U}_{\mathbf{inlet\_gap}}}{\mathbf{U}_{\mathbf{inlet\_}core}}=1$	$\frac{\mathbf{U}_{\mathbf{inlet\_gap}}}{\mathbf{U}_{\mathbf{inlet\_}core}}=0.1$
Tritium generation rate in PbLi (mol/s)	9.72e-8	9.72e-8
Tritium inventory (mol)	2.64e-6	3.57e-6
Tritium exit rate from outlet (mol/s)	9.60e-8	9.44e-8
Tritium permeation rate (mol/s)	1.16e-9	2.81e-9
Losses percentage (%)	1.2%	2.9%

5.5.4 Discussion of the Results

Results of the tritium transport and permeation for the case of a DCLL U-shaped channel have been presented in the previous section. The following remarks can be made:

- Tritium concentration has a strong dependence on velocity. High tritium concentration in Hartmann gaps is observed because of the low velocities, and low tritium concentration in side gaps is observed because of relatively high velocities. Meanwhile, local concentration peaks appear near the bend areas due to the local circulated flow.
- Tritium permeation flux is higher through Hartmann walls due to a higher tritium concentration in Hartmann gaps.
- The contribution of the inlet manifold has a strong effect on tritium permeation. A lower mass flow rate in the gap provides a higher tritium concentration in the gap and thus increases the tritium permeation rate. Under the given conditions, the case of $\frac{\mathbf{U}_{\mathbf{inlet\_gap}}}{\mathbf{U}_{\mathbf{inlet\_}core}} = 1$ gives a lower tritium loss of 1.2% of the tritium production, while tritium loss increased by nearly 140% for the case of $\frac{\mathbf{U}_{\mathbf{inlet\_gap}}}{\mathbf{U}_{\mathbf{inlet\_}core}} = 0.1$. It results in a higher tritium losses of 2.9% of the tritium production.

5.6 Tritium Transport in the HCLL Breeder Units and Comparison with the DCLL Case

5.6.1 Background Information

Tritium transport in a LM blanket is an important issue and a complicated phenomenon. The framework of the predictive capability has been developed which can predict tritium transfer in multi-materials in 3D geometry with flowing liquid metal. To compare HCLL and DCLL blanket concepts based on tritium transport and permeation, a 3D simulation of tritium transport in a HCLL-type blanket was performed. This blanket concept is characterized by a low velocity of the liquid metal breeder, which is about 2 orders of magnitude lower than in the DCLL concepts since the Pb–17Li is only used for tritium extraction not for heat extraction. This means that typical Pb–17Li velocities in the HCLL module are in the order of mm/s. The geometry under study consists of two breeder units (BU) separated by stiffening plates. Each unit contains five cooling plates (Figure 55). All of the walls are electrically conducting. The liquid metal starts in the feeding distributing gap and distributes among the cooling plates, flowing into the second connected breeder unit by passing through an opening near the first wall. After distributing into the second BU, the fluid is collected in the draining poloidal distributing gap. A detailed description of HCLL blanket design specifications is reported in reference [7].

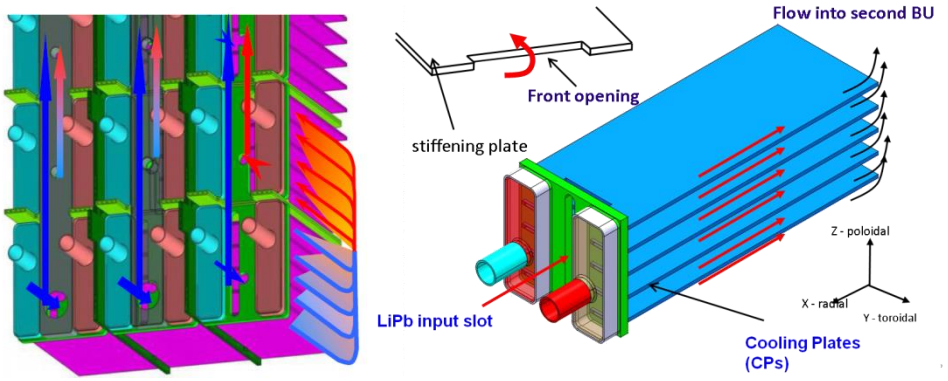

Figure 55. HCLL breeder unit geometry.

5.6.2 Estimates of Tritium Transport and Permeation for HCLL Concept

The velocity field is obtained by performing a 3D simulation with a magnetic field strength of 1.852*T* and with an inlet mass flow rate of liquid metal of 0.33 kg/s. With this figure, the liquid metal velocity will be ~0.8 mm/s in the BU cross-section. Tritium transport calculation is performed by solving a fully 3-D mass transfer problem with appropriate boundary conditions at various interfaces. The tritium generation rate was taken from experimental results in Figure 10.

Figure 56 and Figure 57 show the velocity profile and the corresponding tritium concentration at the middle plane of the geometry. The velocity distributions show that the

stiffening plate has a stronger influence on the velocity profile than the cooling plate, which causes a larger flow rate at the stiffening plate. In the duct cores, a rough uniform velocity distribution is observed, with a small increase in the side layers along the cooling plates. This kind of velocity distribution would be preferred due to its benefit on tritium permeation reduction. The distribution of the tritium concentration in the breeder units shows lower values in the first breeder unit and accumulation along the PbLi pathway. Along the poloidal direction the tritium concentration increases as the channel aspect ratio increases. The second channel of the top breeder unit has highest tritium concentration. The top channel of the first breeder unit has the lowest tritium concentration due to the relatively high velocity there. In the duct cores, we can see a rough uniform tritium distribution, and there are no high local tritium concentrations near the structure walls. This kind of distribution would be good to prevent tritium permeation and reduce tritium loss to helium coolant.

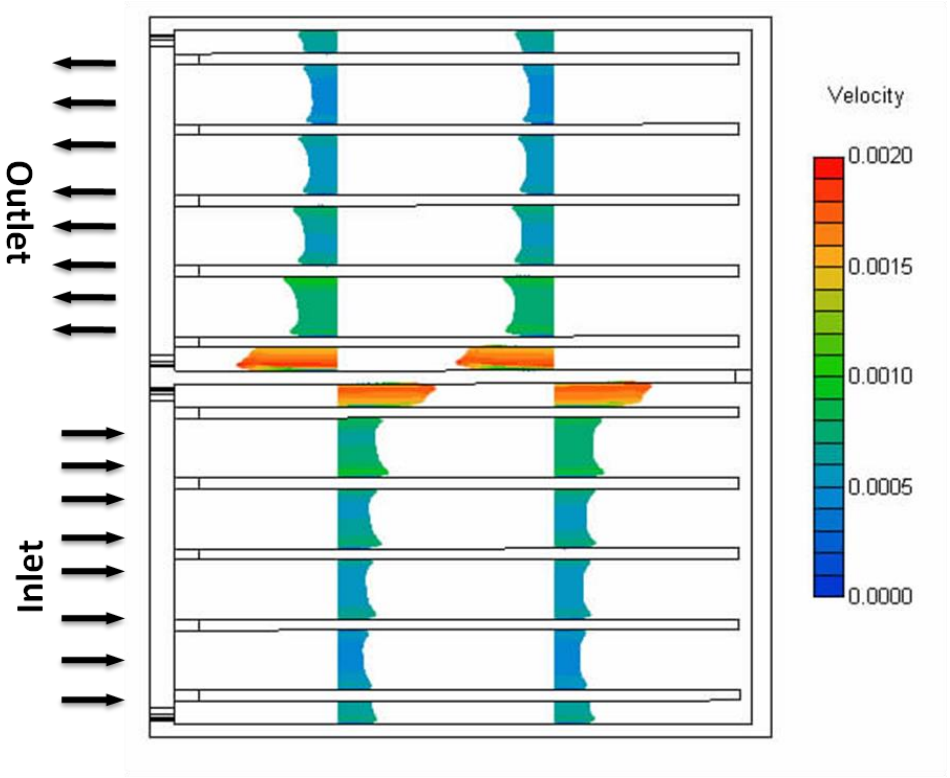

Figure 56. Velocity profile in the HCLL breeder units shows higher velocities near stiffening plate and small increasing in the side layers along the cooling plates.

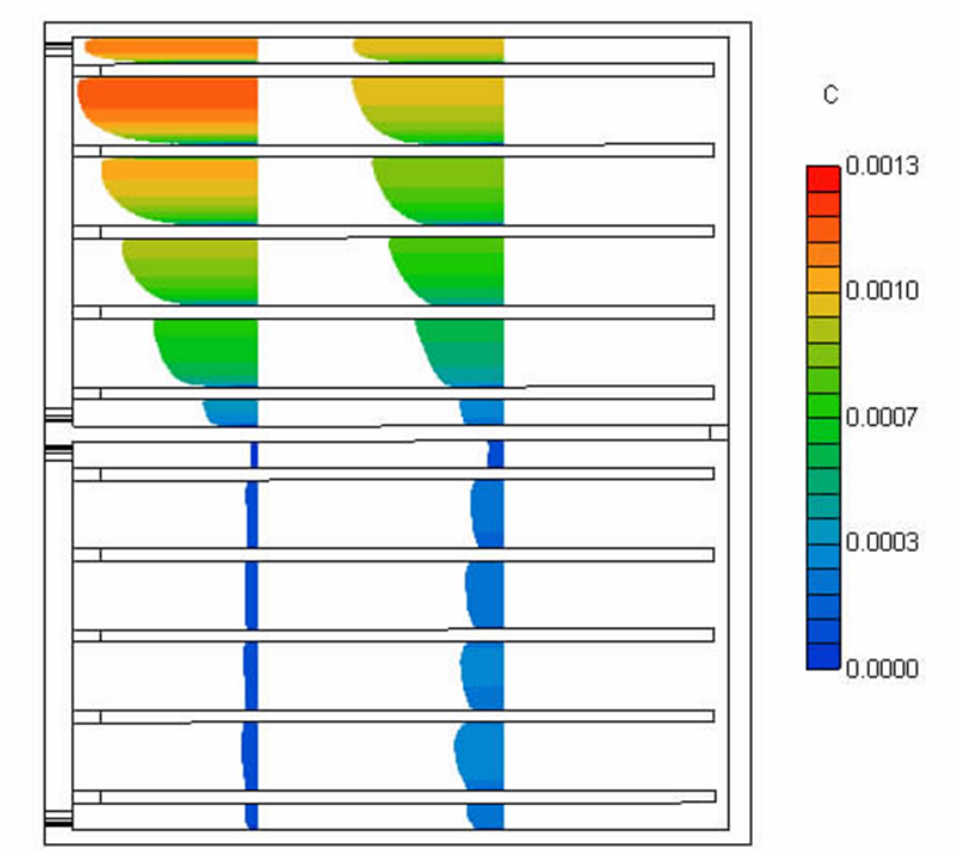

Figure 57. Tritium concentration (mol/m^3) in the HCLL breeder units shows tritium concentration increases as the channel aspect ratio increases along the poloidal direction.

5.6.3 Comparison with DCLL Concept

The overall tritium generation, inventory, and permeation losses for the HCLL's two breeder units and the DCLL's U-shape channel are compared in Table 8. Because the LM flow rate in the HCLL concept is about 2 orders of magnitude lower than in the DCLL concept, the tritium inventory and permeation for the case of the HCLL concept will be much higher than the case of the DCLL concept. For the analyzed HCLL's two breeder units and DCLL's U-shape channel, tritium inventory per volume in PbLi for the case of HCLL increased by over 4 times compared to the case of DCLL. Tritium permeation loss is about 17% of the tritium production for the HCLL breeder units, which is more than 10 times higher than for the DCLL U-shape channel. To control these permeation losses, efficient tritium permeation barriers as well as efficient tritium extraction systems from the helium coolant are necessary for the HCLL concept.

Table 8. Summary of tritium generation, inventory and permeation for the analyzed HCLL two breeder units and DCLL U-shape channel

	HCLL BU(2)	**DCLL U-shape channel**
Pb–17Li average velocities	~0.8mm/s	~0.07m/s
Volume (m^3)	0.026	0.0324
Permeation area (m^2)	1.99	1.45
Tritium generation rate in PbLi (mol/s)	2.49e-8	9.72e-8
Tritium inventory per volume in PbLi (mol/m^3)	4.38e-4	8.15e-5
Tritium exit rate from outlet (mol/s)	2.06e-8	9.60e-8
Tritium permeation rate (mol/s)	4.31e-9	1.16e-9
Tritium permeation flux per area (mol/m^2s)	2.16e-9	8.00e-10
Losses percentage (%)	17%	1.2%

5.7 Initial Analysis of the Effect of the He Bubbles on Tritium Transport

A detailed tritium transport model needs to account for (1) the possible helium bubble nucleation and its coalescence, (2) bubble transport in liquid metal, (3) tritium diffusion and recombination at bubble surface and wall interaction. Some works have been started at the Technical University of Catalonia (UPC), Technology for Fusion (T4F), Barcelona, Spain (such as Batet et al. and Fradera, et al.).

Helium bubble phenomena are too complicated to analyze as a whole from the start. This can be a new research topic. In this work, some initial analysis of the effect of the helium bubbles on tritium transport was carried out and hereafter presented for future reference.

5.7.1 Tritium Transport Modeling Considering Helium Bubbles

Tritium stays in dissolved form (T) in LM, however, if He nucleates, tritium may be absorbed into He bubbles as the new forming phase T_2. We assume tritium and helium bubbles do not change liquid metal properties nor flow behavior, so that tritium can be represented as a passive scalar. Hence, the passive scalar advection/diffusion type equations have been implemented as:

$$\frac{\partial c_{T\_LM}}{\partial t} + \mathbf{u}_{LM}\nabla c_{T\_LM} = \nabla\cdot(D_{LM}(T)\nabla c_{T\_LM}) + S_T - J_{T\_LM-bubble} \tag{45}$$

$$\frac{\partial c_{T2\_bubble}}{\partial t} + \mathbf{u}_{LM} \nabla c_{T2\_bubble} = \frac{1}{2} J_{T\_LM-bubble} \quad (46)$$

Where:

c_{T_LM} = tritium concentration (mol/m^3) within the PbLi, at spatial coordinate r and time t;

S_T = volumetric tritium generation rate, at spatial coordinate r and time t, (mol/m^3/s)

$J_{T\_LM-bubble}$ = tritium flux through PbLi/bubbles interface, at spatial coordinate r and time t, (mol/m^3/s)

D_{LM} (T) = tritium diffusion coefficient (m2/s) in the PbLi as a function of the temperature T;

$\mathbf{u}_{LM}$ = velocities (m/s) in the PbLi MHD flow.

5.7.2 Modeling at the Liquid Metal – Bubble Interface

Generated T stays dissolved but, if He bubbles exist, tritium may be absorbed into the new forming phase, and the He nano-bubbles could act as effective T trap sites. At this point, many questions arise due to lack of experimental data. Tritium transfer phenomena have not been extensively studied for this system.

In order to simplify the model, we assume dissociation and recombination proceeds at a rate fast enough that there is effectively equilibrium between gaseous and LM solute.

Sievert's law applies, relating the equilibrium concentration of solute atoms in the metal to the gas partial pressure inside the bubbles. The form of the solution relation is

$$c_{T\_LM} = K_{S\_LM} P_{T2\_bubble}^{1/2} \tag{47}$$

Where P_{T2_bubble} is the tritium partial pressure inside bubbles, and K_{S_LM} (mol/m^3·Pa$^{0.5}$) is the solubility coefficient for Sievert's law.

Because there are also discontinuities in the concentration profile and continuous flux at the boundaries between liquid and bubble phases, we use same approach used in LM-SM interface, apply a special type of boundary condition using the stiff-spring method, which would define continuous flux conditions that, at the same time, force the concentrations to the desired values:

The flux boundary condition at the LM side can be expressed as:

$$\begin{aligned} J_{T\_LM-bubble} &= (-D_{LM}\nabla c_{T\_LM} + c_{T\_LM}\mathbf{u}_{LM})\cdot\mathbf{n} \\ &= M\cdot a\cdot(K_{S\_LM}\sqrt{P_{T2\_bubble}} - C_{T\_LM}) \end{aligned} \quad \text{at } \partial\Omega^{LM/bubble} \tag{48}$$

The flux boundary condition at the bubble side can be expressed as

$$\begin{aligned} J_{T2\_bubble\_LM} &= (-D_{bubble}\nabla c_{T2\_bubble})\cdot\mathbf{n} \\ &= \frac{1}{2} M\cdot a\cdot(C_{T\_LM} - K_{S\_LM}\sqrt{P_{T2\_bubble}}) \end{aligned} \quad \text{at } \partial\Omega^{bubble/LM} \tag{49}$$

Where

a = the interfacial area;

$\partial\Omega^{LM/bubble}$ = the interface belongs to LM domain;

$\partial\Omega^{bubble/LM}$ = the interface belongs to bubble domain;

5.7.3 Effect of the Volume Fraction of He Bubble on the Tritium Trapping

The purpose of this analysis is to investigate the importance of helium bubbles on tritium transport when the volume fraction of helium bubble and the reference tritium partial pressure are changed. In Figure 58, the percent of tritium trapped into helium bubbles as a function of the volume fraction of helium bubble are compared for the four reference tritium partial pressure in PbLi. It shows that the amount of tritium trapped into helium bubbles is insignificant at low tritium partial pressure regime, which occurs in DCLL concept, However, at high tritium partial pressure regime, which occurs in HCLL concept, the amount of tritium trapped into helium bubbles is markedly high.

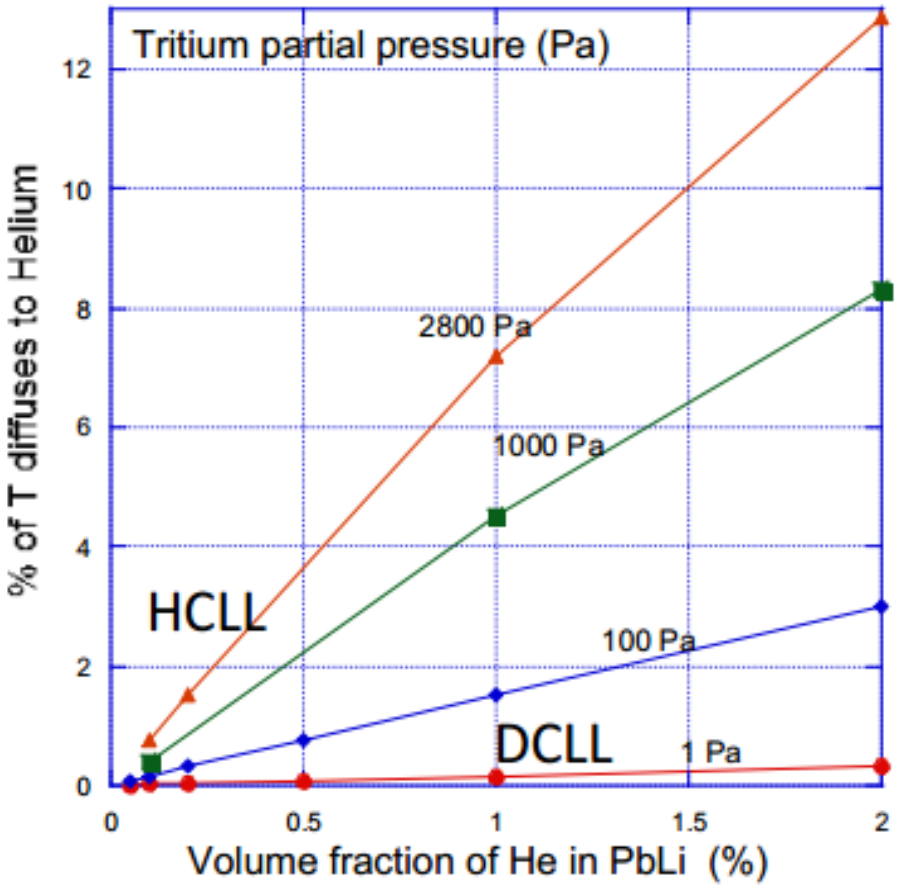

Figure 58. The amount of tritium trapped in He bubbles when the volume fraction of helium bubble and the reference tritium partial pressure are changed

5.8 Overall Summary of the Parametric and Case Studies

The numerical results discussed this chapter are summarized in Table 9. Looking at the reported values, we can summarize the parametric study stating that the most relevant parameters in tritium migration in PbLi blanket are:

- Gap velocity of the liquid metal;
- Tritium solubility in PbLi Ks;
- Hartmann number Ha;
- FCI electric conductivity.
- Helium bubble trapping effect for the HCLL blanket

The less important factors in tritium migration in PbLi blanket are:

- Presence of PES;
- Tritium diffusivity in PbLi;
- Helium bubble trapping effect for DCLL blanket

Table 9. Summary Results of the Sensitivity Study

Ranged parameter or design factors	Case	Results
Hartmann number		Tritium losses
0	Duct flow	2.98e-10 mol/s
1000		1.25e-10 mol/s, drop by 60%
Tritium solubility in PbLi		Tritium losses
5e-4 $mol \cdot m^{-3} \cdot Pa^{-1/2}$	Duct flow	1.5e-10 mol/s
1e-2 $mol \cdot m^{-3} \cdot Pa^{-1/2}$		2.4e-11 mol/s, drop by 80%
Tritium diffusivity in PbLi		Tritium losses
1e-9 m^2/s	Duct flow	1.41e-10 mol/s
1e-8 m^2/s		1.67e-10 mol/s, drop by 18%
Buoyancy effect		Tritium losses
		1.88e-8 mol/s
Downward flow		1.55e-8 mol/s, drop by 18%
		Inventories
Upward flow		4.71e-4 mol
		9.53e-5 mol, drop by 80%
PES effect		Tritium losses
No PES	Duct flow with	1.76e-10 mol/s,
PES in the wall // B	FCI and PES	1.87e-10 mol/s, increase by 6%
PES in the wall ⊥ B		1.99e-10 mol/s, increase by 13%
Electric conductivity of FCI		Tritium losses
5 $\Omega^{-1}m^{-1}$	Duct flow with	4.8e-10 mol/s
1000 $\Omega^{-1}m^{-1}$	FCI and PES	2.2e-10 mol/s, drop by 55%
Velocity of PbLi		Tritium losses
		1.2% of generation
U ~ 0.675 m/s (DCLL)	DCLL U-shape	17% of generation, increase by 10 times
U ~ 0.8 mm/s (HCLL)	HCLL 2BUs	Average Inventory
		8.15e-5 mol/m^3
		4.38e-4 mol/m^3, increase by 4 times
Volume fraction of helium bubble		Amount of T trapped in He bubbles
2% for DCLL		0.2%
2% for HCLL		13%

5.8 References

1. B. Schulz, Fus. Eng. Des. 14 (1991) 199.
2. P. Hubbertsey, T. Sample, M. Barker, J. Nucl. Mater. 191–194 (1992) 283.
3. F. Reiter, Solubility and diffusivity of hydrogen isotopes in liquid Pb-17, Fusion Eng. Des. 14 (1991) 207–211.
4. A. Pisarev, T. Tanabe, T. Terai, G. Benamati, M. Mullin, J. Nucl. Sci.Technol. 39 (4) (2002) 377.
5. A. Aiello et al. "Hydrogen isotopes permeability in EUROFER 97 Martensitic steel" Fusion Science and Technol. Vol. 41 872-876 (2002)
6. RA. Causey et al. / Tritium migration in vapor-deposited β-silicon carbide, Journal of Nuclear Materials 203 (1993) 196-205
7. P. NORAJITRA, L. BUHLER, A. UENAVENTURA, E. DIEGELE, U. FISCHER, E. UTTER, R. KRUESSMANN, S. MALANG, J. REIMANN, A. ORDEN, D. WARD, G. VIEDER, and F. WASASTJERNA, "Conceptual Design of the dual-coolant blanket in the frame for the EU power plant conceptual study (TW2-TRP-PPCS12D)", Forschungszentrum Karlsruhe Report FZKA 6780 (2002).

8. S. Xu, N. Zhang and M. Ni, “Influence of Flow Channel Insert with Pressure Equalization Opening on MHD Flows in Liquid Metal Blanket”, To be appeared in Fusion Engineering and Design.
9. C.P.C. Wong, M. Abdou, et.al., “Design Description Document for the U.S. Dual Coolant Pb-17Li (DCLL) Test Blanket Module”, 2005
10. E. MAS DE LES VALLS, L.A. SEDANO, L. BATET, I. RICAPITO, A. AIELLO, O. GASTALDI and F. GABRIEL, "Lead-lithium eutectic material database for nuclear fusion technology", J. of Nuclear Materials 376 (2008) 353-357.
11. M.J. Pattison [24, TRITIUM TRANSPORT IN POLOIDAL FLOWS OF A DCLL BLANKET, Fusion Science and Technology, FST10-309
12. C. MISTRANGELO and L. BUHLER, "Electric flow coupling in the HCLL blanket concept", Fusion Engineering and Design 83 (2008) 1232-1237.

Chapter 6

Summary and Recommendations

The primary purposes of this study are: 1) to develop mathematical models and computational codes to quantify tritium distributions throughout the blanket and permeation rate from liquid metal to helium coolant, 2) to evaluate the important factors, such as geometric configuration of the blanket, MHD flow, and uncertainties of transport properties that govern tritium permeation and distributions.

The proposed model in this work includes multiple tritium transfer processes which are adequately coupled, such as LM MHD flow, mass transfer at fluid-solid interfaces, and convection-diffusion in liquid metal. Appropriate boundary conditions have been selected to link the different mass transport mechanisms for the different physical regions. The framework of the computational code has been developed. The coupled partial differential equations, which describe the mass transfer in the three-dimensional multiple domains, are solved by a finite volume method in a commercial thermo-fluid mass transfer code. Customized numerical schemes have been implemented in the code for calculating mass transfer across material interfaces. Data mapping utilities were also developed to pass MHD

velocity and temperature profiles to mass transfer code to study the advection and temperature effects.

The computer code has been validated with experimental data from US-JA collaborations and analytical solutions and showed reasonably good agreement. Parametric studies including the MHD effects, buoyancy effects, and PES effect have been carried out. The difference of tritium inventory and permeation rate between DCLL and helium-cooled lead lithium (HCLL) blanket concepts has been quantified. The range of permeation rate change on the basis of uncertainties of solubility and diffusivity is also provided in this work.

The cases investigated were: (1) parametric studies to identify the MHD effect, material properties (e.g. solubility, diffusivity), and the buoyancy effect on tritium transport and permeation; (2) tritium transport in a DCLL-type poloidal duct with PES in FCI to evaluate PES effects on tritium concentration and permeation; (3) tritium transport and permeation in a DCLL U-shaped flow which represents the current US DCLL design; (4) tritium transport and permeation in HCLL configuration and comparison with the case of DCLL concept. Based on the analyses carried out for different cases, the following observations are made:

1. The MHD effect will impart certain benefits in terms of reducing the tritium permeation rate due to the high velocity in the near-wall region under MHD conditions. Tritium concentration peaks close to the walls without MHD, while it becomes more

concentrated in the center as Hartmann number increases. As a result of lower tritium partial pressure near the wall, the permeation rate through the wall will be reduced. However, the rate of decrease due to increase of the Hartmann number becomes slower at higher Hartmann numbers.

2. The calculation results indicated that the effect of the uncertainty in the values for tritium solubility in PbLi on tritium permeation is quite strong, especially for the reference range, in which tritium permeation rate is most sensitive with the values of tritium solubility. The current data results in a ~ 80% difference in permeation rate. A higher tritium solubility provides a lower tritium permeation rate.

3. The diffusion coefficient markedly affects the tritium permeation rate by controlling the amount of tritium diffusing from PbLi to the PbLi/FS interface. A higher tritium diffusivity provides a higher tritium permeation rate.

4. In the buoyant PbLi MHD flows analyzed, there exists a strong shear layer at the center of the channel and there is a region of buoyancy-induced reverse flow near the front wall for the downward flow. As a result, the calculated permeation loss is about 20% higher than the permeation loss for the case of upward flow. Tritium inventory for the case of upward flow dropped nearly by 80% compared to the case of downward flow.

5. PES in the FCIs changed the velocity profiles and thus changed the tritium concentrations in the core and gaps. High tritium concentrations are always associated with low-speed velocities. Under the given conditions, the case of a non-PES duct gives the lowest tritium loss of 1.25% of the tritium production, while tritium loss increased nearly by15% to 1.42 % for the case of a PES opening parallel to the magnetic field. This is attributed to the increasing of the permeation through the front wall due to the velocity reduction in side gaps when the PES is introduced.

6. The electrical conductivity of the FCI clearly affects the tritium permeation rate by changing the velocity in the gaps. A higher electrical conductivity of FCI provides higher velocity in the gap and thus a lower tritium permeation rate.

7. The contribution of the inlet manifold has a strong effect on tritium permeation for a DCLL U-shaped channel. A lower mass flow rate in the gap provides a higher tritium concentration in the gap and thus increases the tritium permeation rate. Under the given conditions, the case of $\frac{\mathbf{U}_{\mathbf{inlet\_gap}}}{\mathbf{U}_{\mathbf{inlet\_}core}}=1$ gives a lower tritium loss of 1.2% of the tritium production, while tritium loss increased nearly by 140% for the case of $\frac{\mathbf{U}_{\mathbf{inlet\_gap}}}{\mathbf{U}_{\mathbf{inlet\_}core}}=0.1$. It results in a higher tritium loss of 2.9 % of the tritium production.

8. Because the LM flow rate in the HCLL concept is about 2 orders of magnitude lower than in the DCLL concepts, the tritium inventory and permeation for the case of HCLL

concept will be much higher than the case of DCLL concept. For the two HCLL breeder units and DCLL U-shaped channel analyzed, tritium inventory per volume in PbLi for the case of HCLL two-breeder units increased by over 4 times compared to the case of the DCLL U-shape channel. Tritium permeation loss is about 17% of the tritium production for HCLL breeder units, which is more than 10 times higher than for a DCLL U-shaped channel. To control these permeation losses, efficient tritium permeation barriers as well as efficient tritium extraction systems from the helium coolant are necessary for the HCLL concept.

The study indicates that the most critical parameters in tritium permeation in a DCLL PbLi blanket are the gap velocities and tritium solubility. It seems possible to further reduce tritium permeation by increasing the gap velocities using a novel manifold design or by increasing the FCI electric conductivity. However, its impact on the MHD pressure drop is yet to be analyzed. A tritium permeation barrier may still be needed for the DCLL blanket to further reduce tritium permeation to meet the tritium permeation requirements.

Recommendations

The tritium transport model that has been presented in this work seems to provide an adequate selection of physical processes and numerical methods and can be used for tritium transport simulation analyses and for assisting lead-lithium liquid metal blanket designs. There are, however, areas in which different physical models and experimental work may be needed to develop more powerful predictive capabilities. On the basis of the indications presented above, the following specific recommendations are proposed for further modeling efforts and planning new experiments:

1. The surface effect. The analyses in this study assume the structural walls are clean. However, oxidized and clean wall surfaces have different surface properties (e.g., adsorption, desorption, and recombination constants). Thus tritium permeation could be affected by the surface conditions. The proposed model in this study is capable of accounting for such phenomena through the use of sticking coefficients. However, more reliable material data under different surface conditions are needed either through experimental methods or by numerical approaches such as molecular dynamics simulations.
2. The helium bubble effect. Preliminary analysis (Section 5.7) in this study shows that the amount of tritium trapped into helium bubbles is insignificant in the low tritium

partial pressure regime, which occurs in the DCLL concept, However, at in the high tritium partial pressure regime, which occurs in the HCLL concept, the amount of tritium trapped into helium bubbles is significantly high. Therefore, further modeling and analyses are necessary to evaluate the impact of helium bubbles especially for the HCLL concept blankets.

3. Experiments of database evaluation. Dedicated experimental campaigns aimed at obtaining more reliable material properties are needed. The effect of the uncertainty in the values for tritium solubility and diffusivity in PbLi on tritium permeation is quite marked, especially for tritium solubility in the reference range, in which the tritium permeation rate is most sensitive to the values of tritium solubility. The current solubility data results in a ~ 80% difference in permeation rate. There is an urgent need to find reliable and agreed-upon data. Moreover, new experiments with tritium aimed to determine more detailed surface properties of structural materials should be carried out. In addition, transport data on other species, which may provide some insights into transport of tritium, should be obtained. Helium transport is potentially an issue for liquid metal blankets as discussed in Section 5.7, especially for the HCLL concept due to high tritium partial pressure and low liquid metal flow rate.

Appendix

A. Unit Conversion

The International System of Units, or SI, is the standard system of measurement used by many scientists. Using the same standards of measurement makes it easier for scientists to communicate with one another. However, for fusion technology and science, non-SI units may be used in some instances. For example, it is convenient to report concentrations in terms of their components—either weight to volume or volume to volume. Listed below are the common conversions between SI units and non-SI units for tritium concentration in PbLi.

Convert from wppb to mol/m^3

$$\text{concentration in } \frac{mol}{m^3} = (\text{concentration in } wppb) \times 10^9 \times \frac{\rho_{PbLi}}{M_T}$$

Where ρ_{PbLi} is the density of PbLi and M_T is the molar mass of tritium.

Convert from concentration in mol/m3 to partial pressure (Pa)

$$\text{Partial Pressure in } Pa = (\text{Concentration in } \frac{mol}{m^3})^2 / {K_s}^2$$

Where K_s is the tritium solubility of PbLi in $\frac{\text{mol}}{\text{m}^3 Pa^{0.5}}$

Convert from wppb to partial pressure (Pa)

$$\text{Partial Pressure in } Pa = (\text{Concentration in } wppb \times 10^9 \times \frac{\rho_{PbLi}}{M_T})^2 / {K_s}^2$$

Convert solubility K_s from (at fr/Pa-0.5) to $\frac{\text{mol}}{\text{m}^3 Pa^{0.5}}$

$$\text{solubility in } \frac{\text{mol}}{\text{m}^3 Pa^{0.5}} = (\text{solubility in } \frac{\text{at} \cdot \text{fr}}{\text{Pa}^{0.5}}) \times \frac{\rho_{PbLi}}{M_{PbLi}}$$

Where ρ_{PbLi} is the density of PbLi and M_{PbLi} is the molar mass of PbLi.

B. Mesh Grid Size Sensitivity

Mesh grid size is an important factor in numerical simulations because resolving of the tritium movements and flow motions depends on the grid size to accurately describe the flows and mass transfer, especially under MHD conditions. As the grid size gets finer, it inflicts a high computational cost. In contrast, if the grid size gets coarser, this leads to poor description of the tritium distribution as well as the flow especially in the regions of Hartmann and side layers. Therefore, using the appropriate grid size is always crucial.

Three grid size samples (fine, medium, and coarse as shown in Table 10 and Figure 59) have been chosen to investigate the grid size effect on the results in a duct flow with 1m length, 60mm*60mm cross-section, and 2mm conducting wall. The grid size was refined in the zone of interest around Hartmann layers and the side layers.

Table 10 Grid Sizes for the Sensitivity Study

Grid size type	**Size of grids in Ha layer (m)**	**Size of grids in side layer (m)**
Fine	8.40e-5, (15 cells in Ha layer)	3.36e-4
Medium	1.26e-4, (10 cells in Ha layer)	5.04e-4
Coarse	1e-3, (5 cells in Ha layer)	1.00e-3

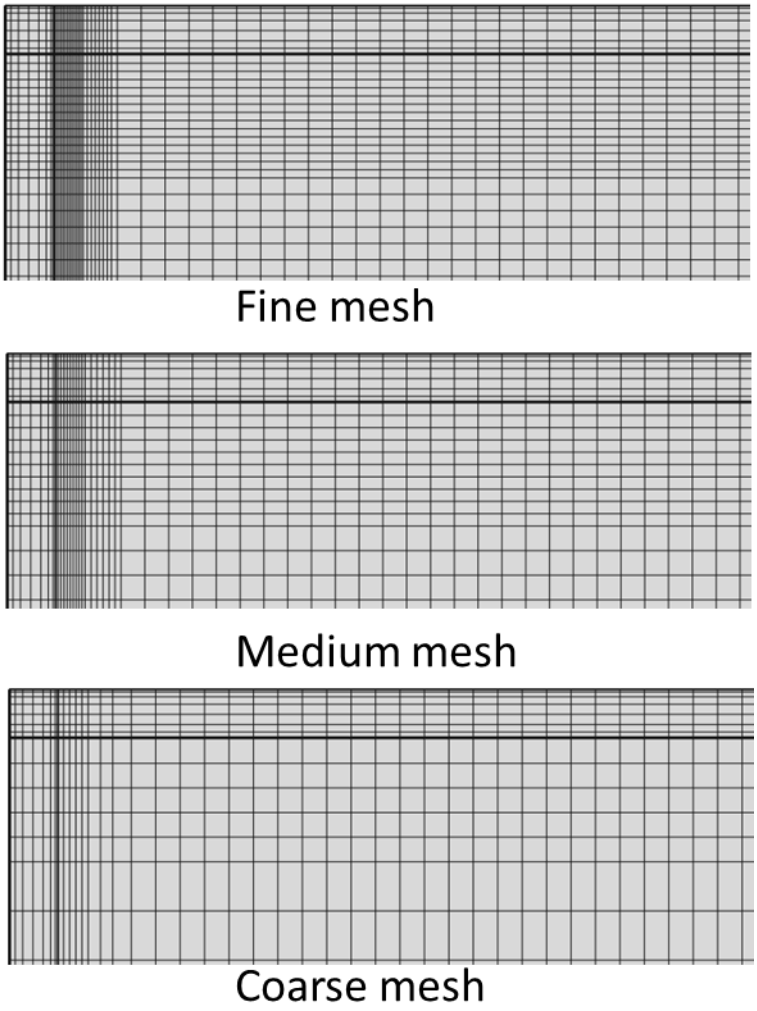

Figure 59. Three mesh sizes shown on the corner of the duct cross-section.

Figure 60 shows the tritium concentration along the side layers for three grid size samples. The results showed similar features but with small differences as expected. From the three grid sizes, the fine meshing (black solid line) reduced the thickness of concentration

peak layer as the model properly resolved the flow in the side layers. However, the computational time was significantly increased compared with the other two meshing.

In contrast, the results using the coarse grid size (blue dash dot line) showed a wider concentration peak layer and it was also shifted away from the wall. However, the simulation result with the medium grid size produces satisfactory tritium concentration descriptions as shown in red dot line.

Figure 61 shows the tritium concentration along the middle-line of the Hartmann layers simulated with the three grid size samples. They results from three grid sizes agreed very well. However, the results using the coarse grid size showed a slight thicker boundary layer.

Therefore, the medium grid size is a good compromise between the fine and coarse grid sizes and therefore we use the medium grid size throughout this study to minimize the long computational time inflicted by the fine grid size but satisfying the engineering solution.

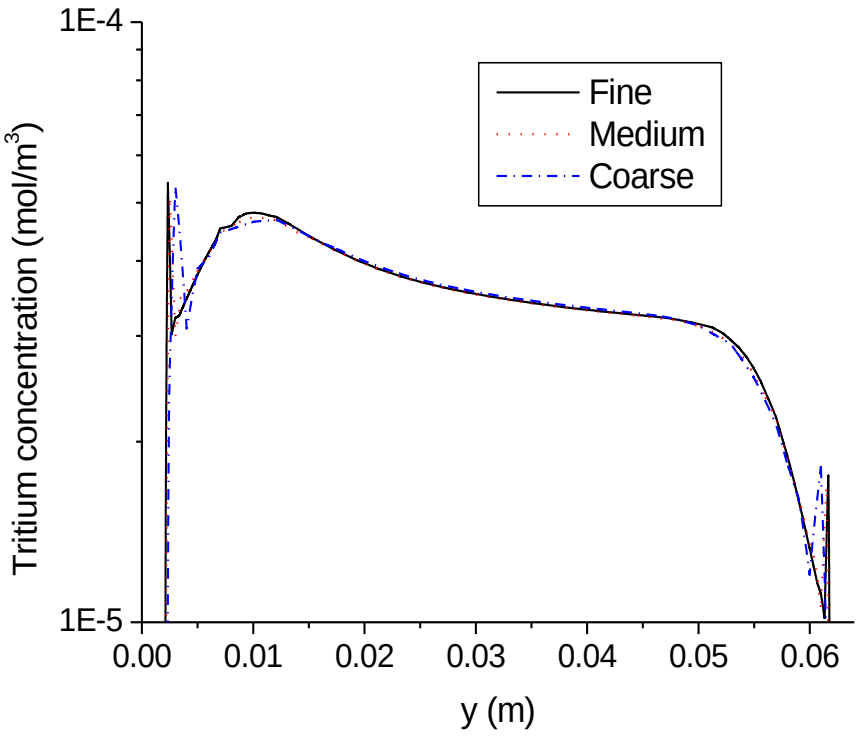

Figure 60. Tritium concentration along side layer simulated with three mesh sizes

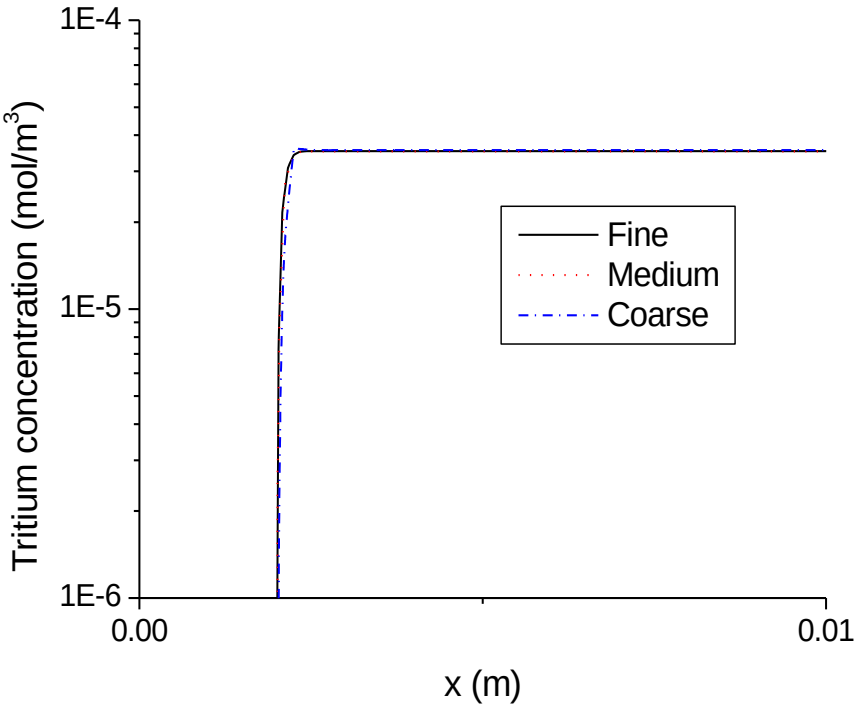

Figure 61. Tritium concentration along Hartmann layer simulated with three mesh sizes